ASPECT INDEPENDENT DETECTION AND DISCRIMINATION OF CONCEALED METAL OBJECTS BY ELECTROMAGNETIC PULSE INDUCTION: A MODELLING APPROACH

Abdulbast Mohamed Elgwel

A thesis submitted in partial fulfilment of the requirements of the Manchester Metropolitan University for the degree of Doctor of Philosophy

School of Engineering

Division of Electrical and Electronic Engineering

Manchester Metropolitan University

2013

Abstract

The work presented in this thesis describes the research, modelling and experimentation which were carried out so as to explore the use of electromagnetic pulse induction for the detection of nearby or on-body threat items such as handguns and knives. Commercially available finite difference time domain electromagnetic solver software, *Vector Fields,* was used to simulate the interaction of a low frequency electromagnetic pulse with different metal objects. The ability to discriminate between objects is based on the lifetime of the induced currents in the object, typically around 100 (μs). Lifetimes are different for a different objects, whether they are weapons or benign objects. For example hand grenades, knives, and handguns are clearly threat objects whereas a wrist watch, mobile phone and keys are considered benign. Electromagnetic pulse Induction (EMI) relies on generating a time-changing but spatially uniform magnetic field, which penetrates and encompasses a concealed metallic object. The temporally changing magnetic field induces eddy currents in the conducting object, which subsequently decay by dissipative (i.e. resistive) losses. These currents decay exponentially with time and exhibit a characteristic time constant (lifetime) which depends only upon the size, shape and material composition of the object, whilst the orientation of the object is irrelevant. This aspect independence of temporal current decay rates forms the basis of a potential object detection and identification system. This thesis investigates the possibility of detecting, resolving and identifying multiple objects if they are close together, for example located on an individual. The mathematical analysis used for the investigation implements the generalised pencil of function (GPOF) method. The GPOF algorithm decomposes the signal into a discrete set of complex frequency components; providing the capability to obtain the time constants from data. It was possible to effectively count and identify multiple metallic objects carried in close proximity providing that the objects do not have very similar time constants. The simulation results, which show that multiple objects can be detected, resolved and identified by means of their time constants even when they are close together, are presented.

Acknowledgments

I would like to take this opportunity to express my sincere thanks and gratitude to Professor Nicholas Bowring and Dr. Stuart Harmer for their continued patience, inspiration, valuable guidance, advice, encouragement, and time.

They guided me through all the stages, giving valuable advice and encouraging me to disseminate results in journals and so provided opportunities to communicate with scientific researchers from different research institutions

I would like to thank to Shaofei Yin, member staff for his continuous support and helping me to learn the simulation program also for the fruitful discussions.

I am also grateful to my mother and my family, especially my wife and my children; they were the biggest motivation in completing my study.

List of Abbreviations

AMMW	Active Millimetre Wave
CW	Continuous Wave
CWD	Concealed Weapon Detection
EM	Electromagnetic
emf	Electromotive Force
EMR	Electromagnetic Resonance
EMW	Electromagnetic waves
ELEKTRA/TR	ELEKTRA transient
FDTD	Finite Difference Time Domain
FEA	Finite Element Analysis
FEM	A finite Element Models
GPOF	Generalised Pencil of Function
IED's	Improvised Explosive Devices
INL	Idaho National Laboratory
IR	Infrared
MMW	Millimetre Wave
NAC	Nonlinear Acoustic
PMMW	Passive Millimetre Wave
RCS	Radar Cross Section
POF	Pencil of Functions
RF	Radio Frequency
SS	Steady state
TR	Transient
TDS	Time Domain Spectra
THz	Terahertz
WAMD	Wide Area Metal Detection

List of Mathematical Symbols

A	Cross Section Area
a	Radius of Sphere (m)
B	Magnetic Field (T)
D	Electric field Displacement (C/m^2)
E	Electric Field Intensity (v/m)
$\mathcal{E}$	Electromotive Force (v)
H	Magnetic Intensity (A/m)
J	Electric Current Density (A/m^2)
L	Inductance (H)
M_{ij}	Mutual Inductance
N	Coil Turns Numbers
R	Radius in Spherical Coordinates
μ_0	Absolute Permeability ($4\pi \times 10^{-7}$ H/m)
σ	Conductivity (S/m)
ϕ	Magnetic Flux (wb)
τ_0	Fundamental Time Constant (ms)
μ	Relative Permeability
ε_0	Absolute Permittivity (8.5×10^{-12} F/m)
ε	Relative Permittivity
δ	Skin Depth (m)
ρ	Electric Surface Charge Density (C/m^2)
χ_m	Magnetic Susceptibility
χ_n	Solution of equation

Contents

List of Tables

List of Figures

Chapter 1

GENERAL INTRODUCTION

1.1 Preview

Technologies for the detection of various concealed and buried metallic objects, especially IED's (Improvised Explosive Devices), are currently of great topical interest. Although there have been many studies, throughout the world, to curb and prevent security threats in public places, such as concealed weapons and explosive devices and buried ordnance (e.g. landmines) there is still no single sensor which provides a complete solution to these problems.

Sensors capable of the detection of concealed, buried and hidden objects, both metallic and non-metallic, which can also discriminate between threat items (suicide vests, guns, knives, hand grenade and other deadly weapons) and non-threat items (mobile phone handsets, jewellery and keys) would provide a very significant enhancement of capability to security forces. These threats represent a considerable challenge facing today's law enforcement community [1]. In this field, the screening techniques used for the detection of buried or concealed metal items are used in banks, airports, public events and entrances of sensitive buildings, as well as at the gates of prisons and courts. However such EMI devices cannot detect hidden objects at any significant distance. To detect hidden objects they must be close to the detection device in order to ensure sufficient sensitivity. According to the research presented here, there is no device that can detect and identify concealed metallic objects on the body with a high certainty of detection and identification and a low probability of false alarms.

1.2 Aim of project

The aim of this project was to demonstrate the feasibility of detection and identification of multiple conducting objects using EMI to excite circulating eddy currents within the object. The results were realised by numerical simulation using a finite element time domain electromagnetic solver that was capable of modelling

metallic objects of both threat and non-threat types. These objects were of different shapes, sizes and materials. Modelling was carried out for singular objects; grouped objects and in a variety of orientations and positions. The results were processed to determine the fundamental time constant for these configurations of objects.

To detect and distinguish concealed metallic objects it is necessary to propagate electromagnetic pulses to induce eddy currents to flow in the concealed or buried of metallic objects. Analysis of the reflected (received) signals that take the form of exponentially damped function field amplitudes provide the basis for the determination of the time constant for the metallic object and thereby permits crude identification of object type.

1.3 Objectives

The objectives of this research are to:

- Design the modelling for several metallic objects of a range of representative materials, threat and non-threat targets, by a Finite Element Simulation program.
- Find the fundamental time constants for many various shapes and sizes such as spheres and cylinders, and other more representative objects separately and with more than one object together, in various degrees of proximity.
- Develop the electromagnetic pulse induction methodology to detect the concealed and buried metallic targets in group and mix items together on the body or in a bag.
- Find and use a robust mathematical analysis technique generalised pencil of function (GPOF) to analyse time decay(s) curves to reliably find the time constants for targets, even when the targets are grouped together.

1.4 Organization of the Thesis

The thesis is organized as follows:

Chapter 1: General Introduction:

This chapter offers an overview of the project topic of the thesis and presents the aims of the research, objectives, structure of the titles, novelty of research and publication papers.

Chapter 2: literature survey

This chapter reviews and discusses many individual methods employed at different frequency bands throughout the wide electromagnetic spectrum currently used or that are the subject of research to detect concealed metal objects, describing their advantages and disadvantages. Also, which of these methods are the most widespread and common, include the devices that are used for this proposal.

Chapter 3: Electromagnetic Concepts

This chapter clarifies and explains the theoretical equations and methods necessary to describe the concepts of electromagnetic induction by using Maxwell's equations and proves the mathematical steps that have been applied and describes the solutions found during the course of this research, such as boundary conditions and quasi-static solutions of Maxwell's equations.

Chapter 4: Simulation Program

This chapter presents the development and building of FE models for a range of objects such as spheres and cylinders, using several materials such as aluminium, stainless steel, titanium and copper, , as isolated items and in proximity. Furthermore, the methods for finding time decay(s) and for calculating the fundamental time constant theoretical for these shapes and comprised with the simulated results.

Chapter 5: Using electromagnetic pulse induction (EMPI) for the detection of concealed metal objects:

This chapter presents the main contribution to new knowledge and the novelty of this research for using electromagnetic pulse induction at low frequencies to detect concealed and buried metallic objects, both from threat and non-threat targets, separately and mixed together as group (more than up to five items) on body or in a bag.

Chapter 6: Conclusion and Future Work

6.1Conclusion: In this section explains and interprets the results and observations that obtained from the simulation work and clarifies the features.

6.2 Future Work: This section presents the steps to the stage of the future and to avoid mistakes and flaws also worthwhile proposals in order to provide adequate solutions to detect these concealed targets.

1.5 List of Publications Relevant to this Thesis

1.5.1 Peer Reviewed Journal Paper

Abdulbast Elgwel, Stuart William Harmer, Nicholas Bowring & Shaofei Yin, Resolution of Multiple Concealed Threat Objects using Electromagnetic Pulse Induction, Progress In Electromagnetics Research, Vol. 26, 55- 68, 2012.

1.5.2 Conference Papers

1. Abdulbast Elgwel, Nicholas Bowring and Stuart Harmer, Detection of Metallic Objects using Electromagnetic Pulses (Threat Targets), Research day at Manchester Metropolitan University, 20th April 2012.

2. Abdulbast Elgwel, Nicholas Bowring and Stuart Harmer, Electromagnetic Pulses Induction for Detection of Metal Items (Non-threat Targets), Research day at Manchester Metropolitan University, 25th April 2013.

1.6 Contribution to Knowledge

The project presented in this thesis led to investigation of the the possibility of detecting and identifying multiple concealed metal objects located on or about the human body. Detection is by means of electromagnetic pulse induction at low frequencies and the investigation is conducted using electromagnetic simulation tools. Models are applied for many objects of different materials, shapes and sizes such as spheres and cylinders also including easily carried weapons, for example a handgun, hand grenade, razor blade and knife, and commonly carried benign objects, such as a wrist watch, mobile phone and key. The materials simulated were (Aluminium, copper, titanium and stainless steel).

In studying these phenomena we utilised a commercial finite difference time domain electromagnetic solver software called vector fields. The model consists of a transmitter coil that generates a primary magnetic field which induces eddy currents to pass and flow on any concealed or buried metallic objects. The resulting electromagnetic pulses (EMP) are induced in the receiver coil positioned some distance away. The exponential decay rate of the induced current provides a time

constant, which depends upon the size, shape and the material from which the object is made. The time constants are aspect independent, providing the basis for concealed object identification.

The project demonstrated the ability to detect a number of objects and identify multiple metal targets in close proximity. The results show that multiple objects can be detected and identified even when the targets are close together.

Chapter 2

Literature Survey

2.1 Background

This chapter examines recent developments in the field of concealed and buried metallic object detection. Many methods and means of utilising electromagnetic fields have been applied to the problem of identifying concealed objects and especially to determining whether the object detected constitutes a threat or not. Such methods include: millimetre waves, x-ray, electromagnetic waves and infrared, and may be passive or active in operation. There are devices available which are hand-held units and also as walk-through (portal) units that are used for concealed weapon detection, also extended-arm type metal detector shown in figure 2-1 that is used to find metal items buried or hidden under the ground, also the extended-arm metal detector is the same type of metal detector typically used in treasure hunting [2].

.

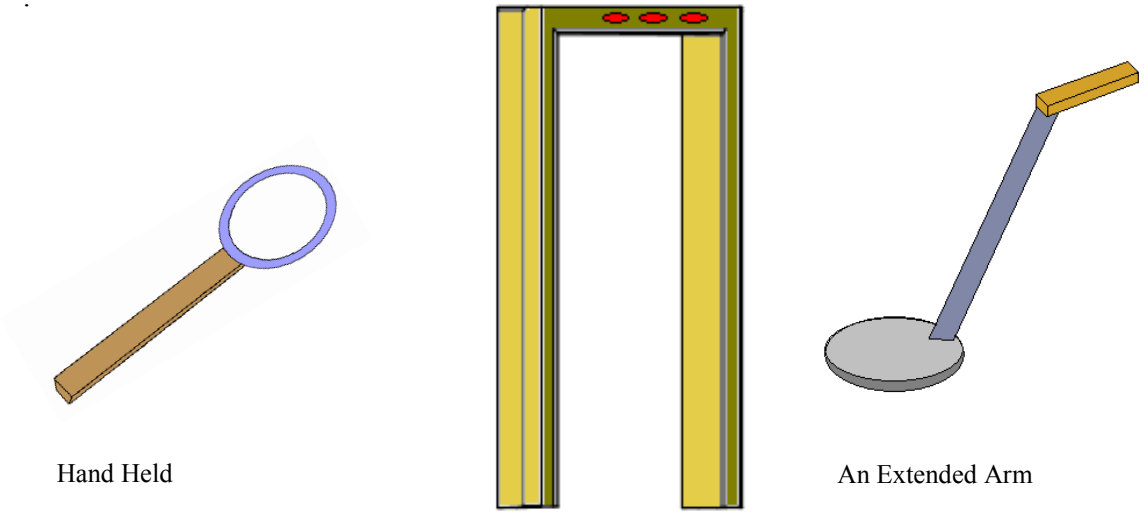

Hand Held

Portal

An Extended Arm

Figure 2-1: Types of metal detectors

2.2 Review of Current Concealed Objects Detection Research

We will look concise for some research and previous study in this field that has been carried out in the past and present with their advantages and shortcomings:

2.2.1 Metallic Objects Detection by Using Gradiometer

This work is based on the principle of distortion in the Earth's magnetic field resulting from ferromagnetic objects such as a hand grenade, handgun, razor blade and wrist watch that are worn by people when passing through the portal see figure 2-2, or used for locating objects buried in the ground, for example landmines and water pipes see figure 2-3, also buried in the wall; for example pipe work and safes.. These types are used in detection systems which are called Gradiometer metal detectors [3] see figure2-2, the model contains two magnetometers connected by

Figure 2-2: Gradiometer for detection metallic objects [4].

Figure 2-3: Magnetic gradiometer system (Bartington Instruments).

electrical at differential mode to reduce the effects of background fluctuations that would otherwise make false alarms. The gradiometer already responds to changes in the magnetic field of the Earth from the moving ferromagnetic objects and based on

the magnitude of these interactions. The system can display the position of the metal object through transit of the portal. This technology was developed like those in the Idaho National Laboratory (INL), see Fig 2-2, which consists of 16 gradiometer located on two sides of the portal system; the data is collected from each gradiometer and the change in Earth's magnetic field is calculated. In this way an image can be generated which reveals the presence of metal objects being carried by the person [5,6].

In figure 2-3 an idea has been implemented by Bartington Instruments [7] which consists of two white cylinders that are the sensors that measure magnetic field strength allowing a computer on the front of the harness to compute the gradient of the Earth's magnetic field. The battery is mounted on the front under the computer. This device is rather heavy. Other advanced electromagnetic techniques, such as a magnetic real-time tracking vector gradiometer using high resolution fluxgate magnetometers has been developed for incorporation into an unmanned underwater vessel to improve mine detection. The unit comprises three primary three axis sensors and one three-axis receive sensor [8].

The gradiometer for metal detection is considered a passive system because it requires ferromagnetic objects; non-ferrous contraband objects such as explosives, electronic batteries and non-ferrous metals like gold, Copper, Lead and Aluminium cannot be detected. For this reason the system is not practical for most cases. Furthermore it is deleteriously affected by vibration or movement induced errors that can cause false alarm events. It may be possible to reduce the effects of motion and vibration using a three-axis accelerometer to measure the change in the position of magnetometer and therefore apply directed magnetic compensation for any vibration or movement, this would clearly increase the additional circuit complexity and cost of the system.

2.2.2 Inductive Magnetic Fields

This unit used to control and detection in open area and indoor to find the objects concealed at these areas, also used to detect hidden objects and contraband items in the bags or on individuals and buried objects as landmines. Each user has different security requirements, such as: airports, railway stations and courthouse security require preventing entry of firearms and metal objects that can be used to injure the people [9]. This technique uses active electromagnetic transmission to detect the metal objects, sees figures (2-4, 2-5). Two coils are used, one is a transmitter coil (source

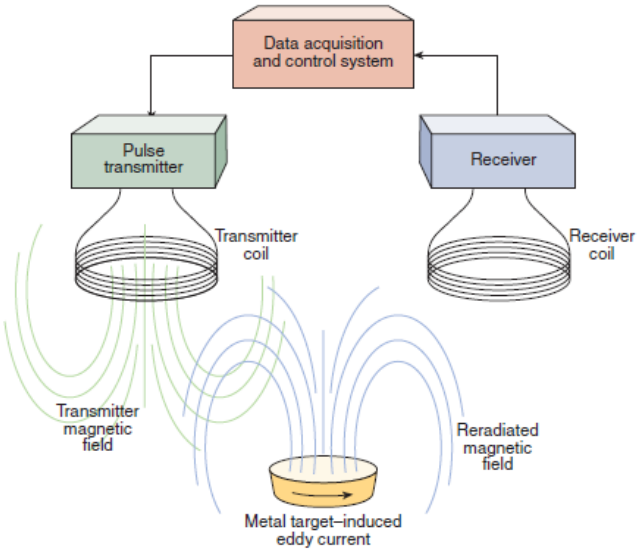

Figure 2-4: Principle of EMI technique for concealed metal detection [10].

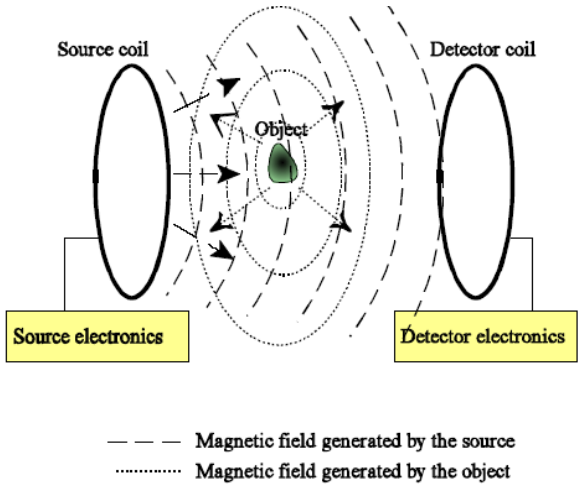

Figure 2-5: Metal detector with an object inside the detection space [2].

coil) and other is a receiver coil (detector coil). When current pulses with frequency content around (5 KHz to 5 MHz) [10,11] flow in the transmitter coil producing a time varying electromagnetic field around the coil that generates the primary magnetic field and induces an electromotive force in the metal object causing eddy currents to flow in the metal which generates the secondary magnetic field that can be sensed by receiver coil. In figure 2-4 the target is located under the coils as in the scenario for the detection of landmines. In figure 2-5 the target located between the coils as may be the case in a walk through portal. In both examples the technique is the same.

Wide Area Metal Detection [12,13] (WAMD) uses the method of pulse induction for generating a time varying electromagnetic and relies on the time constants of the induced eddy currents as a method of target identification. The sensors use a 3D steerable magnetic field sensor [14] to generate and measure 3D time decay responses of the magnetic field of the target see figure 2-6. WAMD works for any electrically conductive or magnetisable objects, making this method a versatile system to scan for prohibited objects. WAMD can also be used for screening in a crowded area, reducing the need to screen for each person to be screened separately and without invading individual privacy see figure 2-7.

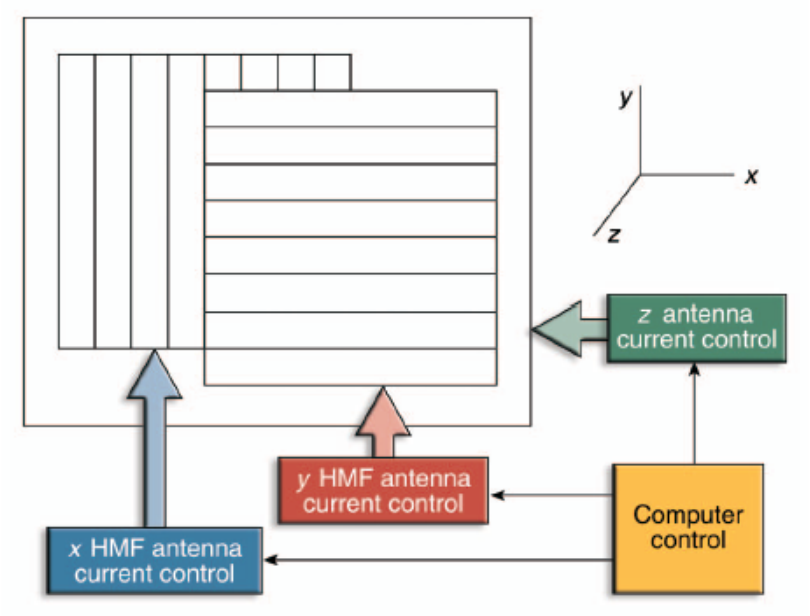

Figure 2-6: Diagram of a 3D steerable magnetic field sensor system [10].

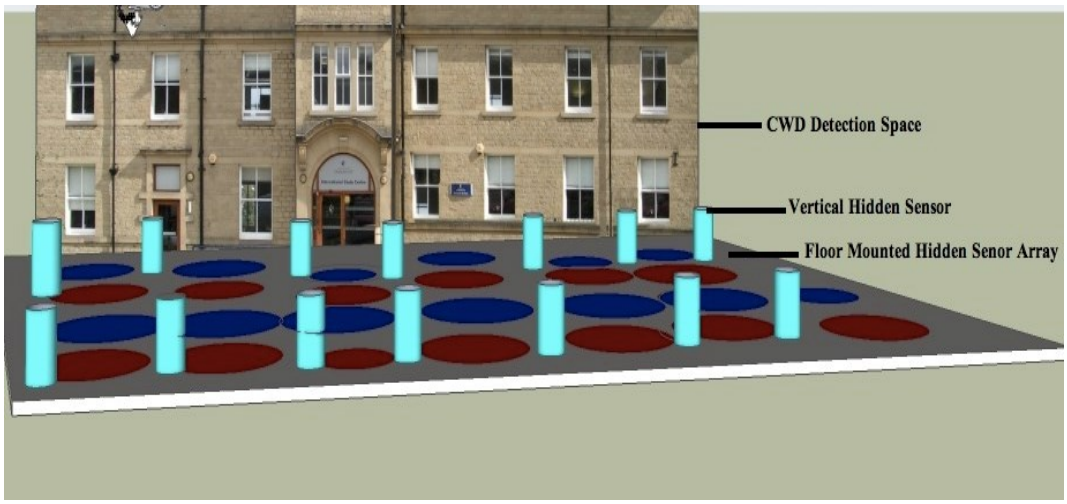

Figure 2-7: Wide Area Metal Detector (WAMD) sensor system concept [12].

There are many techniques developed by a number of researchers, such as those conducted at the University of Newcastle, using electromagnetic imaging techniques for the detection and classification of threat and non-threat objects [15].

The inductive magnetic field method is not complete and still suffers a clear deficit in the inability to detect low conductivity and non-conductivities materials and also metal objects which are small in size. This difficulty arises because the signal generated by the body is comparable to that generated by the small objects and then the object passes undetected.

2.2.3 Acoustic and Ultrasonic Detection

The emission of acoustic waves with ultrasonic frequencies (> 20 kHz) into materials, whether metallic or non-metallic, can be used to ascertain physical properties of concealed objects. However the effects are dependent upon the shape, orientation, size and hardness of material, also the diameter of the detector antenna, wavelength of the acoustic signal emitted power [16] and it is therefore not a reliable method for identifying objects concealed on the human body. The antenna size and wavelength affect the minimum size of objects that can be detected on the body or buried in the ground , for example landmines pipes or in investigation of both shallow and deep sub bottom layers [17]. The sonic wave reflects from boundaries between materials with different acoustical properties, and audio frequencies (low frequency) can be

penetrate clothing or rough surfaces to detect and show hidden objects [18], while ultrasonic detectors cannot penetrate thick clothing which makes it difficult to detect concealed objects under such scenarios [19].

There are some hand held weapon detectors that work by emitting acoustic waves and these systems generally function at ranges of 1m – 5m . JAYCOR advanced Technology Company have developed a system which is a combination of radar and ultrasound for producing ultrasound images and can operate at 5m-8m distance [19].

As shown in figure 2-8 [20,21] a nonlinear acoustic method (NAC) for CWD has been developed which uses two sets of transducers to produce two ultrasonic beams of differing frequencies, f1 and f2, to project sonic waves over long distances and onto a small spot on the person. The ultrasonic frequencies are converted from ultrasonic to audio frequencies by non-linear interactions which produce the frequencies f1, f2, f1-f1, f1+f2. The difference, or beat frequency, frequency (f1-f2) is chosen for detection and since the low frequency, i.e. audio frequency range, can penetrate clothing and interact with the subject to detect concealed objects. Parametric acoustic arrays can be used to produce nonlinear acoustic effects and the concealed objects detection is dependent on acoustic signatures [22,23].

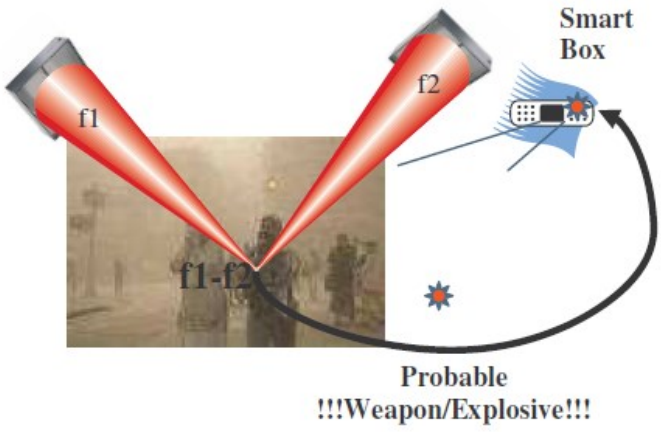

Figure 2-8: Crossed beam ultrasonic nonlinear acoustic generator for CWD [23].

This technique is sensitive to solid objects and doesn't inflict any harm on the body. Ultrasound can also be used for holographic imaging to detect the concealed objects [24], but some shortcomings are evident because there cannot be reliable differential or discrimination between threat serious items and contraband and also

between benign items. Thick, dense clothing such as leather causes high acoustic reflection and targets concealed under it are difficult to detect.

2.2.4 Target Recognition Using Electromagnetic Resonance

Metal object detectors are used as instruments to search for dangerous or nuisance metal objects that can be hidden in baggage, containers or on the body. These devices are in some cases based on electromagnetic resonance (EMR) which utilise radar with frequencies (200 MHz – 2 GHz). At these frequencies the Radar Cross Section (RCS) varies in a rapid and oscillatory manner with frequency as is seen in Mie scattering. The resonant response in the object is related to its physical size and composition but is crucially also independent of the object's orientation and is called a natural resonance frequency that can be used to characterize the object [25]. The Resonance based scattering exhibits some additional features that make it attractive for object identification programs as follows:

- The scattered is larger in the resonance region than it is below this region (Rayleigh region).
- The natural resonances are independent of the orientation of the object.
- The resonance patterns of object uniquely identify the object. .
- Several natural resonances can characterize an object over a large frequency band.

The RCS depends on the ratio of wavelength to an object's linear size [26] and the RCS scattering falls in three regions which are termed Rayleigh, resonance (Mie) and the optical region. The RCS of a sphere as function of its circumference, measured in wavelengths, and normalized to the geometric cross section of the sphere can be seen in figure 2-12. The resonance region of the sphere has many peaks that correspond to the natural resonances of the sphere. When the circumference is large compared to a wavelength, the oscillatory behaviour vanishes and the normalised RCS is now independent of frequency and equal to the physical cross section of the sphere.

The target space is illuminated with either a pulse or swept frequency source and the signal reflected by the objects in the target space provides an electromagnetic signature for the objects [2]. The objects' signatures are then compared to known signatures to determine whether or not these objects are present in the target

space [27]. This technique is considered safe and low power, hence suitable for human exposure, and also doesn't invade the privacy of individuals.

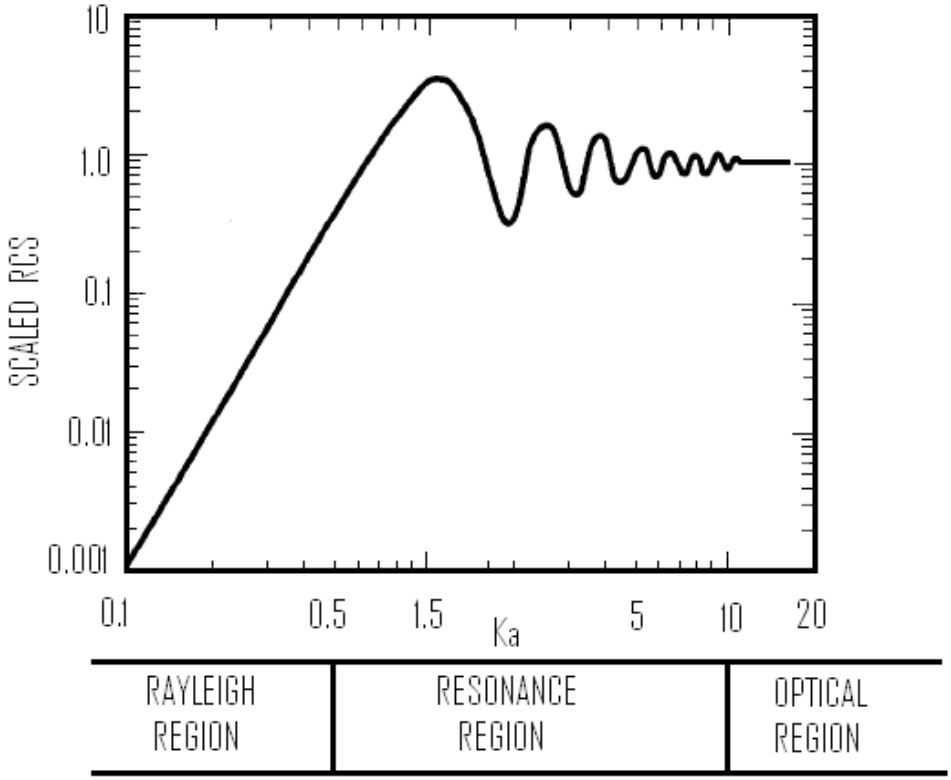

Figure 2-9: Radar Cross Section is enhanced in the resonance region [25].

In spite of, the EMR has good specifications of safety for human and can be penetrates to away range for detection the concealed or hidden objects. However, the EMR has some inabilities, as noise corresponding to the signature of people contaminates the return signal. The signatures of people are different from person to person; also the signature of person with any object such as weapon can be similar to another person without weapon, potentially leading to false alarm high rates [28].

2.2.5 Concealed Object Detection Using Millimetre Waves

Millimetre wave (MMW) imaging, offers the possibility for remote screening of persons for concealed metallic and non-metallic materials. Plastic explosives, drugs and other contraband concealed under layers of clothing can be seen in many circumstances when viewed in the millimetre-wave region of the electromagnetic

spectrum. For the detection of concealed objects, the system is based on three major factors: The apparatus is suitable in terms of over almost the entire millimetre-wave region. The MMW region does not present health risks and observations can be made remotely and with discretion as required. Active MMW systems emit very little radiation; the emitted power is some ten thousand times smaller than that emitted by a typical cell phone (the maximum rate (SAR) mobile standard for 2009 is 1.6 to 2 W/kg). MMW images are less physically revealing than x-ray images, and this technology eliminates the problems with the use of ionizing radiation, as with x-ray systems [29]. Millimetre waves can see through clothing and display the resulting image, with a reduced capability of revealing intimate anatomical details, also MMW systems have an enhanced standoff capability, when compared to x-ray imaging scanners and as such can be used to scan crowds and be used in public places. Furthermore, millimetre wave sensors measure the emission temperature through the black body radiation that is emitted and (in the case of active systems) reflected from the source that reflects from the target whether metallic such as weapons or grenades, or non-metal, plastic explosives, bottles and other boxes [30,31].

There are two types of MMW screening systems, namely active and passive sensors. Active sensors are by formed by generating and emitting signals that are focussed onto the objects/target in question, interact with them and where signals are reflected back to the sensor, because the self generated (emitted) signals have known properties and often signal processing is used to enhance very weak emitted target signals from noise sources, for example, when detecting landmines. For example, in the work of Bosqetal, a novel active hyperspectral MMW scanning system was developed to detect of buried landmines that used a vector network analyzer collecting the backscattered MMW radiation from any buried objects [32]. This method has demonstrated an ability to detect metallic object buried under 3 inches of dry soil [33]. The limitation of this method is that the emissions are usually weak.

Passive MMW sensors operating at 94 GHz and other wavelengths have been reported [34]. Here, a set of receivers are spatially scanned over a target that form an emissivity map, where objects concealed on the boy [35] show up because of differing contrast, see figure 2-10. At microwave and millimetre wave frequencies surfaces emit radiation that depends on parameters such as temperature and the amount of emissivity. Metal surfaces have are strong reflectors of RF that masks the natural

emissivity and which produce reflections from other sources in the scene, with the most significant being the sky. Figure 2-11 shows a passive MMW image formed from the temperature differences emitted from the target or reflected from the source. The output of the sensor is emissivity signals of objects in the MMW spectrum

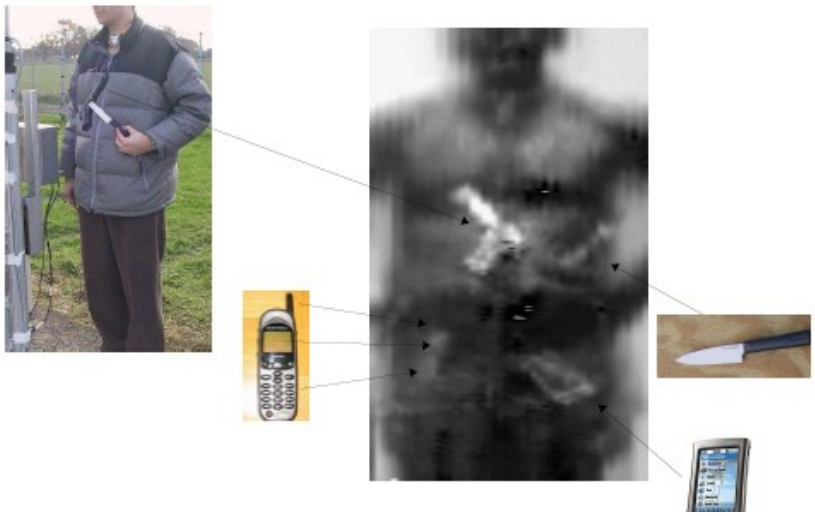

Figure 2-10: Images resolution of the MMW system using 94 GHz [35].

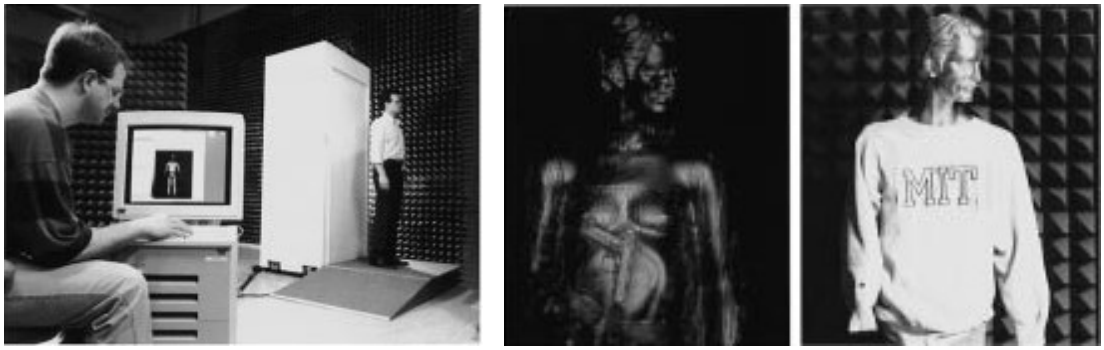

Figure 2-11: MMW images (imaging system) [36].

and measure with receiver [36]. The MMW sensors can be penetrated clothing to detect concealed metal objects due to low emissivity and high reflectivity of objects such as metallic gun [28]. An imaging sensor working at 220 GHz has been demonstrated for passive MMW imaging [37], which shows an acceptable image quality for detection of metallic and non-metallic objects. At this relatively short wavelength the MMW imaging is high resolution and clear for metallic and non-metallic objects, the penetration of clothing is reasonably good, so the objects can be visually detected. The detection ability of concealed objects is dependent on the

operating wavelength and the wavelength dependent on object properties (e.g. the type of material and the size of the object). This system is basically FM diffraction limited radar, with diffraction limiting the spatial resolution and consequent object recognition. Developments of millimetre-wave systems for several years have led to commercial MMW systems, mainly operating at 30 GHz, 94 GHz or 220 GHz, designed for a range of checkpoint and stand-off people screening applications and these are now beginning to become more widely used in this the field [38].

2.2.6 THz waves for concealed threat detection

Since the past several years, there has been an increased interest in the potential of the technology for non-destructive and non-intrusive detection of concealed, buried objects such as weapons, explosives, electronic cells, contraband also chemical, biological agents and related devices. There are two methods to generate THz based on optics and electronics. The optics method uses a single frequency far-infrared laser, where THz wavelengths are generated by the mixing of two laser frequencies in a photo conducting antenna, or using femto-second laser pulses (time domain spectra TDS). These types of source are still at laboratory stage kind is developing, see figure 2-12 [39-41]. The electronic method is by using electronic components, for example superconductor-insulator-superconductor (SIS), Schottky-burrier diode (SBD) hot electron bolometer HEB) mixer like heterodyne detectors [42]. There are three techniques for generating THz using an electronic method, harmonic multipliers, backward wave oscillators and quantum cascade lasers [43]. These types are now readily available and are replacing the laser mixing or pulsed laser approaches.

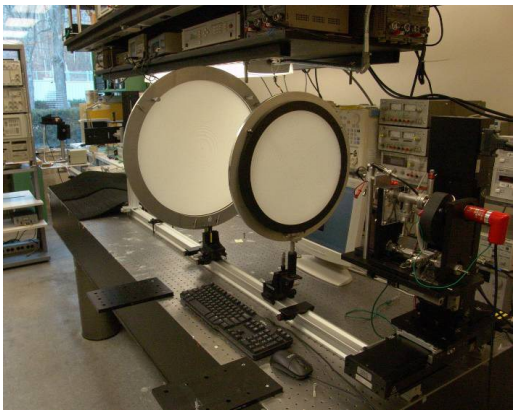

Figure 2-12: Illumination of Fresnel optics with THz source from 3m [39].

Terahertz radiation can penetrate most non-metallic materials such as thin layers of cloth, plastics and (partially), leather whereas metals completely block or reflect THz waves. Thus, this technology can be used in imaging detection systems suitable for the screening of personnel [44]. An example of sub-THz images taken at 640 GHz is shown in figure 2-13. Here, a range of items are shown in pairs pairs, with the visible image shown on the left and the 640 GHz image on the right.

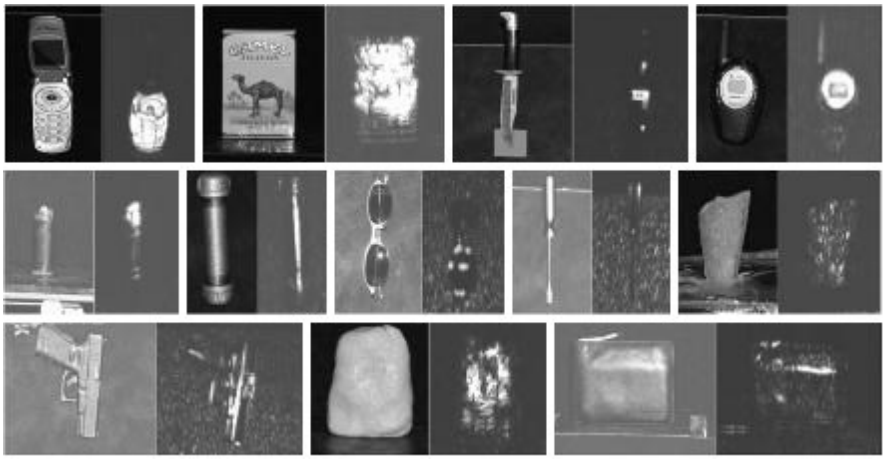

Figure 2-13: A range of threat and non-threat items imaged in the visible spectrum and at 640 GHz. The 640 Ghz image is on the right and and the visible image is shown on the left [45].

So, when an object is carried on the body, whether metal or non-metal will show up as an area of contrast on a THz image when compared to the body alone. The human body has a high liquid content that will absorb nearly all T-Rays, with the energy being harmless for the skin. Figure 2-14: shows an active THz image of a person carrying a handgun, with the clothing appearing partially invisible and with a reflection of the weapon, but the person's skin appears substantially dark [45].

There are some barrier materials that mask concealed threats, with every material having its own characteristic THz transmission spectra that must be taken into account. The detection of land mines using THz waves imaging has some unique considerations in terms of barrier materials, because the anti-personnel landmines are small items and contain minimal amounts of metal and ground penetrating radar systems, due to limited spatial resolution, cannot distinguish these small mines from rocks [46,47].

Figure 2-14: 640 GHz image (left) of a toy gun under shirt. Visible image (right) [45].

THz waves have advantages of high resolution, the availability of a wide THz spectrum and the use of a non-ionizing form of radiation to illuminate human body [48]. However there are some drawbacks: THz has a limited output power when using electronic methods of generation (e.g. harmonic multipliers) and they are affected by the atmosphere, with strong absorbance at high frequencies [49]. They are high cost, complex and require significant processing. Additionally, they require special power sources, the scanning rate is slow (typically between 0.5 and 8 frames per second) and the video output still poor. For the images shown here, the wavelength close the infrared wavelength at femto-second laser as radiation source [50].

2.2.7 Infrared Imaging

During the last couple of decades a considerable effort has been expended on developing methods of detecting metal and non-metal objects concealed on a person beneath clothing, in detecting contraband, devices or buried in the ground and walls, these methods have included the use of infrared imaging technology. This technology is primarily used for night vision applications and the principle of the theory is that the infrared radiation emitted by the human body is absorbed by clothing after that re-emitted. In figure 2-15 infrared radiation is used to show the image of a concealed weapon with two clothing types, both a thin cotton shirt and a medium weight jacket.

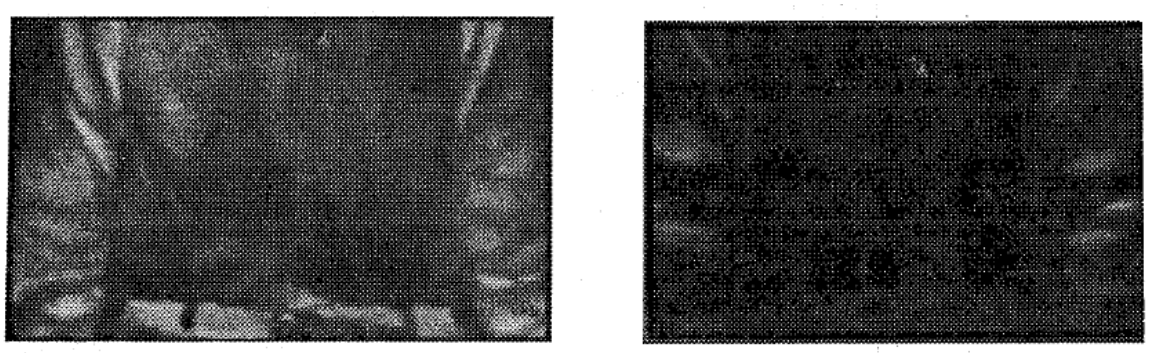

Figure 2-15: Image of weapon concealed beneath a thin cotton shirt (left) and a medium weight jacket (right) with mid wave (3-5 micron).

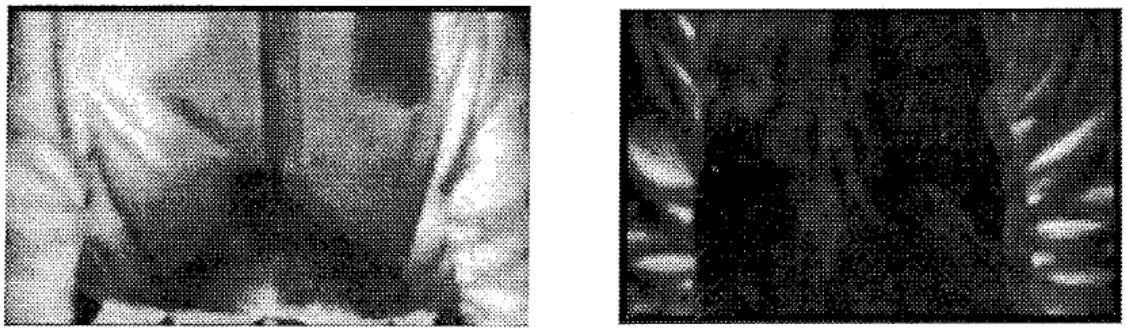

Figure 2-16: Image of weapon concealed beneath a thin cotton shirt (left) and a medium weight jacket (right) with long wave (8-12 micron).

In the case of a weapon concealed beneath cloth using a mid-wavelength infrared between (3-5 micron) the image of concealed weapon is partly clear. In figure 2-16, the wavelength has been lengthened to 8-12 micron consequently, the image of concealed weapon will be clearer as they should penetrate fabric better. Normally, in the cases of loose and thick clothing, the emitted infrared radiation will be diffused over a large area, which reduces the ability to detect hidden objects [51].

The infrared radiation (IR) is generally transmissible through the air, can penetrate through smoke and mist more readily than visible radiation. However, IR is affected by atmospheric conditions such as rain or fog. So, IR is attenuated by the processes of scattering and absorption, with IR and visible radiation exhibiting similar degrees of attenuation, with gaps caused by absorption of various molecules, as shown in

figure 2-17 [52]. IR can be used for detection of buried objects as the landmines and pipes. This study relied on the soil thermal diffusivity and meteorological parameter and the shape [53]. The difficulty in observing IR from concealed

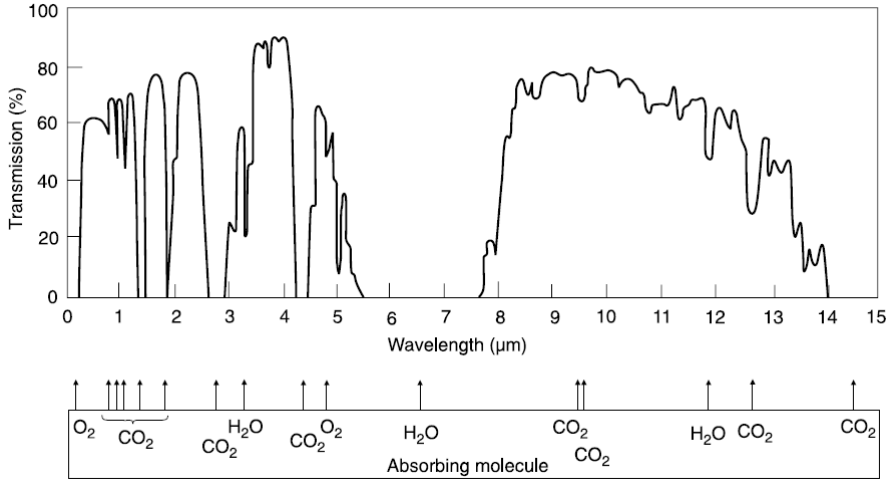

Figure 2-17: Transmission of visible and IR radiation through the atmosphere [51].

objects becomes worse as the object temperature approaches that of the body, which is likely to occur when the object is concealed on the body for a reasonable amount of time, because the maximum contrast on an IR image is strongly dependent on the temperature of the body and the object [54].

2.2.8 X-ray Imaging

The x-ray technology employed in these devices for detecting illicit hidden objects is of low energy and penetrates few millimetres into body. Variants of the technology are deployed for the inspection of items and baggage at security checkpoints in airports [55]. This technique of x-ray differs from devices used in the medical field. In the medical field, x-ray imaging relies on the absorption of incident x-rays for imaging, whereas the x-ray system of concealed object detection relies on the interaction of an x-ray photon with an electron bound to an atom and is called Compton scattering or the backscattering effect/phenomena in quantum mechanics [2]. This interaction occurs when an electron absorbs some of an x-ray's energy, whereas the absorbed energy is transferred to the kinetic energy that reduces the energy of the x-ray photon interacting with an electron, with the scattered x-ray photon used for imaging. X-ray imaging systems can provide high spatial resolution to identify concealed and hidden objects on the body, within cases and containers and

in the ground, also its ability to penetrate clothing is high and, as such, the technique can be usefully employed for the detection of metallic and non-metallic objects [56,57], consequently weapons, explosives, chemicals, drugs, biological agents, landmines and related devices can be found, see figure 2-18.

The x-ray system is sufficiently fast for high productivity applications, so within a few seconds can make scans of person with high precision.

Figure 2-18: Sample X-ray Images [55].

There are some shortcomings of using x-ray imaging, these x-ray systems emit low dosages, however, there may be safety concerns surrounding ionizing x-ray radiation and the United State Food and Drug Administration (USFDA) does not have an official position on the safety of these devices. In addition when an examination the person requires multiple scans, , furthermore it raises privacy issues.

2.3 Discussion

The literature survey has presented a limited study in the field of the detection of concealed and buried objects, using different methods that are either deployed or which are the subject of relevant research. The detection has to rely on the signal responses from object picked by the sensors. However, many technologies are currently employed for the detection of concealed objects. Many kinds of detection sensors are in the process of being developed or are currently deployed, together with many signal processing techniques which aim to improve the detection accuracy from both an academic and an industrial aspect, including using the Gradiometer, inductive the magnetic fields, acoustic and ultrasonic, millimetre waves, THz technology, infrared imaging, x-ray imaging and electromagnetic resonance. The outline is

illustrated in figure 2-19 to show EM spectrum used to detect the hidden objects by the techniques described here.

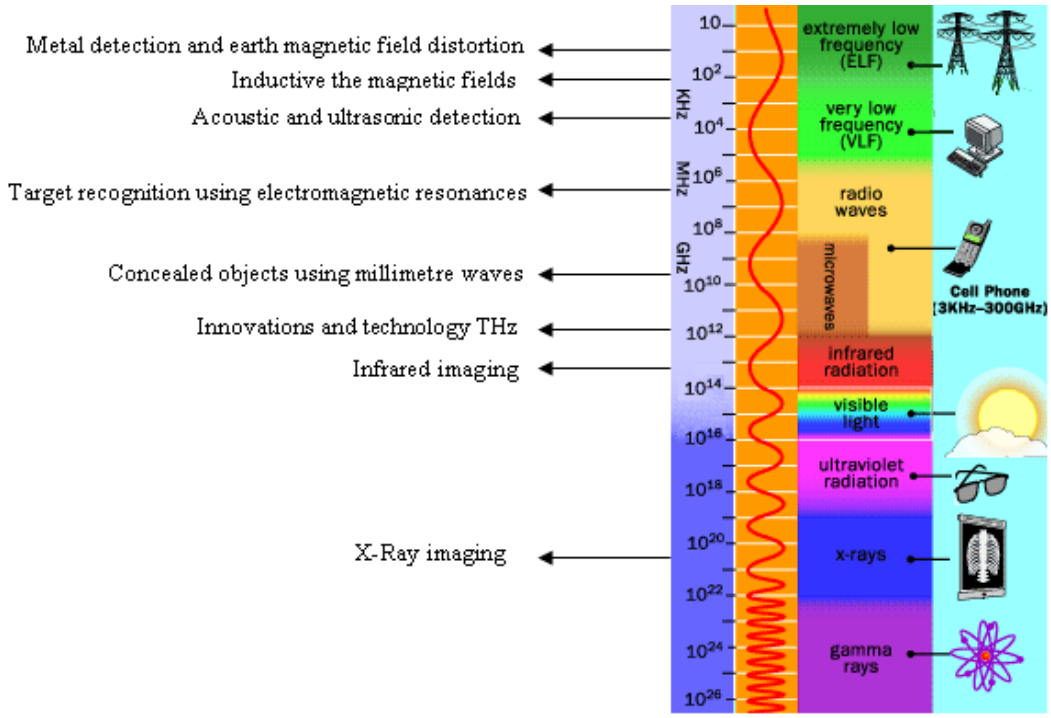

Figure 2-19: Electromagnetic spectrum and corresponding technologies.

The technologies described in this section form a summary of their lead purpose, their deficiencies in performance in terms of vulnerability to weather factors, lights and distance from the devices. Here they are summarised in terms of their performance and the following definitions indicate to knowledge threat or contraband hidden objects and ban it:

1. Detection: the discrimination process for targets of possible interest from their environs.
2. Identification: determination of threat or contraband.
3. Classification: determination of the contraband or threat's characteristics.

Table 2-1 briefly refer to the techniques used in terms of their response to items as well as its form and the energy used for interrogation at the detection distance, the portability of the devices and proximity at which they operate.

Table 2-1: The different techniques for detection concealed objects

No.	The Technique Devices	Signature	Distance	Portability
1.	The Gradiometer	Passive	Near	Transportable & Portable
2.	Inductive the magnetic fields	Active	Near	Transportable
3.	Acoustic & ultrasonic detection	Active	Far	Portable
4.	Electromagnetic resonances	Active	Far	Transportable
5.	Millimetre waves	Passive or Active	Far	Transportable & Portable
6.	THz technology	Active	Near	Transportable
7.	Infrared imaging	Passive	Far	Transportable
8.	X-ray imaging	Active	Near	Transportable

The Gradiometer is one device for the identification and detection of ferromagnetic objects only; it has high ability for penetration and it is harmless passive system. A challenge identified for Gradiometer is that it cannot detect non-ferromagnetic objects and the Gradiometer is dependent on the distortion of the earth's magnetic field, which changes from day to night; this affects the sensitivity of device. From a general review of papers, it can be assumed that the device is large, expensive and costly. As for the inductive magnetic field type systems (i.e. conventional metal detectors), these are active system with a high penetration ability, but metallic objects only can be detected and identified; also the technique requires a signature database to compare with a target. This technique has low sensitivity and small size metal materials typically remain undetected when carried on the body. With regard active acoustic technology, whether sonic or ultrasonic, these are harmless, but detect rigid objects, including metal or non-metal. Furthermore the technique suffers through a lack of penetration through many clothing types and it does not distinguish between threat and non-threat items. The electromagnetic resonance (EMR) is an active system safe for humans also it has penetration ability from a short distance to detect concealed items, whether they be metal or non-metal targets. However the EMR suffers from an inability to distinguish between threat or benign equipment and tools, because the technique requires a signature database for people which are different from person to person. Furthermore, EMR has a limited

ability to detect buried items in the ground such as landmines and distinguish between them and, cans or pipes which can cause false alarms. The MMW technique is commonly used for the detection of hidden objects or in the search for contraband and more is an appropriate technology for deployment at airport security gates, as well as in the detection and the search for buried land mines or pipe bombs. MMW systems, whether they be active or passive, are portable or transportable by vehicle or movable by hand. The MMW wave is not ionizing and consequently is harmless to the body and it has high penetration ability for most clothing types. In some cases it can detect both metallic and non-metallic objects. However, MMW detection is mostly based on an imaging technology approach, and usually requires complex automated image analysis software for object classification, making the system complex and costly. THz technology can be used for active imaging systems, has high resolution and detects metallic and non-metallic items. Such systems do, however, have some drawbacks: it isn't necessary capable of stand=off detection, is affected by the atmosphere and THZ can be absorbed by the atmosphere at low frequencies consequently the imaging quality produced is poor. Furthermore, the technology is very expensive, making multiple pixel imagers very difficult to achieve. Infrared imaging (IR) technology is a passive system and is known to be used at night to detect both metallic and non-metals hidden targets. However IR imaging has low penetration through all but very thin clothing and cannot differentiate objects at the same temperature, furthermore IR is affected by atmospheric factors (e.g. rain, fog). X-rays are active systems, with an ability to penetrate all clothing and baggage, and high resolution. Similarly they also can detect metals and non-metallic objects. The disadvantages are safety concerns for the body and a violation of privacy. The ability to detect concealed threats at standoff distances is severely restricted.

2.4 Summary

Through this study of techniques and technologies, old and modern, which has identified and briefly described a range of current detection methods, it can be concluded that more research and development is required to overcome gaps in the capability matrix. There is no technique that is fully capable of detecting hidden, buried and concealed objects, without drawbacks. Table 2.2 identifies the main capabilities of technologies that operate within the electromagnetic

spectrum Table 2-2: A summary of the techniques that have been described in this Chapter, with their respective capabilities and the characteristics:

Table 2-2: Main issues of the different techniques for detection concealed objects

No.	The Technique Devices	Penetrable	Objects	Disadvantage
1.	The Gradiometer	High	Ferromagnetic metallic targets	Non-ferromagnetic targets undetectable
2.	Inductive magnetic fields	High	Only metals	Location information is lacking & not enough sensitivity.
3.	Acoustic & ultrasonic detection	Medium	Hard objects	Penetration deficient & scanning deficient
4.	Electromagnetic resonances	High	Metals & others	High false alarms & needs a signature database.
5.	Millimetre waves	High	Metals & others	High cost & complex system
6.	THz technology	Medium	Metals & others	Lack of stand-off detection capability, can be absorbed & expensive
7.	Infrared imaging	Low	Metals & others	Low penetration, affected by the atmosphere and by temperature
8.	X-ray imaging	High	Metals & others	Safety concerns, & privacy violation. Lack of standoff capablility.

All of these variant technologies are used in the detection of hidden or buried objects, whether metal or non-metal, some of which presents an image and whereas others produce different signals that denotes existence of an item. For instance, x-ray imaging technology has the best results to show and detect concealed objects; it has a high penetrative ability, produces an exceptionally clear image, it is the most modern equipment suitable for the detection of hidden objects metals and others, but it has implications for the health of the body and its users, as well as privacy issues. Also

studied and presented here are EM spectra alone or by combination (EM induction, EM resonance and Gradiometer), which are complementary approaches to make an improved system capable of operation in more circumstances.

The research presented in this thesis outlines a method of detecting concealed objects using a variation of the commonly accepted method of Electromagnetic Pulse Induction (EMPI). The variation on this existing method allows for the detection and potential identification of multiple objects concealed in close proximity. The identification of the concealed object enables classification algorithms to provide information about it, for example if the object is considered as a threat or benign.

Chapter 3

Electromagnetic Induction concept

3.1 Introduction

The inductions of electromotive force by changing magnetic flux were first observed by Faraday and by Henry in early nineteenth century from their pioneering experiments have developed modern generators, transformers, etc. This chapter is primarily concerned with the mathematical formulation of the law of electromagnetic induction.

3.2 Maxwell's Equations

Maxwell brought together a unifying set of equations which relate all electromagnetic field quantities. These equations are usually written in vector notation as

$$\nabla \times \mathbf{H} = \mathbf{J} + \frac{\partial \mathbf{D}}{\partial t} \qquad (3.1)$$

$$\nabla \times \mathbf{E} = -\frac{\partial \mathbf{B}}{\partial t} \qquad (3.2)$$

$$\nabla . \mathbf{D} = \rho \qquad (3.3)$$

$$\nabla . \mathbf{B} = 0 \qquad (3.4)$$

where **J** (A/m^2) is the electric current density and **ρ** (C/m^2) is the surface charge density, **E** (V/m) is the electric field and **B** (T) is the magnetic induction, **H** (A/m) is the magnetic intensity, **D** (C/m^2) is the electric field displacement. Each of these equations represents a generalization of certain experimental observations:

- Equation 3.1 represents is a time varying extension to Ampere's law.

- Equation 3.2 is the differential form of Faraday's law of electromagnetic induction.

- Equation 3.3 is the Gauss's law for electricity, which in turn derives from Coulomb's law.

- Equation 3.4 is the Gauss's law for magnetism, usually said to represent the fact that single magnetic poles (monopoles) have never been observed, i.e. the net magnetic flux entering any volume is zero, consequently a magnetic flux line is continuous; there are no "sources" of magnetic flux.

The electromagnetic field is described by four field vectors; **E**, **B**, **D** and **H**. Then the relationship between them are required to solve the electromagnetic field equation, the electric displacement **D** is defined as

$$\mathbf{D} = \varepsilon_o \mathbf{E} + \mathbf{P} \qquad (3.5)$$

Where ε_0 is permittivity= $\varepsilon_o = 1/\mu_o c^2$, and equals ($8.5 \times 10^{-12}$ F/m). In the absence of dielectric material, the polarization **P**=0. For the following work, it will be assumed that all materials are non-polarisable, and thus the electric field and the electric displacement are directly proportional

$$\mathbf{D} = \varepsilon_o \mathbf{E} \qquad (3.6)$$

The magnetic intensity **H** is defined to be related to **B** through the intrinsic magnetization M is

$$\mathbf{H} = \frac{1}{\mu_o}\mathbf{B} - \mathbf{M(H)} \qquad (3.7)$$

This equation **M** is explicitly written as a function of **H**. The magnetization vector **M** is defined as the average magnetic moment per unit volume in the material or, equivalently, the magnetic dipole polarization per unit volume.

For a non-magnetic material, such as copper, there is no magnetization (**M**=0) and thus the magnetic intensity and the magnetic field density are related simply by

$$\mathbf{B} = \mu_O \mathbf{H} \qquad (3.8)$$

The functional relationship of the magnetization with the magnetic field, **M(H)** helps classify the three main classes of magnetic materials: diamagnetic, paramagnetic, and

ferromagnetic. The constitutive laws for the different magnetic materials are shown in figure 3-1. In diamagnetic and paramagnetic materials the magnetization **M** and has relationship with the magnetic intensity **H** and depend on the nature of magnetic material. In large class of materials there exists an approximately linear relationship between **M** and **H**, if the material is isotopic as well as linear.

$$M = \chi_m H \qquad (3.9)$$

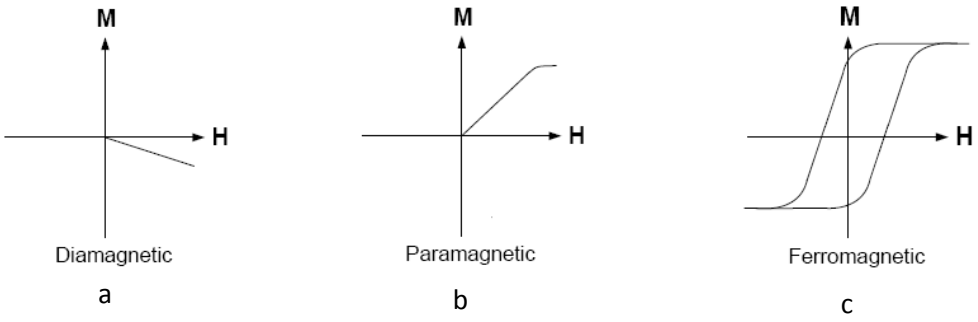

Figure 3-1: Different types of magnetic material: Diamagnetic (a), Paramagnetic (b) and ferromagnetic materials (c).

where χ_m is the magnetic susceptibility at figure 3-1(a,b) and the magnetic susceptibility of a diamagnetic material is negative [58-60] and the magnetic induction is weakened by the presence the material. The paramagnetic materials have positive susceptibilities and the magnetic induction is strengthened by the presence the material. In spite of χ_m is function of the temperature and sometimes varies quite drastically with temperature, it is generally safe to say that χ_m for paramagnetic and diamagnetic materials is quite small i.e ($\chi_m << 1$).

Metals derived from iron or steel are ferrous metals. In ferromagnetic materials it is more energetically favourable for the permanent magnetic moments throughout the material to be aligned. This is in contrast to a dipole interaction; it is not energetically favourable to have dipoles moments aligned. Throughout a ferromagnetic material there exist domains in which all moments are aligned. The orientation of

magnetization varies from domain to domain. When an external field is applied to the material, domain walls move such that regions that are magnetized opposite to the field are reduced in size.

3.3 Boundary Conditions

The boundary conditions that must be satisfied by the electric and magnetic fields at an interface between two media are deduced from Maxwell's equations exactly as in the static case. The boundary condition applied to the magnetic induction from the Maxwell's equation as equation 3.4 [61]. Maxwell's equations in differential form describe the field at points where the divergence and curl of the fields exist. These requirements thus exclude surfaces where Eand Hare discontinuous. Conditions on the field vectors at the surface are derived by using the integral form of Maxwell's equations. The derivation of boundary conditions can be found in numerous texts [62,63] and only the final results will be listed here. The normal component of the electrical field is a discontinuous function at an interface that separates regions of different conductivity and the normal component of magnetic flux density is a continuous at an interface that separates regions of different magnetic permeability.

$$\hat{\mathbf{n}}.(\mathbf{D}_1 - \mathbf{D}_2) = \frac{\rho}{\varepsilon_o}$$

$$\hat{\mathbf{n}}.(\mathbf{B}_1 - \mathbf{B}_2) = 0 \qquad (3.10)$$

where ρ is surface charge density. The tangential components of electric and magnetic fields are continuous functions.

$$\hat{\mathbf{n}} \times (\mathbf{E}_1 - \mathbf{E}_2) = 0$$

$$\hat{\mathbf{n}} \times (\mathbf{H}_1 - \mathbf{H}_2) = 0 \qquad (3.11)$$

3.4 Quasi-static Solution of Maxwell's Equations

When using Maxwell's equations, the displacement current term $\partial \mathbf{D}/\partial t$ in equation 3.1 will be omitted. To establish the validity of this assumption we can follow the steps [64]. The curl of equation 2.1 can be combined with equation 3.2 and Ohm's law $\mathbf{J} = \sigma \mathbf{E}$ to give a dimensionless equation in **E** alone.

$$\nabla \times H = J + \frac{\partial D}{\partial t} \tag{3.12}$$

$$\frac{\partial \mathbf{D}}{\partial t} = \varepsilon\, \varepsilon_0 / \sigma \mathbf{E} \tag{3.13}$$

And $\mathbf{E} = E_0 e^{i(k.r-\omega t)}$ (3.14)

Then the ratio is

$$\frac{\mathbf{J}}{\frac{\partial \mathbf{D}}{\partial \mathbf{t}}} >> 1 \tag{3.15}$$

when applied Ohm's law and equation (3.13), the equation (3.15) becomes

$$\left| \frac{\sigma}{i\, \omega\, \varepsilon\, \varepsilon_0} \right| >> 1 \tag{3.16}$$

Where $\omega = 2\pi/\tau$, $\varepsilon = 1$, $\varepsilon_0 = 8.85 \times 10^{-12}$ F/m, $\sigma \cong 10^6$ S/m, and

$$\tau = \frac{\sigma\, \mu_0\, a^2}{\pi^2}$$

where a=0.1 m, $\mu_0 = 4\pi \times 10^{-7}$ (H/m),

Then the ratio of the coefficients (equation 3.16) is 7.4×10^{13}.

3.5 Electromagnetic Induction

In 1824, Oersted discovered that current passing though a coil created a magnetic field capable of shifting a compass needle. After a few years, Faraday and Henry discovered just the opposite. They have noticed a changing magnetic field would induce current in closed circuit. This process of generating electrical current in a conductor by placing the conductor in a changing magnetic field is called electromagnetic induction or just induction. It is called induction because the current is said to be induced in the conductor by the magnetic field. Induction is measured in unit of Henries (H). When induction occurs in an electrical circuit and affects the flow of electricity it is called inductance. The inductance is divided into two types.

3.5.1 Self Inductance

Any electric circuit which produces a magnetic field and it carries current, if the current changes then the magnetic field will change and causing flux linkage with the circuit [65] see figure 3-2 (a,b).

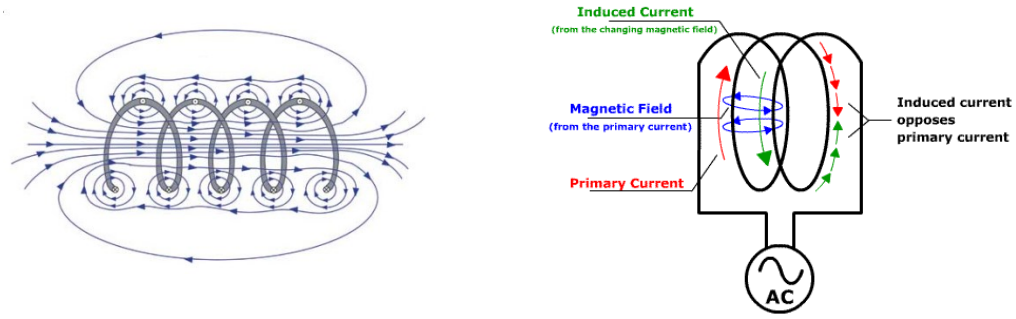

Figure 3-2: (a,b): Electromagnetic induction - self-inductance circuits.

Thus for a rigid stationary circuit the only changes in flux result from changes in the current. That is,

$$\frac{d\Phi}{dt} = \frac{d\Phi}{d\mathbf{I}}\frac{d\mathbf{I}}{dt} \qquad (3.17)$$

Then $(d\Phi/d\mathbf{I})$ is a constant, equal to $(\Phi/\mathbf{I})$ and called the incremental inductance. In any case, the inductance L is defined as

$$L = \frac{d\Phi}{d\mathbf{I}} \qquad (3.18)$$

and $$\mathcal{E} = -\frac{d\boldsymbol{\Phi}}{dt} \qquad (3.19)$$

from equations (3.17), (3.18) and (3.19) it follows that the expression for the induced electromotive force (emf)

$$\mathcal{E} = -L\frac{dI}{dt} \qquad (3.20)$$

where $\mathcal{E}$ the electromotive force.

As an illustration of the use of equation (3.18) for the calculation of inductance the self inductance of a solenoid coil will be calculated, such a coil is shown in figure (3-2)b. From Ampere's law the magnetic induction inside the Solenoid coil is

$$\mathbf{B} = \frac{\mu_o N \mathbf{I}}{l} \qquad (3.21)$$

where, N is number of turns, l the length and **I** the current in the coil. So the flux at each turn is

$$\Phi = \frac{\mu_o N^2 \mathbf{I} A}{l} \qquad (3.22)$$

The inductance is then simply:

$$L = \frac{d\Phi}{d\mathbf{I}} \frac{\mu_o N^2 A}{l} \qquad (3.23)$$

The (mks) unit of inductance is the Henry (H), A is the cross section area of coil.

3.5.2 Mutual Inductance

If one circuit induces current flow in a second nearby another circuit will produce mutual inductance show figure 3-3 (a,b).

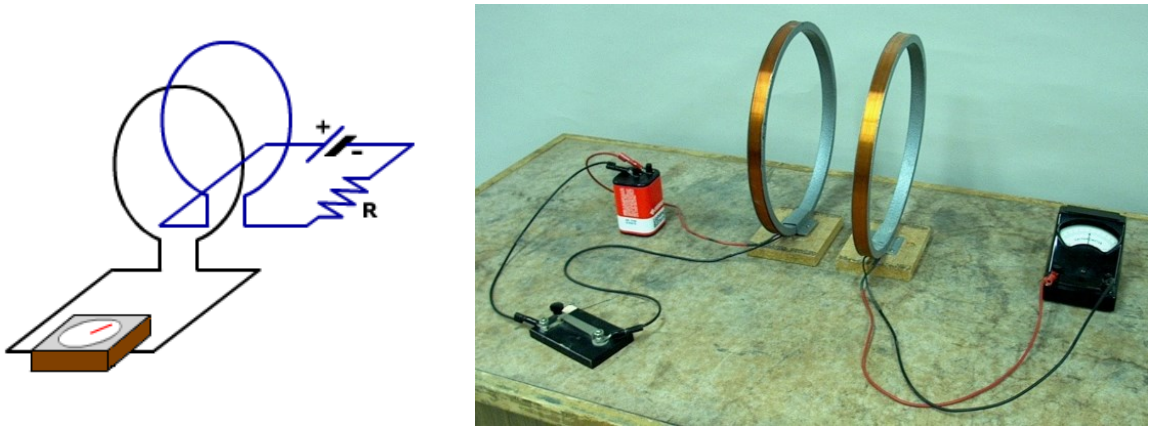

(a) **(b)**

Figure 3-3 (a,b): Electromagnetic induction - Mutual-inductance circuits.

This restriction can be lifted by assuming that there are n circuits, labelled 1,2,3,…n. The flux linking one of these circuits, say one labelled i, can be written

$$\Phi_{\mathbf{i}} = \Phi_{\mathbf{i}1} + \Phi_{\mathbf{i}2} + \Phi_{\mathbf{i}3} + \ldots\ldots\ldots\ldots\ldots\Phi_{\mathbf{in}} = \sum_{\mathbf{j}=1}^{\mathbf{n}} \Phi_{\mathbf{ij}} \qquad (3.24)$$

The emf induced in the circuit can then be written as

$$\mathcal{E} = -\frac{d\Phi_i}{dt} = -\left\{\frac{d\Phi_{i1}}{dt} + \ldots\ldots\ldots\ldots + \frac{d\Phi_{in}}{dt}\right\} = -\sum_{j=1}^{n} \frac{d\Phi_{ij}}{dt} \qquad (3.25)$$

If each of the circuit is a stationary circuit, the only changes in the flux is that the result from changes in the current, thus

$$\frac{d\Phi_{ij}}{dt} = \frac{d\Phi_{ij}}{d\mathbf{I}_j}\frac{d\mathbf{I}_j}{dt} \qquad (3.26)$$

The coefficients ($d\Phi_{ij}/d\mathbf{I}_j$) are constants, independent of the current.

The mutual inductance between circuit I and circuit j is defined by

$$M_{ij} = \frac{d\Phi_{ij}}{d\mathbf{I}_j}, \qquad i \neq j \qquad (3.27)$$

The (mks) unit of mutual inductance are the Henries (H).

To calculate the magnetic induction for this situation that produces from first winding

$$\mathbf{B} = \frac{\mu_o N_1 \mathbf{I}_1}{l} \qquad (3.28)$$

And consequently fluxes:

$$\left.\begin{aligned} \Phi_{11} &= \frac{\mu_o N_1^2 \mathbf{I}_1 A}{l} \\ \Phi_{21} &= \frac{\mu_o N_1 N_2 \mathbf{I}_1 A}{l} \end{aligned}\right\} \qquad (3.29)$$

From these fluxes the inductances can be became

$$L_1 = \frac{\mu_o N_1^2 A}{l} \tag{3.30}$$

$$L_1 = \frac{\mu_o N_1^2 A}{l} \tag{3.31}$$

From equation 3.18, then

$$M_{21} = \frac{\mu_o N_1 N_2 A}{l} \tag{3.32}$$

Reversing the procedure and considering a current from another winding is

$$L_2 = \frac{\mu_o N_2^2 A}{l} \tag{3.33}$$

$$M_{12} = \frac{\mu_o N_1 N_2 A}{l} \tag{3.34}$$

thus demonstrating that for this case $M_{12} = M_{21}$. Furthermore the equations (3.21), (3.22) and (3.23) may be combined to yield

$$M_{12} = \sqrt{L_1 L_2} \tag{3.35}$$

3.6 Skin Depth

In discussion steady currents we noted that the current density was uniform over the cross section of a cylindrical conductor show figure 3-4, if the source is oscillatory of some frequency, then the current is pushed toward the surface of the conductor [66].

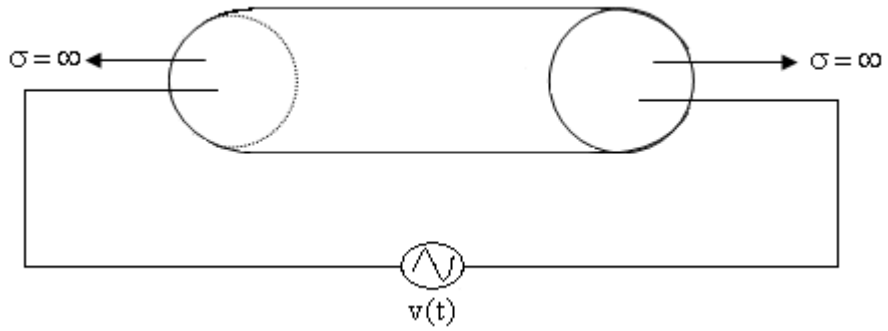

Figure 3-4: Types of metal detectors.

The eddy currents can only be carried between the outer surface and a level (layer) of the metallic material, this phenomenon called ***skin depth*** **(** δ **)**, and we simply state that calculated by

$$\delta = \frac{1}{\sqrt{\pi \mu_r \mu_0 \sigma f}} \qquad (3.36)$$

where f is the frequency, σ is the conductivity of metal material, μ_0 is magnetic permeability and. $\mu_r = 1$. The SI unit of skin depth is meter (m) [67].

The skin effect due to effective resistance of the metallic materials also the skin depth is low where high frequency and vice versa, i.e. the skin depth changes with frequency and causing varies in the electrical field distribution on the surface layer. Farther more the skin depth depends on the conductivity of the metal and vary according the used the conductivity [68].

3.7 Summary

This chapter provided a concise review the electromagnetic induction that relates with theoretical basic in this research and concept of the Maxwell's equations and their application and impact of this project. As well as to clarify aspects of the simulated models to obtain on the good results and to avoid errors related to this project.

Chapter 4

Simulation Program and Building the Model

4.1 Introduction

The most important concepts for pre-processing, analysis and post-processing of Opera-3d models are introduced. Building a geometry using the modeller, exploiting the symmetry to reduce the size of model to be solved and generating the finite element mesh are covered. Setting up the analysis by choosing appropriate material characteristics, solution type and a solver module are also discussed. Finally, the Post-Processor is used to obtain and present results from the analysis.

The simulation program is called Vector fields, version 13.0 - Opera-3d (an Operating environment for Electromagnetic Research and Analysis) is the pre and post-processing system for well known electromagnetic analysis programs including TOSCA, ELEKTRA, SCALA, CARMEN, SOPRANO, DEMAG, QUENCH and TEMPO.

Finite element discretization forms the basis of the methods used in these analysis programs. This widely applicable technique for the solution of partial differential equations requires special enhancements to make it applicable to electromagnetic field calculations. Access to these features is supported by the Opera-3d Geometric Modeller and pre-processor. These programs provide facilities for the creation of finite element models, specification of complicated conductor geometry, definition of material characteristics including, for example, nonlinear and anisotropic descriptions and graphical displays for examination of the data.

Similarly, the Opera-3d Post-Processor provides facilities necessary for calculating electromagnetic fields and displaying them as graphs and contour maps. The Opera-3d Post-Processor can also calculate and display many derived quantities and can plot charged particle trajectories through the calculated fields.

This work used the ELEKTRA Transient Mode to build the models simulate the interacyion of electromagnetic fields with objects.

4.2 ELEKTRA Transient Mode

ELEKTRA Transient (ELEKTRA/TR) analyses time dependent electromagnetic fields, including the effects of eddy currents, in three dimensions. There are three analysis options: the time variation can be transient (TR), steady state ac (SS) or eddy currents can be induced in moving conductors with a specified linear or rotational velocity in the presence of a static field (VL). VL can be applied to situations where the motion does not change the geometry, e.g. infinitely long rails or rotating disks.

4.3 Model Great

The Geometric Modeller provides facilities for creating models for use with the Opera-3d analysis modules and Post-Processor. The Modeller manipulates any defined objects through operations such as transformations and combinations. Basic objects (blocks, cylinders, spheres, cones, pyramids and solenoids) can be created at any position in space Special primitives can be defined in the Modeller to define standard conductor shapes. These include racetrack coils, solenoids and others see figure 4-1(a,b).

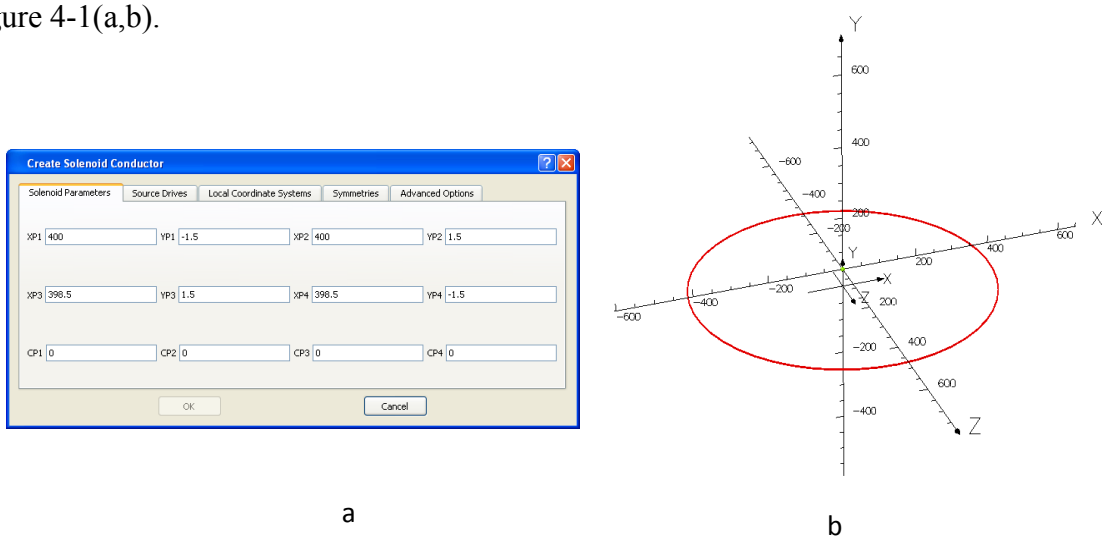

a b

Figure 4-1: (a) solenoid great with parameter, (b) Solenoid dimension.

4.4 Defining Material Properties

The permeability of the magnetic materials will be defined using a nonlinear characteristic curve. If the analysis is run linearly the initial slope of the curve will be

used. If the analysis is run nonlinearly the curve will be used to match the permeability of each element to the flux density. The materials will be treated as isotropic. Material properties are assigned to material labels defined for each cell in the model. In order for eddy currents to flow in the radiation shield electrical conductivity must be defined.

4.5 Boundary of Model

Boundary conditions are used in two ways. Firstly they can provide a way of reducing the size of the finite element representation of symmetrical models. Secondly they are used to approximate the magnetic field at large distances from the model (far-field boundaries). On individual far field surfaces a boundary condition is applied. Valid boundary conditions are either relevant field components or perfect insulator. Boundary condition BCRADIUS is associated with the curved surface of a cylinder or sphere see figures 4-2(a,b).

One of the NORMAL or TANGENTIAL field conditions or the radiation condition should be applied on all exterior boundaries and must be defined the sides of boundary.

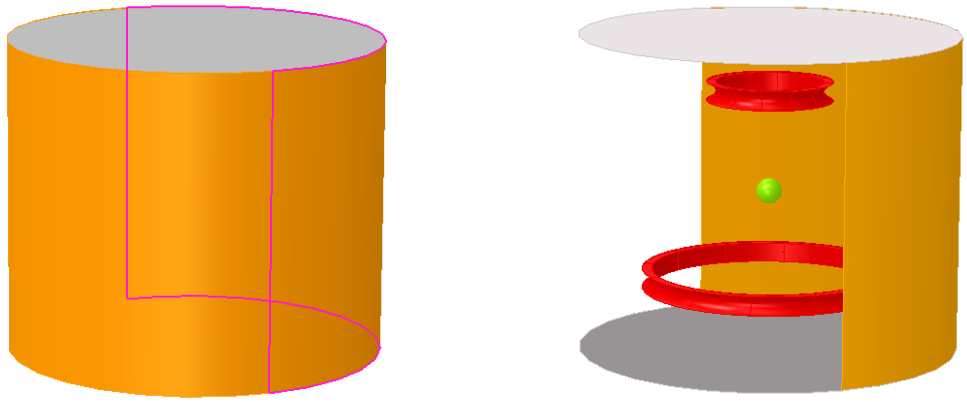

Figure 4-2: (a) Model boundary, (b) Cross section of model boundary.

The magnetic field must be determined in the free space that surrounds the magnet, and this must also be included as part of the model. In the real world, this space extends to infinity. In a finite element model though the free space region is

terminated at a finite distance from the region of interest, such that the termination does not significantly affect the accuracy.

4.6 Mesh Size

The final stage before creating a database and solving it is to create the model body and mesh the model. The mesh generation of the finite element mesh is performed in the Modeller and is a two stage process:

• Surfaces of models (cells) are initially meshed into triangles.

• Starting from the surface mesh, each cell is subdivided into a tetrahedral.

To prepare the model for meshing, the user must first execute the step model create model body. This selects all entities as bodies, and performs a Boolean Union, without regularisation. The result is one body with all cells retained.

4.7 Mesh Control

The element size can be controlled on vertices, edges, faces or cells within a model. This allows the mesh to be refined in areas of interest where high accuracy is required or where the field is changing rapidly. The element size can be controlled in several ways [69]

• The **Maximum element size** is the maximum side length of an element. As each cell is meshed it is high-lighted by its outline. Constructing the volume mesh takes a few minutes and results in a mesh with about 280,000 elements and about 50,000 nodes,. These numbers of elements and nodes depend on the design and structure of the model.

• The **Maximum angle between elements** defines the maximum angle between the normal to adjacent elements on a curved surface.

• The **Maximum deviation from surface** defines the maximum distance between the centroid of the planar surface element and the real curved surface it represents see figure 4-3(a,b,c).

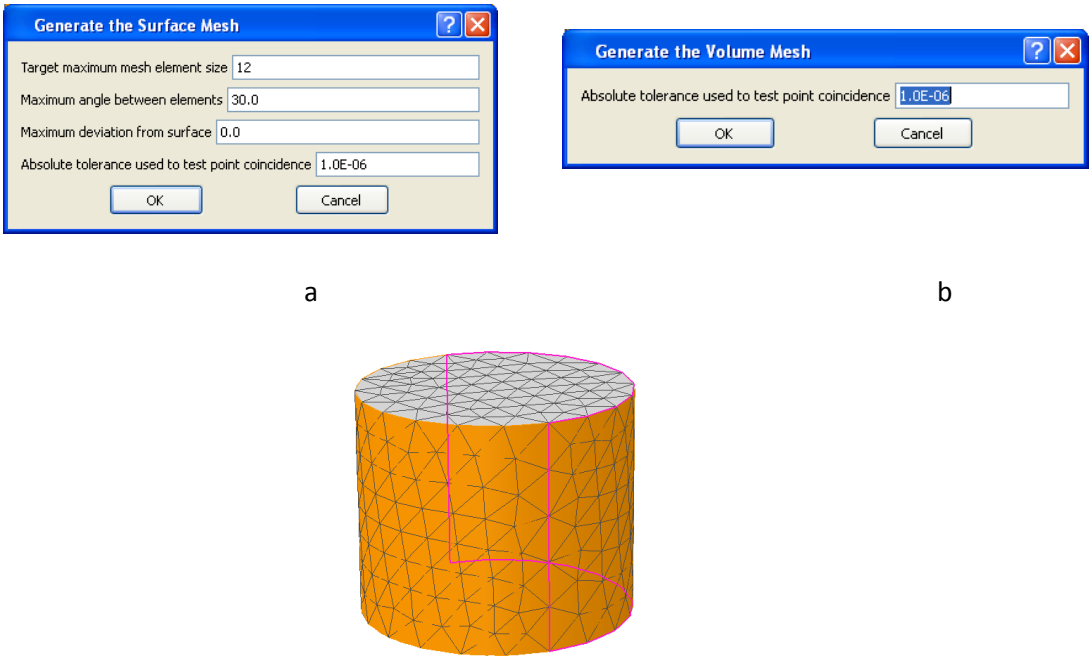

Figure 4-3: (a) Surface mesh parameter, (b) Volume mesh parameter, (c) Model meshing.

4.8 Skin Depth and Meshing

The electromagnetic skin effect is the penetration depth of the field inside conductive materials is dependent on the three parameters: electric conductivity, magnetic permeability and frequency.

The skin/surface meshing is controlled by two considerations, the penetration depth according to the perpendicular to the conductor, and the gradient of the state variable according to the tangent. The meshing on the surface is related to the type of element, and the skin meshing in boundary accurate check of the element sizes quadrangular mesh form anisotropy, automatic meshing based on spatial distribution of the mesh size. To fine layer elements, the material is modelled by its boundaries with boundary finite elements on which particular boundary condition are introduced.

4.9 Post Processing

When the analysis has finished, the model starts running the solver, the database is automatically activated and the results generated are stored. There are two ways in which the model can be saved to file, first the model geometry and information on materials and analysis settings can be saved in (an opc file) which can be read by

edited by the Modeller, second and analysis database (an op3 file) must be saved for ELEKTRA/TR to analyse.

This chapter presents the software and the simulation models used to investigate the electromagnetic induction using cylinders and spherical models of varying dimensions and materials including copper, titanium, aluminium, and stainless steel. In addition, a comparison between the theoretical and simulation results is presented.

4.10 Simulation Program and Building the Model

Numerical simulation is carried out using the commercially available finite element, time domain, electromagnetic solver software from *Vector Fields*. The first issue that is addressed in modelling of the various EMI scenarios is that of specifying the external magnetic field. This field should be spatially uniform over a sufficient volume that the modelled objects can be moved within this volume without unwanted effects from spatial magnetic field gradients across the objects. The effect of a spatially varying magnetic field across the object would be to introduce a degree of aspect dependence to the time constants and thus degrade the property of aspect independence upon which the method relies. A large, circular coil is suitable for the purpose of generating a spatially uniform field. The magnetic field is uniform over distances that are commensurate to typical concealed metallic objects such as weapon sizes (~20 cm) providing the coil is much larger than this size. Accordingly, a coil 4 metres in diameter was chosen as being suitable for this purpose and called transmitter coil that can transmit step pulse of current causing eddy currents to flow and excited in target metal object. The eddy currents scatter a signal that will be detected by a receiver coil. The receiver coil is 2 metres in diameter that receives the signal after being reflected from the object and take exponential form of decaying transient at the same time following sudden changes in the magnetic field. Yet not so large as to render computation time excessive on a standard PC. It should be stated that this choice of magnetic field source may very well be suboptimal when consideration is given to the design of a practicably deployable device. In this case, several smaller coils may be arranged to give a plane where the magnetic field is uniform or long parallel wires carrying current may instead be used to achieve uniformity of field in the desired sensing region.

In order to study the effect that varying object separation has on the ability to detect and discriminate objects within close proximity using EMI it is necessary to be able to alter the position of the various objects within the coil, without moving the object(s) into a region where there is significant magnetic field gradient see Figure 4-4.

A graph illustrating the calculated magnitude of magnetic field gradient, expressed as a percentage (i.e. % change per metre), from a 4 metre diameter coil as a function of distance from the coil centre and distance from the plane of the coil. The magnetic field strength is normalised by the axial field magnetic strength in the plane of the coil, evaluated at the coils centre.

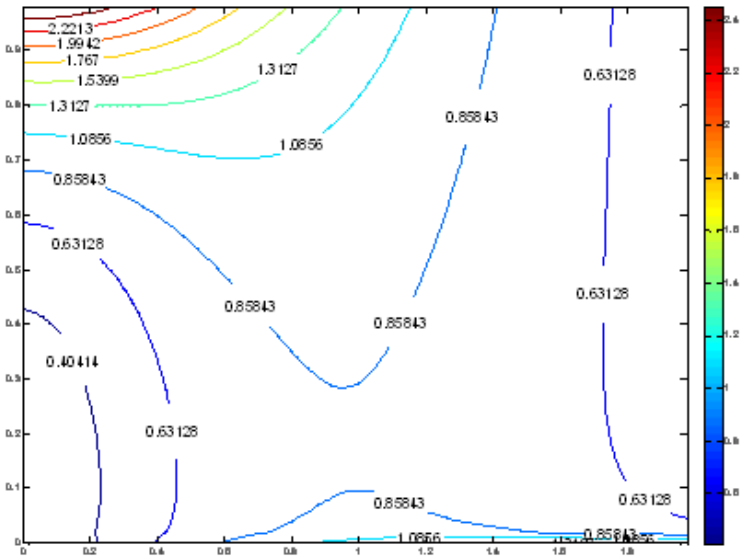

Figure 4-4: Variation of magnetic field gradient with distance from the centre of coil.

In fact the 4 metre diameter coil provides a very uniform magnetic field over a considerable region around the coil centre; see Figure 4-5. The axial and radial field components are normalised by to the axial component of the magnetic field, in plane and at the coil centre. The central region of the coil, extending one metre from the centre and one metre from the plane of the coil, has a normalised magnetic field gradient which is less than 2.5% per metre giving a maximum change of ~ 0.5% for a 20 cm sized object. This value is more than adequate for this EMI application; therefore we may move our objects within a ~3 m^3 cylindrical volume located at the centre of the coil without encountering problems.

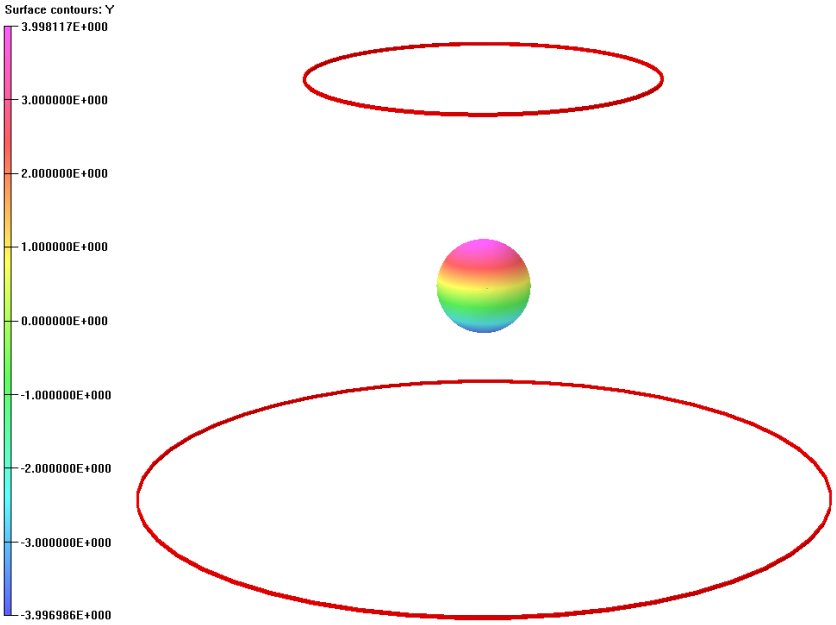

Figure 4-5: Simulation model – sphere between the transmitter coil and receiver coil.

The finite time domain solver creates a mesh (of finite elements) on which Maxwell's equations is solved, the mesh must have an element size which is sufficiently small to resolve the interaction of the electromagnetic fields within the conductor. The scale of the mesh size required can be judged by computing the skin depth of the metal conductors from which the objects are being modelled.

4.11 Electromagnetic Theory for targets Detection and Identification

There is published work in the field of EMI for a variety of uses, concealed metallic objects detection; ground penetrating radar for unexploded ordnance detection and mining. These applications rely on the same phenomena and share a common theoretical underpinning.

4.11.1 Time Constant for Sphere

In studying the electromagnetic induction for regular shape sphere in the three axes show figure 4-6 the expression for the vector potential outside sphere is [70-73]

$$A_{\phi}^{e} = 3K\, B_{0z}\, a^{3}\, R^{-2} \sin\theta \sum_{s=1}^{\infty} \frac{e^{-q_s t}}{[\kappa_s^{2}\, a^{2} + (K-1)(K+2)]} \qquad (4.1)$$

The quantities of equations are defined as follows:

$$q_s = \frac{\kappa_s^2}{\sigma \mu_0} = \frac{\pi^2 s^2}{\sigma \mu_0 a^2} \tag{4.2}$$

$$\kappa_s = \frac{\pi s}{a} \qquad \text{where, } s = 1,2,3,\ldots.. \tag{4.3}$$

$$K = \frac{\mu_1}{\mu_2} \tag{4.4}$$

''t'' is a time of initiation of the current step, and R is the radius in spherical coordinates.

$$\mathbf{B} = \nabla \times \mathbf{A}$$

$$\mathbf{E} = -\frac{\partial \mathbf{A}}{\partial \mathbf{t}} \tag{4.5}$$

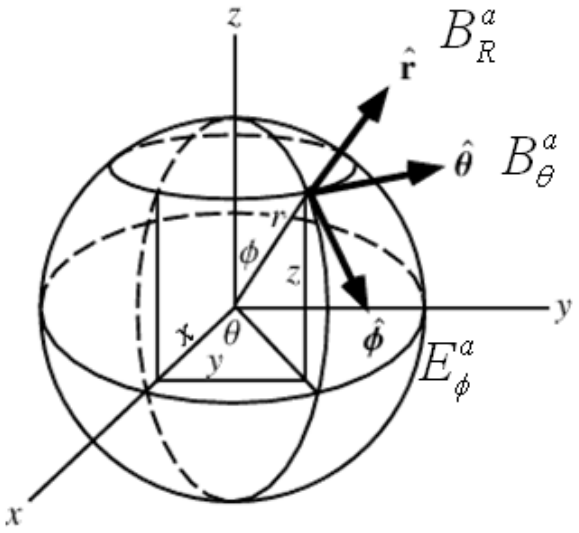

Figure 4-6: The magnetic fields caused by currents induced in the sphere.

By using quasi-static solution of Maxwell's equations, the primary magnetic field around the sphere increases by amount due to currents induced flowing through the sphere and after applied equation 4.5 over equation 4.1, and then can obtain the following expression for three axes of the fields:

$$E_\phi^e = 3K\, B_{0z}\, a^3\, R^{-2} \sin\theta \sum_{s=1}^{\infty} \frac{q_s\, e^{-q_s t}}{[\kappa_s^2\, a^2 + (K-1)(K+2)]} \tag{4.6}$$

and

$$B_R^e = \frac{6K\,B_{0z}\,a^3}{R^3}\cos\theta\sum_{s=1}^{\infty}\frac{e^{-q_s t}}{[\kappa_s^2\,a^2+(K-1)(K+2)]} \tag{4.7}$$

$$B_\theta^e = \frac{3K\,B_{0z}\,a^3}{R^3}\sin\theta\sum_{s=1}^{\infty}\frac{e^{-q_s t}}{[\kappa_s^2\,a^2+(K-1)(K+2)]} \tag{4.8}$$

where, $E_\phi^a, B_R^a, B_\theta^a$ are the only components of the anomalous fields caused by current induced in the sphere and expressed in spherical coordinate system centred on the sphere [74-76].

There are three different parts of time response of electromagnetic fields as follows:

- The early stage (early time).
- The intermediate stage (intermediate time).
- The late stage (late time).

Thus, during the early stage of time domain behaviour at ($t \approx 0$), the electromagnetic field is

$$B_R^e(t) = B_{oz}\frac{a^3}{R^3}\cos\theta[1-\frac{6}{\sqrt{\pi}}(\alpha t)^{1/2}] \tag{4.9}$$

$$B_\theta^e(t) = B_{oz}\frac{a^3}{2R^3}\sin\theta[1-\frac{6}{\sqrt{\pi}}(\alpha t)^{1/2}] \tag{4.10}$$

The early stage (early time response) behaviour persists over longer times. In particular in the case of a perfectly conducting sphere, induced currents are present only on the surface of the sphere at all time and, in theory they do not decay [77].

Next consider the behaviour at relatively large times, during the late stage of time domain field, the field is almost entirely determined by the exponentials

$$B_R^e = \frac{6\,B_{oz}}{\pi^2}\frac{a^3}{R^3}e^{-\pi\alpha t}\cos\theta \tag{4.11}$$

$$B_{\theta}^{e} = \frac{3\,B_{oz}}{\pi^2}\,\frac{a^3}{R^3}\,e^{-\pi\alpha t}\sin\theta \qquad (4.12)$$

$$B_{\phi}^{e} = \frac{3\,\alpha\,B_{oz}}{R^2}\,a^3\,e^{-\pi\alpha t}\sin\theta \qquad (4.13)$$

The late time is defined by inequality

$$t \geq \frac{1}{\pi^2\alpha} \qquad (4.14)$$

Then, the late time for transient field will be observed and the components of the electromagnetic field and can be written as

$$B_{R}^{e} = \frac{6\,B_{oz}}{\pi^2}\,\frac{a^3}{R^3}\,\cos\theta\;e^{-t/\tau_0} \qquad (4.15)$$

$$B_{\theta}^{e} = \frac{3\,B_{oz}}{\pi^2}\,\frac{a^3}{R^3}\,\sin\theta\;e^{-t/\tau_0} \qquad (4.16)$$

$$B_{\phi}^{e} = \frac{3\,\alpha\,B_{oz}}{\tau_0\,\pi^2}\,\frac{a^3}{R^2}\,\sin\theta\;e^{-t/\tau_0} \qquad (4.17)$$

The parameter $\frac{1}{\pi^2\alpha}$ is called the time constant τ_0 for the spherical conductor, and

$\alpha = \frac{1}{\sigma\,\mu_0\,a^2}$,, hence

$$\tau_0 = \frac{1}{\pi^2\alpha} = \frac{\sigma\,\mu_0\,a^2}{\pi^2} \qquad (4.18)$$

where, μ_0 is absolute permeability of free space and equals ($4\pi \times 10^{-7}$ H/m), σ is conductivity and a is radius of sphere.

The equation (4.18) is important for determine the time constant theoretically for the sphere and already applied in these results.

4.11.2 Mesh size calculation for Models

The maximum mesh size required is $\frac{\lambda}{\gamma}, \frac{\delta}{\gamma}$, where γ might typically be 10 (i.e. 10 is target maximum mesh element size at generate surface mesh in the model). The

electromagnetic frequency can be well estimated by taking the reciprocal of the fundamental time constant for a sphere, also with Equation (3.36), where $\mu_r = 1$. Substituting this into Equation (4.18) gives the expression and the typical frequency constant of decaying electromagnetic field:

$$f = \frac{1}{\tau_0} = \frac{\pi^2}{\mu_0 \sigma a^2} \tag{4.19}$$

and topical λ of decaying in the vacuum:

$$\lambda - \frac{c}{f} = \frac{c \mu_0 \sigma a^2}{\pi^2} \tag{4.20}$$

then the topical skin depth in object is:

$$\delta = \frac{a}{\pi^{3/2}} \tag{4.21}$$

For example the typical object in (a = 0.1 m) and conductivity ($\sigma = 10^6 - 10^7 \, S.m^{-1}$) the skin depth can be calculated from equation (4.21) as

$$\delta = \frac{0.1}{\pi^{3/2}} = 1.8 \text{ cm}$$

4.11.3 Time Constant for Cylinder

To study the electromagnetic induction for regular shape solid cylinder in the three axes show figure 4-7 the equation of the vector potential is:

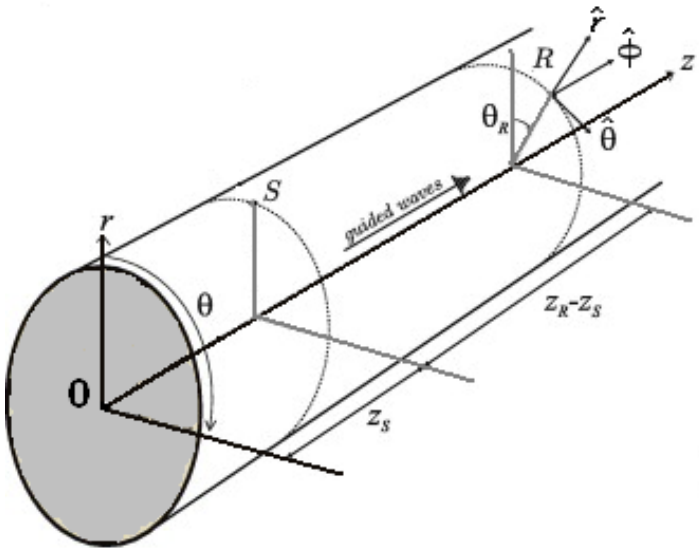

Figure 4-7: The magnetic fields caused by currents induced in the cylinder.

For using quasi-static solution of Maxwell's equations, the magnetic field flows through the cylinder and produces the eddy currents around the cylinder, the step response function in time domain is [78]

$$s(t) = 2\pi a^3 \left\{ 2\frac{(\mu_r - 1)}{(\mu_r + 2)} - \sum_{\alpha=1}^{\infty} \frac{6\mu_r e^{S_\alpha t}}{(\mu_r + 2)(\mu_r - 1) + (\alpha\pi + \beta_\alpha)^2} u(t) \right\} \qquad (4.22)$$

In terms of the positive real decay time constants

$$\tau_\alpha = -\frac{1}{S_\alpha} \qquad (4.23)$$

and the roots of the transcendental equation given the time constants:

$$\tau_\alpha = \frac{a^2 \mu_0 \sigma}{(\alpha\pi + \beta_\alpha)^2} \qquad (4.24)$$

the magnetic polarizability is derived

$$M(t) = 2\pi a^3 \left\{ -\partial(t) + \sum_{\alpha=1}^{\infty} \frac{6\mu_r e^{-t/\tau_\alpha}}{(\mu_r + 2)(\mu_r - 1) + \mu_0 \sigma a^2} u(t) \right\} \qquad (4.25)$$

where $\partial(t)$ is dirac delta function and $u(t)$ is step function, and by a Fourier or Laplace transform could be taken to give the relative permeability of the shape as function of frequency to find the roots. These roots would give the magnetic polarizability in frequency domain, then the equation becomes [78]:

$$s(t) = -50\, a^3 \sum_{n=1}^{\infty} \frac{e^{-t/\tau_0}}{n^2 \pi^2}\, u(t) \qquad (4.26)$$

with

$$\tau_0 = \frac{\sigma \mu_0 a h}{18} \qquad (4.27)$$

where, h is height of cylinder. The equation (4.27) is time constant for solid cylinder.

4.11.4 Time Constant of Simulation Models

The time constant can also be determined from the models by using simulation program for any metallic objects. The time domain dependence of the induced voltage on the secondary of the receiver coil can be expressed [79-81] as

$$V(t) = \delta(t) - \sum_n A_n \exp\left(-\frac{t}{\tau_n}\right) \tag{4.28}$$

where A_n and τ_n are the amplitudes and time constants respectively, of the n^{th} eddy current mode circulating in the object. In general, an analytic solution giving the values of A_n and τ_n is not possible for all, but a few very simple cases where symmetry allows for an analytical expression. A conducting sphere is one such case [82,83]. For a sphere of radius R; conductivity σ and relative permeability μ_r, the time constants τ_n are given by

$$\tau_n = \frac{\mu_r \mu_0 \sigma R^2}{\chi_n^2} \tag{4.29}$$

where χ_n are the solutions of the equation

$$\tan(\chi_n) = \frac{(\mu - 1)\chi_n}{\mu - 1 + \chi_n^2} \tag{4.30}$$

The time dependence given by Equation (4.23) simplifies further for times which are long, when compared to the time constants of the higher ($n \geq 2$) order modes. In this late time regime, after the excitation pulse or the switching off of the current in the primary coil that provides the spatially uniform magnetic field, the voltage induced in the secondary coil is simply

$$V(t) \approx A \exp\left(-\frac{t}{\tau_1}\right) \tag{4.31}$$

Thus we may identify an object by its aspect independent, fundamental time constant which is dependent only upon the shape, size and material that form the object.

When M multiple objects are present within the magnetic field the detected signal, again for times which are long compared to high order modes, will simply be the superposition of the signals for the objects individually,

$$V(t) \approx \sum_{n=1}^{M} A_n \exp\left(-\frac{t}{\tau_0}\right) \qquad (4.32)$$

And equation (4.32) can be written

$$V(t) \approx \sum_{n=1}^{M} A_n \exp(-bt) \qquad (4.33)$$

Where $b = \frac{1}{\tau_0}$, i.e b is the quantity that obtained from fitting curve by MATLAB.

The results obtained are processed with MATLAB program (non-linear fitting algorithms) for calculation the time constant, and the fitting curve applied to sphere is shown in figure 4-8 and an exponential decay curve appears as straight line with slop being the time constant. The slop of line (time constant) is extracted by curve fitting of transformed data.

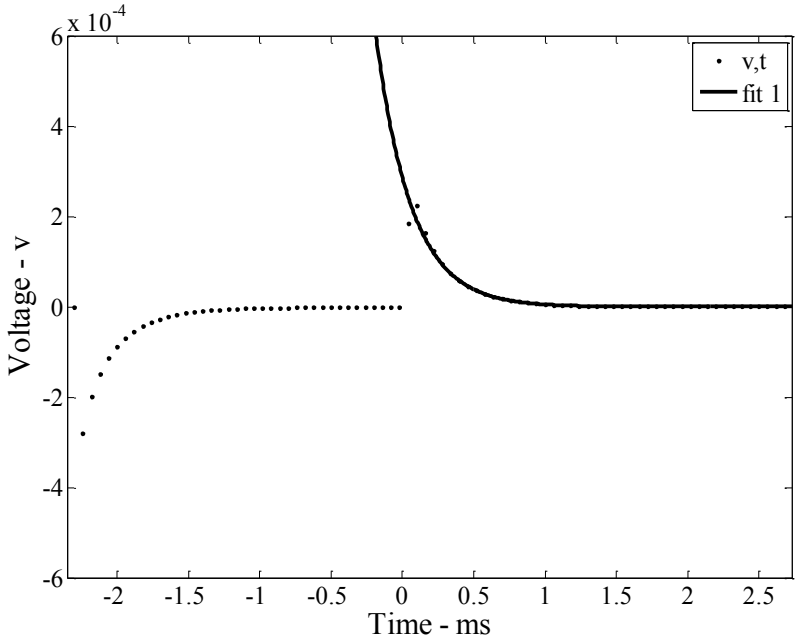

Figure 4-8: Curve fitting of time constant for sphere.

4.12 Determination Time Constant of Sphere

In this section calculate time constant for sphere theoretically and from the simulation models shows table 4-1 below. The expression shows the potential of using the time constant in identifying a many spheres for different radii and many materials (Stainless steel, Titanium, Aluminium and Copper). All spheres of different materials and the same radii will be characterised by a scattered electromagnetic field and time constant will be different. Thus the spheres can be classified, at least within the precision with which the time constant of the decaying magnetic field can be determined.

Table 4-1: Equation of time constant of sphere (modeling and theoretically)

Time constant from Simulation τ_0 (s)	**Time constant from Theoretical equation** τ_0 (s)
$\mathbf{V(t)} = A_n \exp(-\frac{t}{\tau_0})$	$\tau_0 = \frac{\sigma \mu_0 a^2}{\pi^2}$

4.12.1 Time Constant for Stainless steel Sphere

Numerical simulation is carried out using the commercially available finite element, time domain. A large, circular coil is suitable for the purpose of generating a spatially uniform field over distances that are commensurate to all sizes and shapes.

The model was validated by simulation of stainless steel spheres of conductivity 1.1×10^6 $S.m^{-1}$ and of different radii. The fundamental time constants from the simulations were compared to theoretical equation and the simulated results agree well with theory, see Table 4-2, and time decays are appeared clearly in the figure 4-9

Table 4-2: Stainless steel spheres for many radii

Material	Radius	$\tau_{Simulation}$ (ms)	$\tau_{Theoretical}$ (ms)
Stainless Steel	3.0 cm	0.1212	0.1260
	4.0 cm	0.2212	0.2241
	5.0 cm	0.3502	0.3501
	6.0 cm	0.5068	0.5042

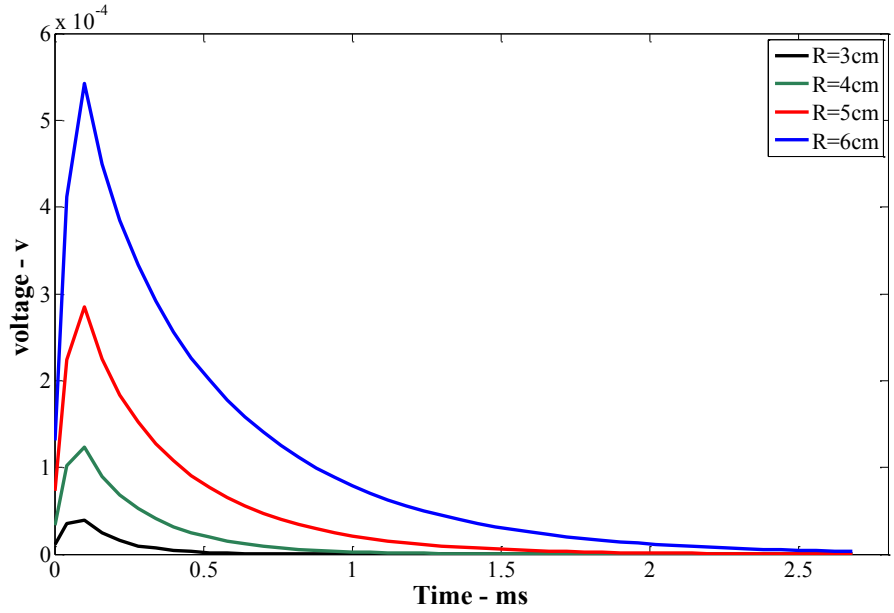

Figure 4-9: Time constant for different radii of stainless steel spheres.

4.12.2 Time Constant for Titanium Sphere

Variations of the simulation and theoretical time constants for titanium spheres of conductivity 1.67×10^{6} $S.m^{-1}$ of different radii are shown in Table 4-3. The decaying time responses of the same spheres are plotted in Figure 4-10.

Table 4-3: Titanium spheres for different radii

Material	Radius	$\tau_{Simulation}$ (ms)	$\tau_{Theoretical}$ (ms)
Titanium	3.0 cm	0.1955	0.1913
	4.0 cm	0.3405	0.3402
	5.0 cm	0.5310	0.5315
	6.0 cm	0.7619	0.7654

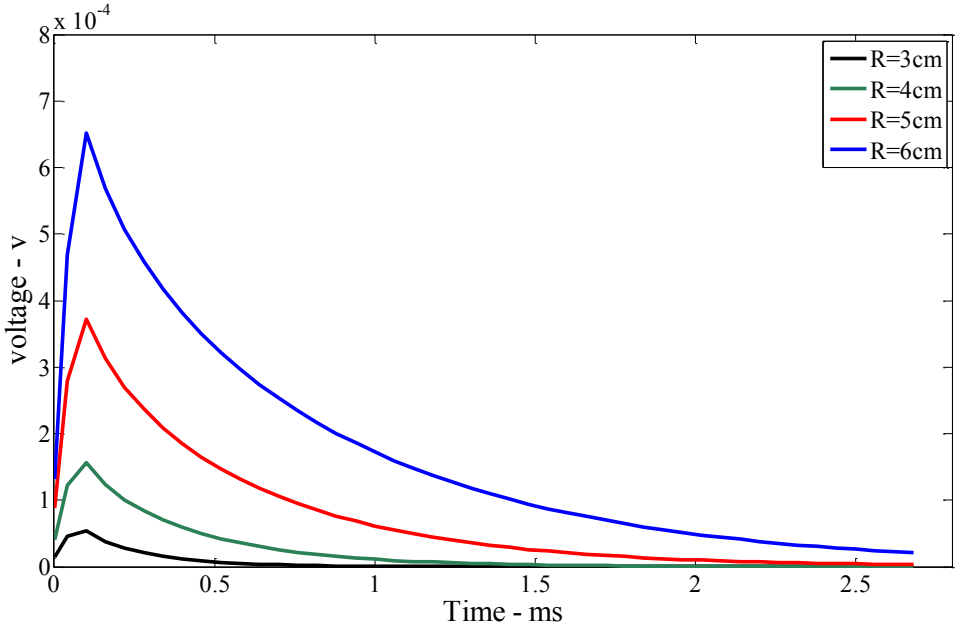

Figure 4-10: Time constant for different radii of titanium spheres.

4.12.3 Time Constant for Aluminium Sphere

Comparison of theoretical and simulation values of the time constants for three Aluminium spheres conductivity 3.38×10^{7} $S.m^{-1}$ with different radii is given in Table 4-4 whilst the decaying time responses are shown in Figure 4-11.

Table 4-4: Aluminium spheres with different radii

Material	Radius	$\tau_{Simulation}$ (ms)	$\tau_{Theoretical}$ (ms)
Aluminium	3.0 cm	4.228	4.4
	4.0 cm	7.707	7.7
	5.0 cm	12.19	12.1

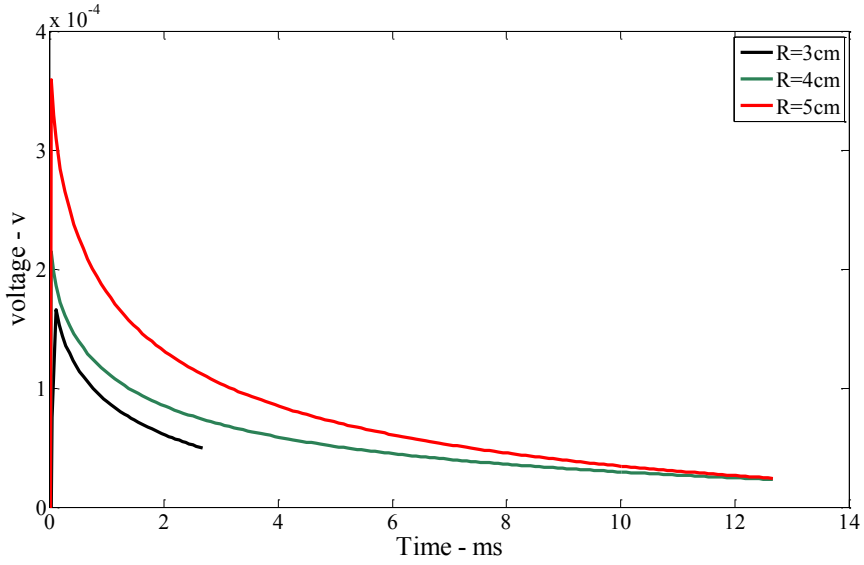

Figure 4-11: Time constant for different radii of aluminium spheres.

4.12.4 Time Constant for Copper Sphere

The conductivity of the Copper sphere is 5.8×10^{7} $S.m^{-1}$ considered somehow large compared to that of Aluminium, Titanium or Stainless steel. The time decays are longer see figure 4-12.

Table 4-5; Copper spheres for two radii

Material	Radius	$\tau_{Simulation}$ (ms)	$\tau_{Theoretical}$ (ms)
Copper	3.0 cm	6.68	6.6
	4.0 cm	11.82	11.6

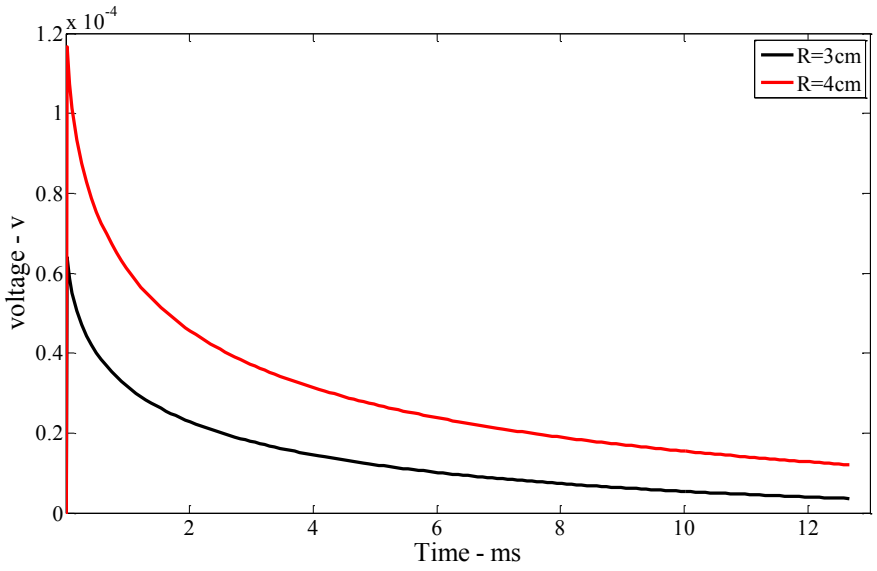

Figure 4-12: Time constant for different radii of copper spheres.

4.12.5 Time Constant for Two Spheres Together

The influence of the separation of two stainless steel spheres radii (4 cm and 6 cm) was simulated at varying separations figure 4-13. The separation indicated between objects is for their closest surfaces and there is no electrical contact for the zero separation case see table 4-6. Both fundamental time constants where accurately recovered irrespective of the separation between the two spheres. This important as it suggests that multiple spheres can be detected and identified by means of their time constants even when they are positioned close together. The radius of sphere one (R=4cm) and the radius of sphere two (R=6cm), Table 4-6.

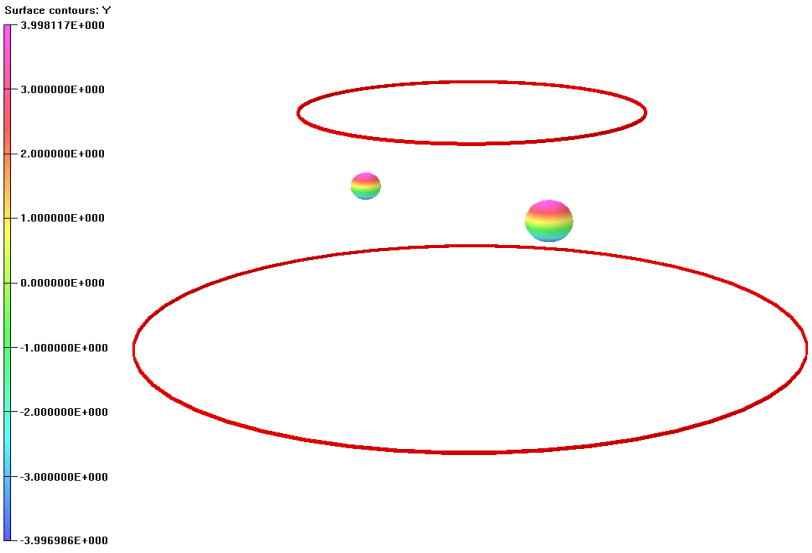

Figure 4-13: Model of two stainless steel sphere (R=4cm and R=6cm).

Table 4-6: Two stainless steel spheres (R=4cm and R=6cm) together

Material	Target	Distance between two spheres	Time constant for sphere 1 0.2212 (ms)	Time constant for sphere 2 0.5068 (ms)
Stainless Steel	Sph.1 & Sph.2	100 cm	0.2208	0.5257
	Sph.1 & Sph.2	50 cm	0.2149	0.5288
	Sph.1 & Sph.2	25 cm	0.2202	0.5268
	Sph.1 & Sph.2	0.2 cm	0.2225	0.5260
	Sph.1 & Sph.2	0.0	0.2218	0.5274

4.13 Determination Time Constant for Cylinder

In this section the cylindrical models of various sizes (radii and length) and materials are studied. The cylinder shapes are a solid cylinder positioned between two coils see figure 4-14. The materials are stainless steel and titanium. The time constant of the induced eddy current decay of the cylinder is obtained theoretically and from simulation models. The results are shown in table 4-7. The cylinder dimensions are the same for the stainless steel and titanium cylinders.

Table 4-7: Equation of time constant of cylinder (modelling and theoretically)

Time constant from simulation τ_0 (s)	**Time constant from Theoretical equation** τ_0 (s)
$\mathbf{V(t)} = A_n \exp(-\frac{t}{\tau_0})$	$\tau_0 = \frac{\sigma \mu_0 ah}{18}$

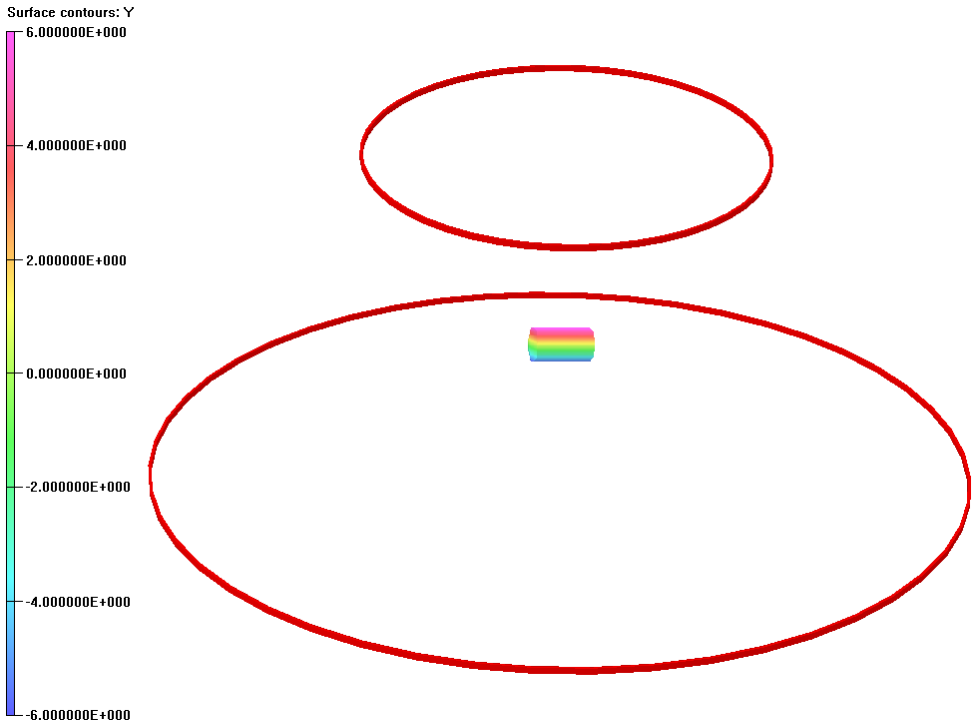

Figure 4-14: Model of cylinder.

4.13.1 Time Constant for Stainless steel Cylinder

A large circular coil is used like the one used previously with the sphere, which is also convenient for cylinder. The coil generates a pulse of uniform magnetic field symmetrical around the cylinder and include, and conductivity 1.1×10^{6} $S.m^{-1}$.

The simulation model is confirmed the simulated results concurred with theoretical ones, see table 4-8, and time decaying responses are in the figure 4-15.

Table 4-8: Stainless steel cylinders for many sizes

Material	Target	Length	Radius	$\tau_{Simulation}$ (ms)	$\tau_{Theoretical}$ (ms)
Stainless Steel	Cylinder_1	4 cm	2 cm	0.0622	0.0614
	Cylinder_2	8 cm	4 cm	0.2483	0.2457
	Cylinder_3	10.0 cm	4.0 cm	0.3088	0.3071
	Cylinder_4	10.0 cm	6.0 cm	0.4607	0.4607

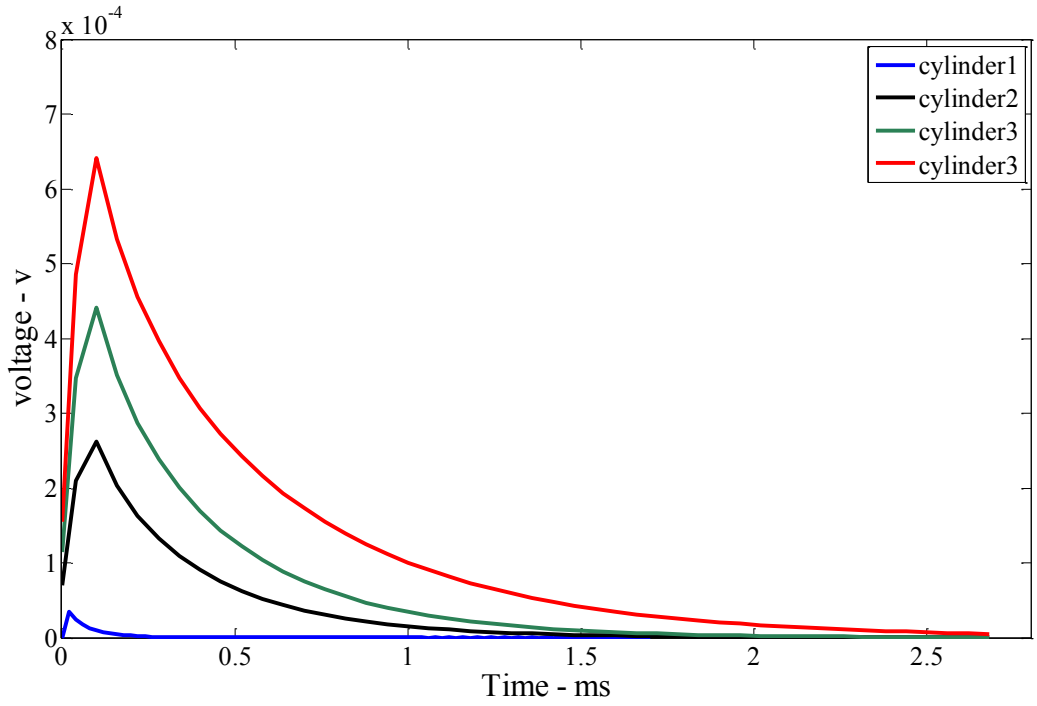

Figure 4-15: Time constant for stainless steel cylinder different sizes.

4.13.2 Time Constant for Titanium Cylinders

Various sizes of Titanium cylinder models with the conductivity 1.67×10^{6} $S.m^{-1}$ were used. The theoretical and simulated values of the time constants are compared in table 4-9 and the decaying time responses are plotted in figure 4-16.

Table 4-9: Titanium cylinders for many sizes

Material	Target	High	Radius	$\tau_{Simulation}$ (ms)	$\tau_{Theoretical}$ (ms)
Titanium	Cylinder_1	2 cm	4 cm	0.0936	0.09327
	Cylinder_2	8 cm	4 cm	0.3736	0.3730
	Cylinder_3	10.0 cm	4.0 cm	0.4660	0.4663
	Cylinder_4	10.0 cm	6.0 cm	0.6990	0.6995

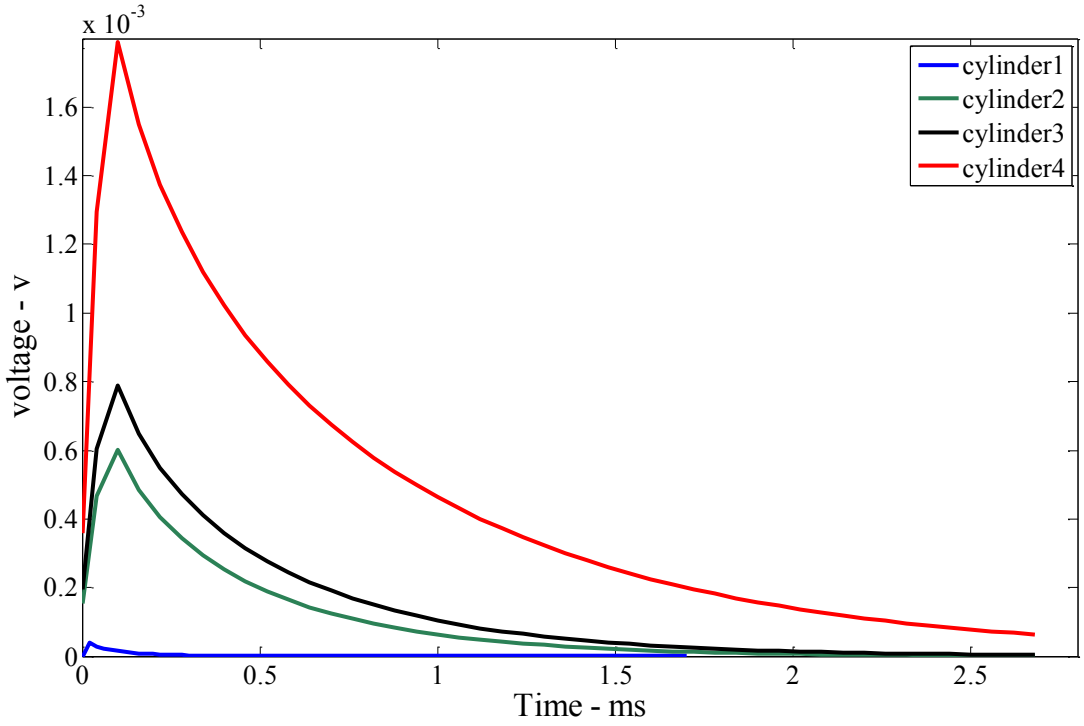

Figure 4-16: Time constant for titanium cylinder different sizes.

4.13.3 Time Constant for Aluminium Cylinder

In the case of Aluminium conductivity 3.38×10^{6} $S.m^{-1}$ only one cylinder size (radius=2 cm, height=4 cm) was used conductivity were used. This was due to the limitation of the simulation software. Hence, only one simulation results is presented in Table 4-10 with the decaying time response plotted in figure 4-17.

Table 4-10: Aluminium cylinder

Material	Target	High	Radius	$\tau_{Simulation}$ (ms)	$\tau_{Theoretical}$ (ms)
Aluminium	Cylinder	4 cm	2 cm	2.1109	2.1

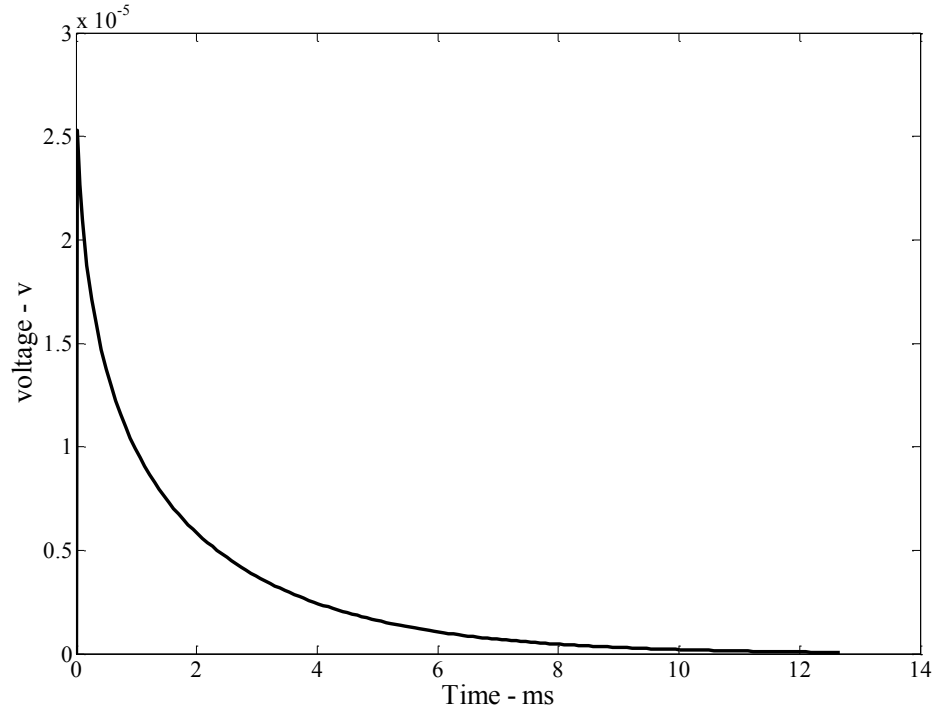

Figure 4-17: Time constant for aluminium cylinder.

4.13.4 Time Constant for Copper Cylinder

For the Copper cylinder models, one simulation model of cylinder with parameter (r = 2 cm, h = 4 cm) and conductivity is 5.8×10^{7} $S.m^{-1}$, because the computer also can not make any processing for high parameter over this size of cylinder. Again, only one simulation result which agrees with the theoretical one, see table 4-11 and decaying time responses of figure 4-18.

Table 4-11: Copper cylinder

Material	Target	High	Radius	$\tau_{Simulation}$ (ms)	$\tau_{Theoretical}$ (ms)
Copper	Cylinder	4 cm	2 cm	3.2016	3.2

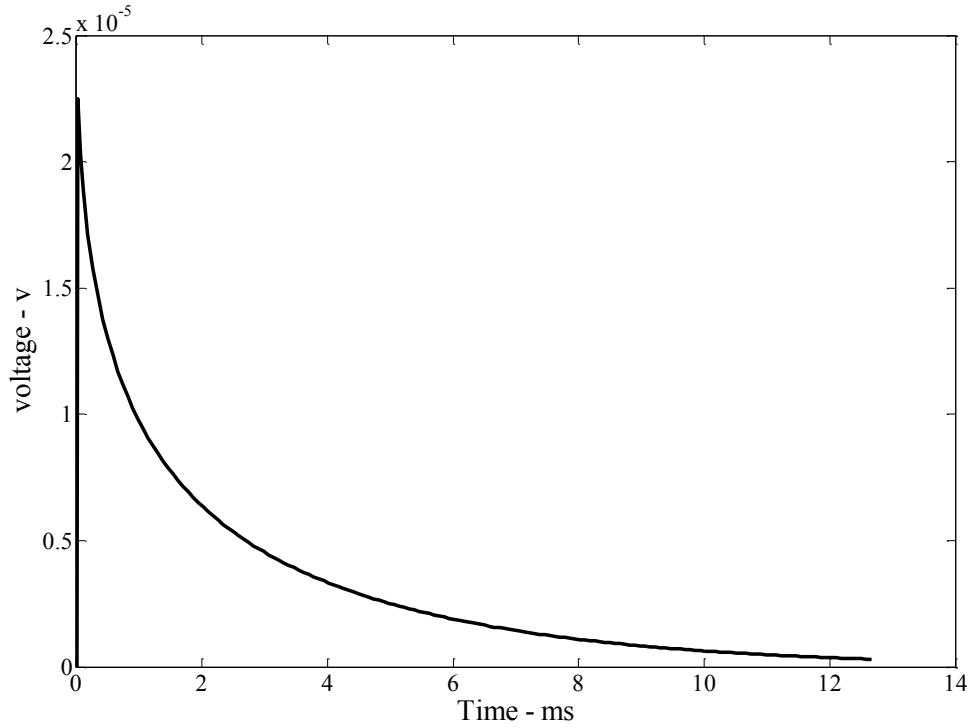

Figure 4-18: Time constant for copper cylinder.

4.13.5 Time Constant for Two Cylinders Together

Two separate cylinders have been used of stainless steel with following dimensions and different distances between them see figure 4-19:

- Cylinder 1 has length 4 cm and radius 2 cm.
- Cylinder 2 has length 8 cm and radius 4 cm.

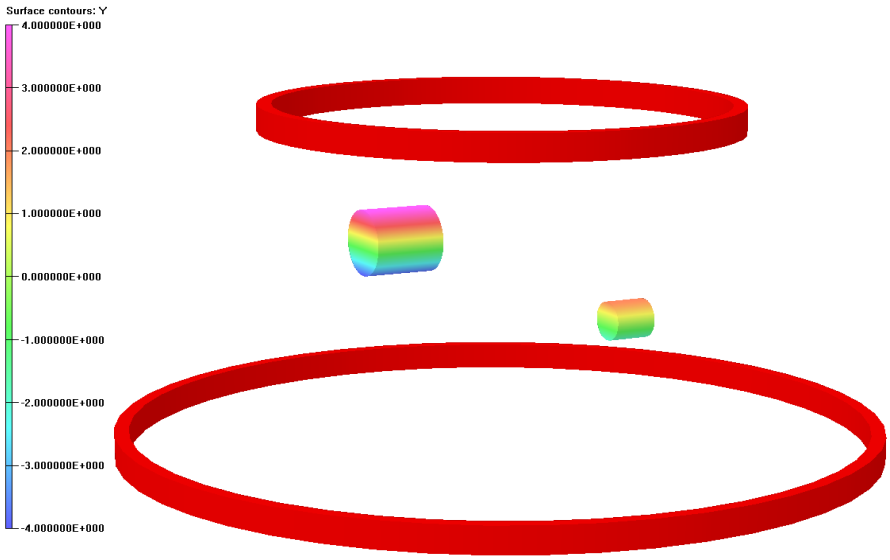

Figure 4-19: Model of two stainless steel cylinders

The time constant is found for many distances of separation of two cylinders and no electrical connect for the zero separation targets and the results are very close and validated see table 4-12:

Table 4-12: Two stainless steel cylinders together

Material	Target	Distance between two cylinders	Time constant for cylinder 2 0.0622 (ms)	Time constant for cylinder 1 0.2483 (ms)
Stainless Steel	Cly.1 & Cly.2	100 cm	0.0620	0.2744
	Cly.1 & Cly.2	50 cm	0.06366	0.2766
	Cly.1 & Cly.2	0.0 cm	0.06287	0.2714

4.14 Summary

The simulation models demonstrate the feasibility of detecting metallic objects which is found to depend on their physical characteristics; size and material composition of metallic spheres and cylinders. These models were applied to several different forms and dimensions individually.

As can be seen the tables from (4-2) to (4-5) and (4-8) to (4-11) there is good agreement between the theoretical and simulation results obtained for the fundamental time constants of various objects of various sizes and materials.

The effect of the separation between two targets was also investigated using two spheres of radii 4cm and 6 cm see table (4-6). Both time fundamental time constants where accurately recovered irrespective of the separation between the two spheres.

Similarly, two cylinders were used as two targets together with different distances and the results are in table 4-9.

This is an important result as it suggests that multiple objects or targets can be detected and identified by means of their time constants even when they are close together, for example when carried in a bag, providing they are not in direct electrical contact. The simulation models have shown that the time decay is sensitive to the shape, size and material composition that affects in the conductivity and which in turn affect the skin depth of target.

Chapter 5

Using Electromagnetic Pulse Induction for the Detection of Concealed Metal Objects

5.1 Introduction

In this chapter, the use of electromagnetic pulse induction to detect concealed and buried metal objects is simulated, with time constants and decay curves calculated for a range of representative cases; both threat non-threat, of several objects with different shapes and sizes. The threat objects are a revolver type handgun, a hand grenade, a knife and a razor blade. The non-threat objects are; a mobile phone, key and wrist watch. The decay curves etc are determined from the objects separately, and two or more together , using stainless steel material. The threat and non-threat objects by themselves or in combination are modelled with a finite element models (FEM) simulation solver program from Vector Fields.

Pulse Induction Techniques for the detection and identification of metallic objects have been reported and studied as a possible method for concealed weapon detection both on the human body and in carried baggage [84-90]. Electromagnetic Pulse Induction (EMI) relies on generating a rapidly changing, spatially uniform magnetic field which penetrates and encompasses the concealed metallic object. The temporally changing magnetic field induces eddy currents in the conducting object which then decay by dissipative (resistive) losses. These currents decay exponentially with time and have a characteristic time constant which depend only upon the size and shape of the object and the materials from which it is made; the orientation of the object does not influence the time constant [91-97] . It this aspect independence which forms the basis of a simple object identification system: a library of time constants, measured *a-priori*, can be compared with the measured time constant of an unknown sample to assess the presence or absence of a particular object or objects of interest. EMI for concealed object detection has one important advantage over resonant electromagnetic aspect independent phenomena: that is the human body has a very

much smaller perturbing effect in EMI than at the microwave frequencies (~ 0.4 – 2 GHz) required for excitation of natural resonances of typical concealed threat objects such as handguns and knives. At microwave frequencies the human body is opaque and therefore scatters and reflects microwave energy very effectively, undermining the ability to extract clean and uncluttered signatures from concealed objects [98-106]. EMI operates at much lower frequencies ~ 10 KHz, where the human body is nearly transparent, does not support appreciable eddy currents and is therefore 'invisible' [107]. In the case where excitation occurs at frequencies where the electromagnetic wavelength is comparable with the concealed object size (Mie scattering regime), resonant effects give a second aspect independent parameter: resonant frequency and decay time. However, because EMI operates at large electromagnetic wavelengths when compared to the object size, the concealed object is electrically small, and there is no resonant condition and consequently there is only one aspect independent parameter. EMI is at a disadvantage here as mapping an object in complex frequency space (two independent parameters) provides a less degenerate and more robust identifier than is possible with a single, aspect independent parameter [108].

5.2 Object Counting and Identification

A pre-requisite of a security screening system based on EMI is the capability to detect and classify multiple objects that may be within close proximity to one another. As an example, a person could quite conceivably be carrying a handgun in a briefcase a knife in their pocket and may well also have a mobile phone and other benign objects on their person. A robust and effective EMI based system is required to detect, count and identify these objects whatever their separations. Without doubt, the most serious problem posed by application of aspect independent EMI techniques is that of a single parameter being used to identify a concealed object, the fundamental time constant.

There is an inherent degeneracy in this approach which may well prevent certain objects that share similar time constants being counted as individual items and therefore discriminated from one another. To ascertain whether this problem is significant enough to seriously limit the effectiveness of an EMI system requires the measurement or simulation of a very wide variety of objects, both threat and non-

threat, which may be encountered. In this study present a representative of seven commonly carried objects: A wristwatch, key and mobile phone handset as representative of benign (non-threat) objects and a knife, handgun, razor blade and hand grenade as representative of threat objects.

Non-linear recursive fitting algorithms are not particularly suitable for the extraction of multiple time constants from a decaying temporal signal of the form of Equation (4-15). The fitting is sensitive to the starting points and is slow and computer intensive. The greatest problem is counting the number of objects present, as this is generally unknown *a-priori* and applying a model with an increasing number of fit parameters, terms and starting points quickly results in an unwieldy and unreliable method.

In this case it is better to use the application of the generalised pencil of function (GPOF) method [109], which is a far more suitable and rapid algorithm for the intended application as it is a generalised Eigen value problem and therefore does not need multiple iterations to arrive at a solution. The GPOF algorithm decomposes the signal into a discrete set of complex frequency components; in the case of an exponentially decaying signal of the form of Equation (4-25), only the real parts of the complex frequency are non-zero and the imaginary (oscillatory) frequencies are ignored. The number of objects M is unknown but can be estimated, in the absence of degeneracy of time constants, by iteratively increasing the model order (the number of complex frequencies expected) of the GPOF algorithm until any new complex frequencies found have amplitude which is lower than a preset threshold value. See Figure 5-1. Comparison of the time constants thus obtained can then be made with a library of time constants for common or expected objects and a list of likely carried objects may then be formed. Output may be an autonomous alarm or informing the user, by a computer screen, that a person is carrying only benign objects or that a person is likely to be carrying a threat object or objects.

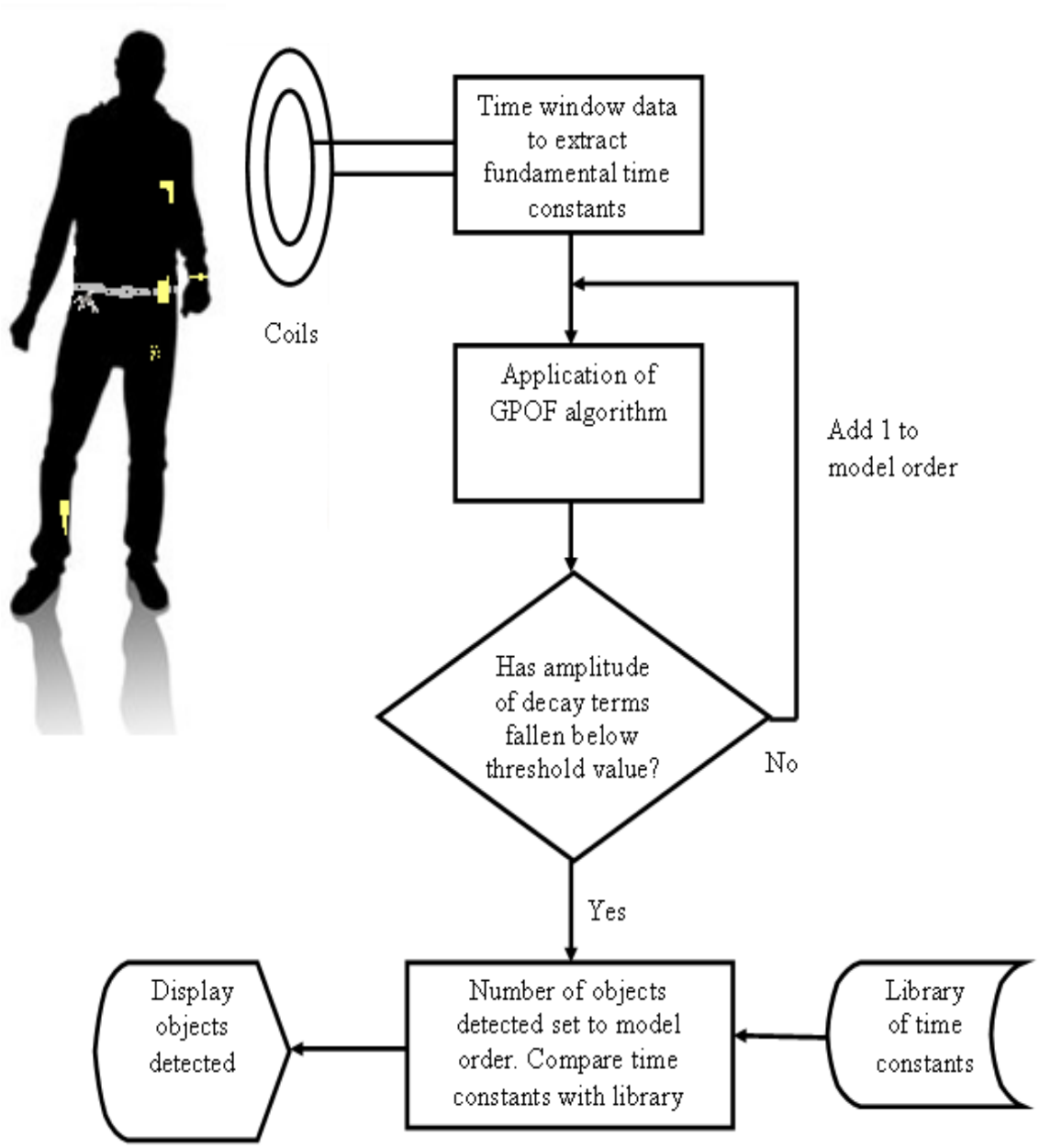

Figure 5-1: Flowchart depicting the processing steps and application of the GPOF algorithm to extract multiple time constants from the receiver coil time data.

5.3 Time Constant of Threat Objects

In this study, the threat metal objects consist of stainless steel that have a relative magnetic permeability and a conductivity of 1.1×10^{6} $S.m^{-1}$. The targets are a hand gun, a hand grenade, a knife and a razor blade, both as a single target and as a set of separated multiple targets, see figure 5-2.

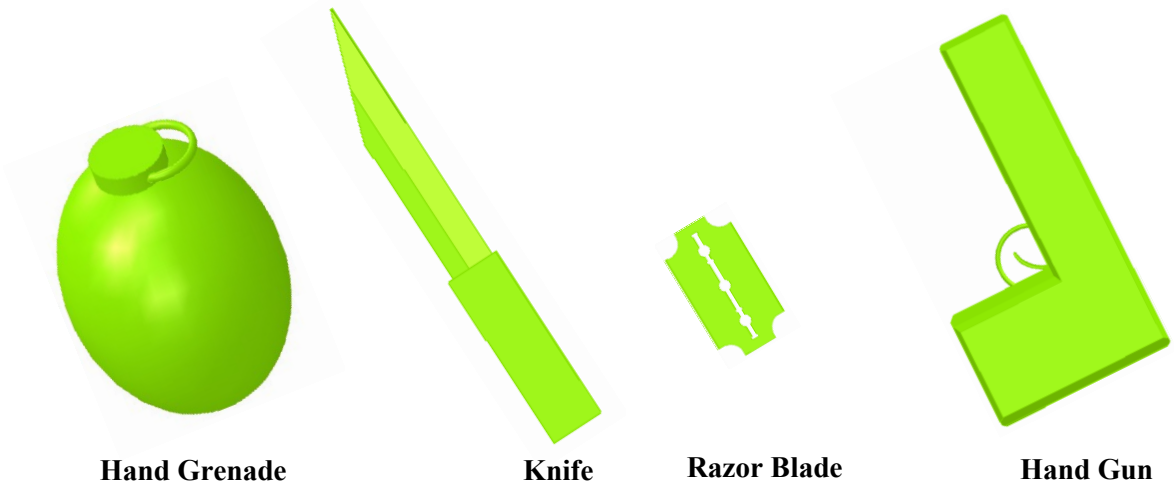

Figure 5-2: Four items of threat objects.

The target is positioned centrally, between the coils, as shown in figure 5-3. The time constant for each target alone is shown in table 5-1 and the calculated decay curve for each can be sees in figure 5-4. The hand grenade has by far the longest time constant, which is related to its near spherical and smooth shape, giving rise to relatively long lived eddy current distributions. The long lasting decay curve of the hand grenade is shown plotted separately in figure 5-5.

Table 5-1: Time constants of threat objects

Material	Targets	Time Constant τ (ms)
Stainless steel	Hand Grenade	0.250
	Hand Gun	0.0724
	Knife	0.0638
	Razor Blade	0.0074

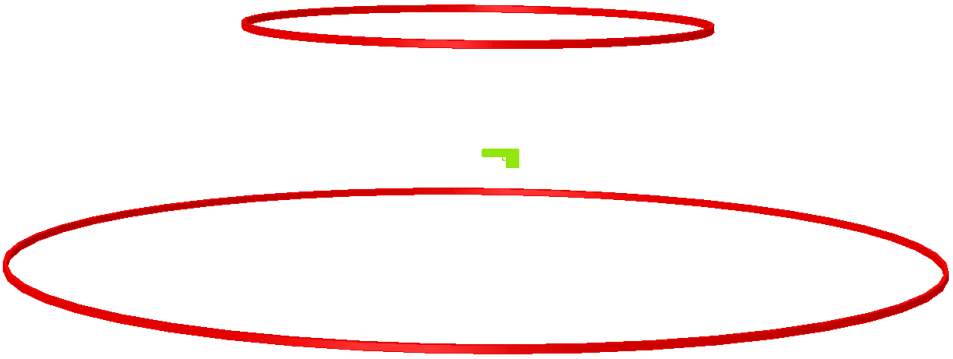

Figure 5-3: Model diagram for gun, showing the size of the coils and positioning of the threat item.

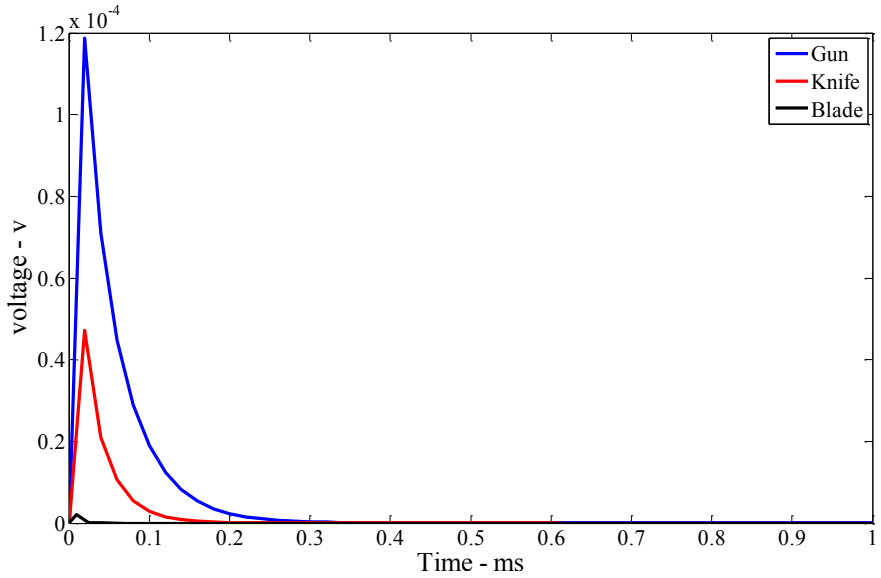

Figure 5-4: Time decays for hand gun, knife and razor blade.

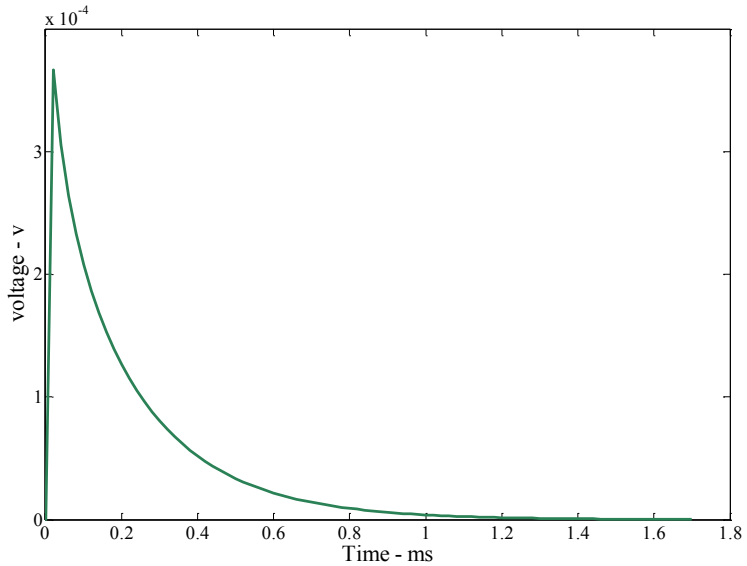

Figure 5-5: Time decay for hand grenade.

The aspect independence of the time constant of objects is the central and key effect on which the potential of EMI for concealed threat screening rests. A handgun was simulated in four different orientations as shown in figure 5-6 and the fundamental time constant recovered, there is little variation between the aspects, see table 5-2.

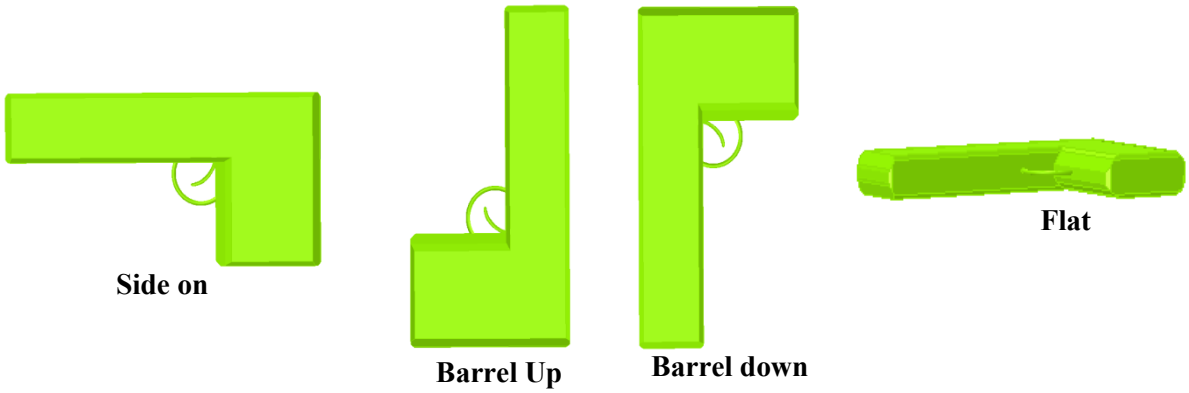

Figure 5-6: Orientations of handgun.

Table 5-2: Influence gun orientation on the time constant

Material	Object & orientation		Time Constant τ (ms)
Stainless steel	Handgun	Side on	0.0724
		Barrel up	0.0721
		Barrel down	0.0720
		Flat	0.0736

Also, the knife was simulated in four different orientations, see figure 5-7. The time constant is validated with minor changes between the results, as shown in table 5-3.

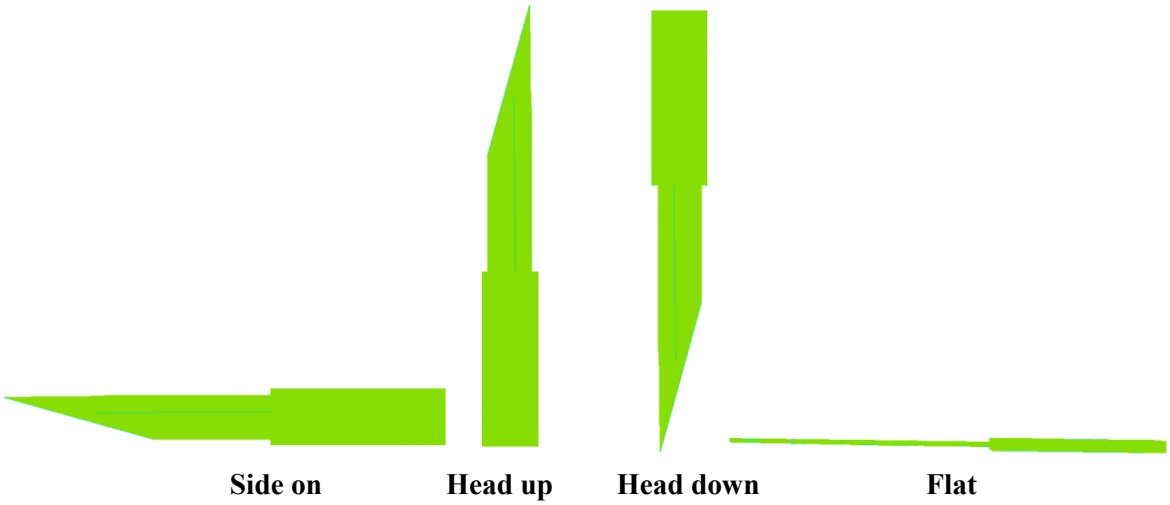

Figure 5-7: Orientations of knife.

Table 5-3: Influence of knife orientation on the time constant

Material	Object & orientation		Time Constant τ (ms)
Stainless steel	Knife	Side on	0.0621
		Head up	0.0612
		Head down	0.0642
		Flat	0.0638

The knife is considered an important and common sample for the detection of threat objects. Simulations using this model verified good and clear results for many orientations. The collapsing magnetic field induces an electromotive force in the metal target and the force causes eddy current to flow in the metal object. There is no energy to sustain the eddy currents, so they begin to decrease with a characteristic decay time that dependent on the size, shape and electrical and magnetic properties of metallic objects. From table 5-3 it can be seen that knife response for each position, the results of positions have similar transient profile. When generating the magnetic field around the knife, consequently the decay currents generate a secondary magnetic field, and the time rate-of-change of the field is detected by magnetic field of the

received coil. The time constant is similar for the four positions. It probes the insensitivity of time constant to target orientation.

Four objects were simulated in single aspect. These were simulated individually and their characteristic time constant obtained by the process described in figure 5-8. The time constants for these objects are presented in table 5-4.

Application of the simple algorithm is described to the simulations of multiple objects, comprising combinations of the four objects listed in table 5-4, successfully retrieves the fundamental time constants of the individual objects reasonably accurately. There is some discrepancy of time constant values, notably in these items that contain more objects. The razor blade seems to pose the greatest problem, the fundamental time constant is not accurately estimated when it is included in a group of other objects. The inaccuracy is probably due to the small size of the razor blade relative to the other objects; the small size giving a much shorter fundamental time constant and a weaker contribution to the signal compared to the other, larger, objects. This results in the signals from the larger objects dominating and a greater inaccuracy in the retrieved time constant.

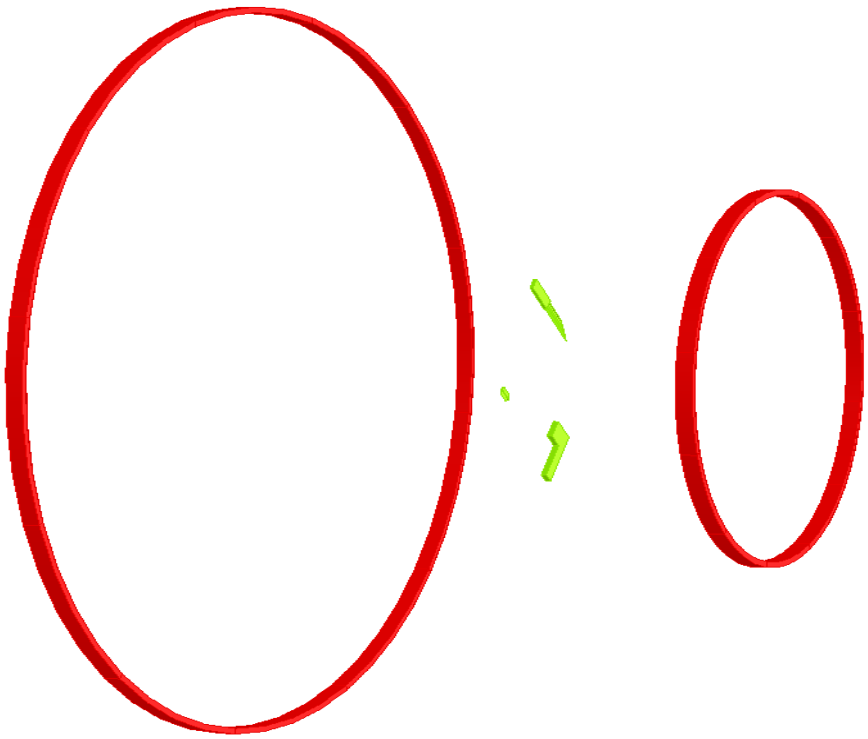

Figure 5-8: Model diagram for gun, knife and razor blade.

Table 5-4: Groups of threat objects and the fundamental time constants. Comparison is made to the time constants obtained for the Individual objects

Objects	Hand grenade 0.250 ms	Handgun 0.0724 ms	Knife 0.0638 ms	Razor blade 0.0074 ms
Hand grenade & handgun	0.250	0.0747	-	-
Hand grenade & knife	0.250	-	0.0663	-
Handgun & knife	-	0.085	0.066	-
Handgun, knife & razor blade	-	0.0776	0.0735	0.0072

5.4 Time Constant of non-Threat Objects

In this section, a study is made of non-threat metal objects of stainless steel material with a relative magnetic permeability of unity and a conductivity of 1.1×10^{6} $S.m^{-1}$. The targets are: mobile phone, key and wrist watch with single target and separated see figure 5-9.

Mobile phone **Wrist watch** **Key**

Figure 5-9: Three items of non-threat objects.

The item is placed centrally, between the coils, as shown in figure 5-10. The time constant and decay curve was calculated for each individual item, see table 5-5.

Table 5-5: Time constant of representitive non-threat objects

Material	Targets	Time Constant τ (ms)
Stainless steel	Mobile Phone	0.0241
	Wrist Watch	0.0516
	Key	0.0172

The wrist watch has comprises a reasonably large shape with enough of metallic material to produce relatively long lived eddy current distributions around the watch, see figure 5-11, followed by the mobile phone and then finally the key. The key poses the greatest difficultly to detect, because the small size giving a much shorter fundamental time constant and a weaker contribution to the signal compared to other benign items. So, a smaller sized object, as expected, produces a shorter time decay when compared to larger objects. However, the data analysis and fitting methods described here produces the possibility of detecting items of a small size and shape hidden or concealed amongst several other items, or in clothing.

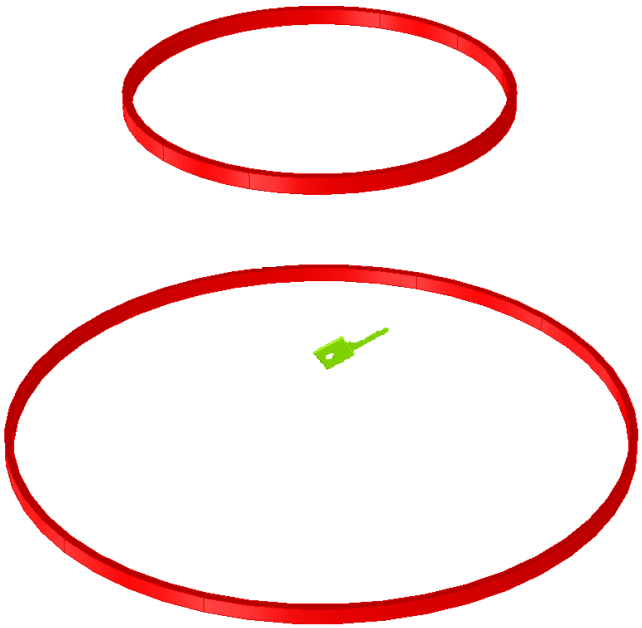

Figure 5-10: Model diagram for key.

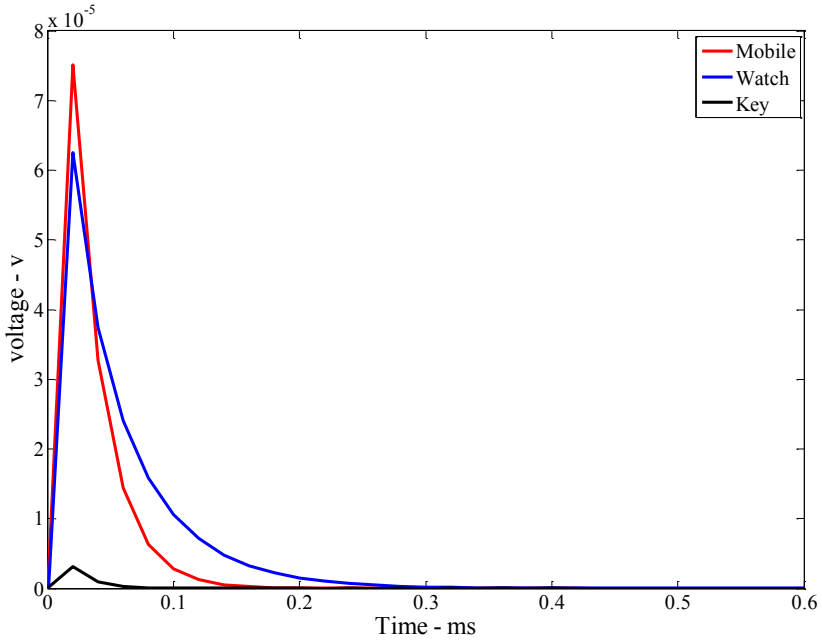

Figure 5-11: Time decays for mobile phone, wrist watch and key.

Three objects mobile phone, key and wrist watch were simulated together in a single aspect. The objects were simulated individually and their characteristic time constant obtained by a mathematical process, see figure 5-12. The fundamental time constants of these objects are presented in table 5-6.

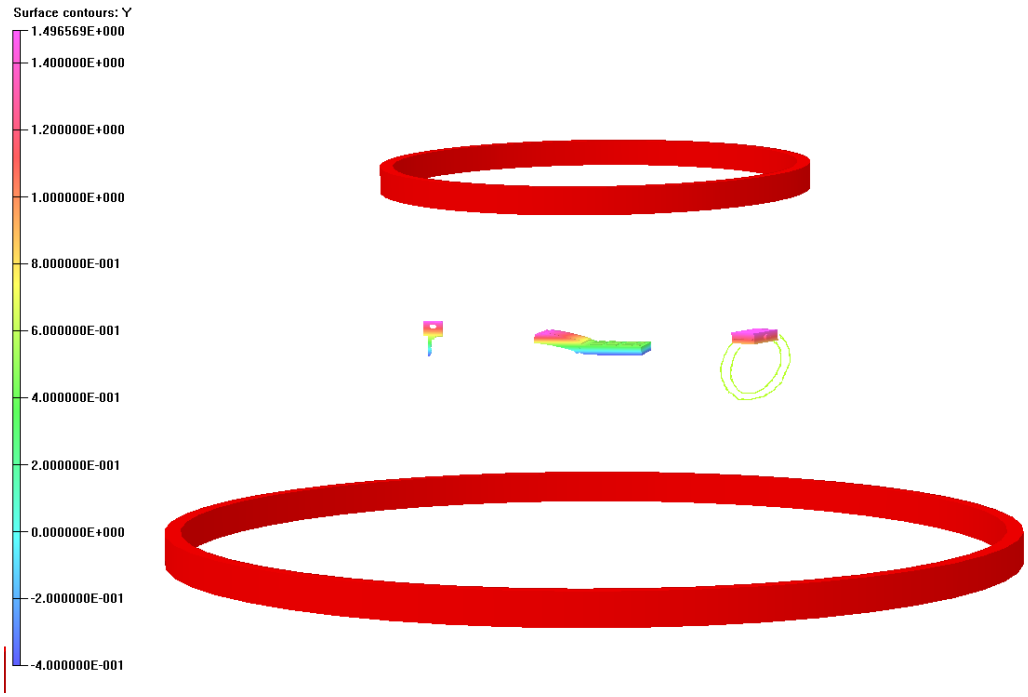

Figure 5-12: Model diagram for mobile phone, wrist watch and key.

Table 5-6: A comparison of two, three objects together and the fundamental time constants comparisons made to the time constants obtained for the Individual objects

Objects	Mobile Phone 0.0241 ms	Watch 0.0516 ms	Key 0.0172 ms
Mobile Phone & Watch	0.0261	0.0541	-
Mobile Phone & key	0.0256	-	0.0153
Watch & key	-	0.0539	0.0124
Mobile Phone , Watch & Key	0.0262	0.0537	0.0118

The results of calculating fundamental time constants for combinations comprising of the three objects were reasonably good when compared with individual objects, to an acceptable precision. There is a slight difference in the results in cases of two objects together and individual result of fundamental time constant. A small object can be difficult to detect because it reflects a weak signal and thus produces a short time decay, as happened with the key.

The time decay of a key was short, which indicates that the key poses a problem requiring more attention. In practical situations, it is possibly too small to present a threat.. The inexactness was probably due to the small size of the key relative to the other items and re going to study with multiple other objects in the next.

5.5 The Detection of Small Objects

5.5.1 Sensitivity the of time constant to Key & Razor Blade

The purpose of this study is to determine the likelihood of detection of small objects, especially those which could constitute serious human threats. This study uses a key and razor blade. The razor blade is important target that can be concealed at any position and around the human body or in a bag. The razor blade is considered to be one of several items that pose a threat to people. These two small objects and different shapes of stainless steel material were simulated together see figure 5-13.

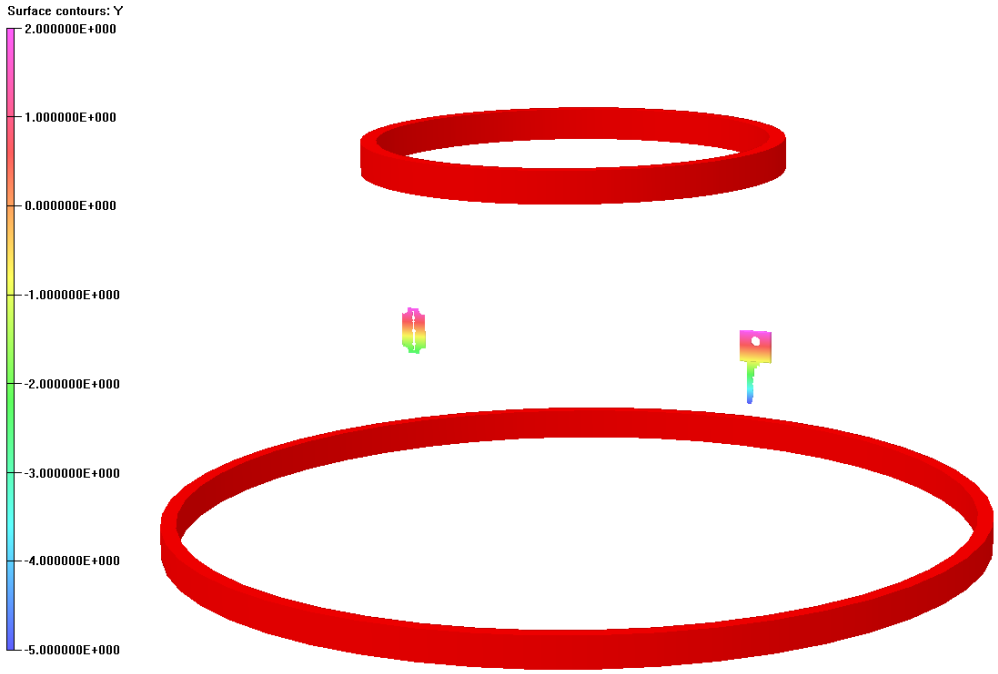

Figure 5-13: Model diagram for key and razor blade.

The targets are placed between two coils towards the middle, the fundamental time constant calculated as see the table 5-7.

Although the two small objects, the simulation results did discriminate between the two objects concealed together, with no significant changes between the razor blade and a small change in the value of the key time constant.

Table 5-7: Two small objects (key & razor blade)

Target	Key 0.0172 ms	Razor Blade 0.0074 ms
Razor Blade & Key	0.0201	0.00734

5.5.2 Sensitivity of time constant to Key, Razor Blade & Wrist Watch

The key, razor blade and wrist watch were modelled together. These objects are two small targets and one larger target (the wrist watch), forming mixed items, both threat and benign, with different shapes and sizes but the same material, stainless steel. The fundamental time constant is determined as displayed in table 5-8.

Table 5-8: Three small objects (key, razor blade & wrist watch)

Target	Watch 0.0516 ms	Key 0.0172 ms	Razor Blade 0.0074 ms
Blade, Key & Watch	0.0556	0.0193	0.0070

This data indicates that a small object does affect other objects within the same group; the razor blade and key fundamental time constant values are changed somewhat. This change will not necessarily be a hindrance in detecting hidden metal objects because the magnitude of the change is within a few percent.. The eddy currents are generated around the biggest object (wrist watch) more than small objects (key & razor blade) and the reflected signal from the watch is significantly stronger than those from the key and blade. Despite this, it still appears to be possible to detect and identify the small items.

5.6 Resolution of Multiple Concealed Metallic Objects by Using Electromagnetic Pulse Induction

Given the importance of detecting metal objects, especially when they are mixed with other items or hidden in bags and clothing, we have applied up to seven targets to the simulation program. The seven objects were simulated in a single aspect and the influence of these objects on the fundamental time constants is investigated. These targets are three (non-threat) benign objects (mobile phone, wrist watch and key) and four threat objects (hand gun, hand grenade, knife and razor blade). These are quite obviously different shapes and sizes, with the same component material being used in each case, stainless steel with a conductivity of 1.1×10^{6} $S.m^{-1}$. The objects were simulated individually and their characteristic time constants obtained by the process described in Figure 5-1. The processing of simulation program applied between two objects up to five objects together by many different and mix targets, threat and non-threat objects, see figure 5-14. The fundamental time constants for these objects are presented in table 5-9, along with the retrieved time constants for groups composed of different numbers of the seven simulated objects. The hand grenade has by far the longest time constant, which is related to its near spherical and smooth shape, giving

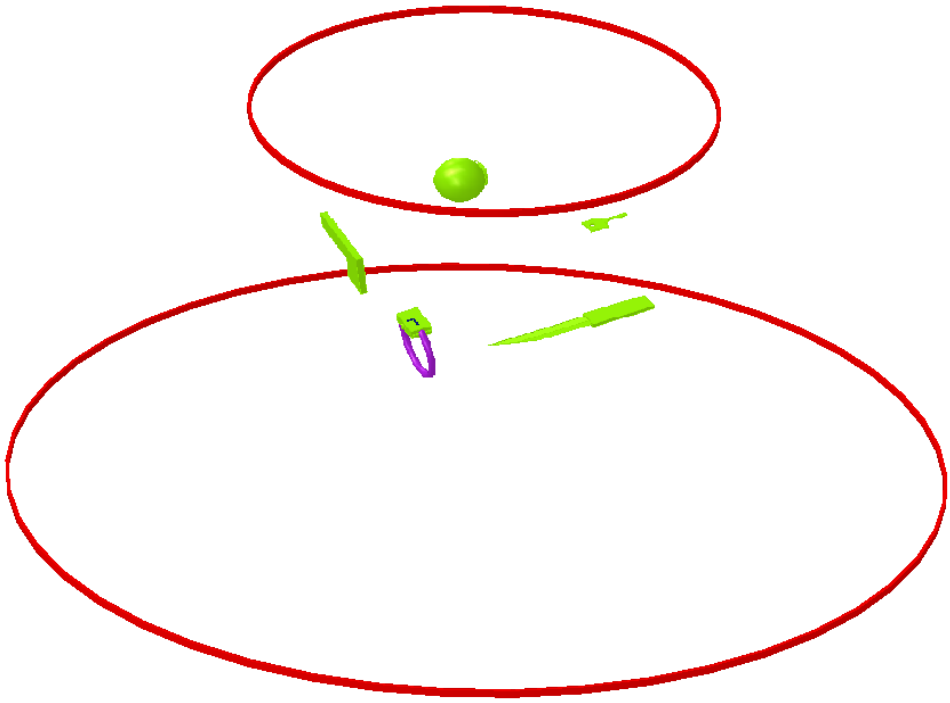

Figure 5-14: Group of different metallic objects.

rise to relatively long lived eddy current distributions. Application of the fitting algorithm described in section (4.11.4) to the simulations of multiple objects, comprising combinations of the seven objects is listed in table 5-9. It can be seen that the algorithm successfully retrieves the fundamental time constants of the individual objects reasonably accurately. There is some inconsistency of time constants with small changes, especially in groups that contain more objects. Once again, the key and the razor blade together pose a problem; here, the fundamental time constant is not accurately estimated when it is included in a group of other objects. Once again, this situation of inaccuracy is probably due to the small size of the key and razor blade ratio to other objects. Because, as already mentioned, small sizes produces much shorter fundamental time constant and weaker contribution to the signal compared to the large objects, which results in the signals from the larger objects dominating and a greater inaccuracy in the retrieved time constant.

Table 5-9: Groups of two to five objects and the fundamental time constants obtained from these groupings; comparison with the Individual objects

Objects	Hand grenade 0.250 ms	Handgun 0.0724 ms	Knife 0.0638 ms	Razor Blade 0.0074 ms	Wrist watch 0.0516 ms	Mobile phone 0.0241 ms	Key 0.0172 ms
Hand grenade & handgun	0.250	0.0747	-	-	-	-	-
Hand grenade & knife	0.250	-	0.0663	-	-	-	-
Handgun & knife	-	0.085	0.066	-	-	-	-
Mobile phone & watch	-	-	-	-	0.0541	0.0261	-
Mobile phone & key	-	-	-	-	-	0.0256	0.0153
Wrist watch & key	-	-	-	-	0.0539	-	0.0124
Handgun, knife & razor blade	-	0.0776	0.0735	0.0072	-	-	-
Mobile phone , watch & key	-	-	-	-	0.0537	0.0262	0.0118
Razor blade , key & watch	-	-	-	0.007	0.0556	-	0.01937
Hand grenade, handgun & wrist watch	0.253	0.086	-	-	0.0520	-	-
Hand grenade, handgun, wrist watch & knife	0.252	0.0774	0.0795	-	0.043	-	-
Hand grenade, handgun, wrist watch, knife & mobile phone	0.250	0.0751	0.0655	-	0.0536	0.0209	-
Hand grenade, handgun, knife, mobile phone & key	0.232	0.0691	0.0656		-	0.0251	0.00925

The simulations demonstrate the feasibility of being able to detect, count and identify a range of commonly carried metallic objects and also a range of weapons. Discrimination of weapons from benign objects is feasible, by the objects simulated, as the fundamental time constants are sufficiently distinct. The presence of multiple objects within the sensor range does not prevent counting and identification, although the accuracy of the determination of the individual objects fundamental time constants is made worse as the number of objects increases. The reason for this worsening of performance is undoubtedly due to the interaction (scattering) of the magnetic fields from the objects, i.e. the eddy currents flowing in one object give rise to a changing magnetic field which induces eddy currents in neighbouring objects and therefore blurs the time constants. The distortion of time constants when multiple objects are present is not so strong as to prevent the counting and identification of up to five objects from one another, with the possible exception of the key. Smaller objects such as a key or razor blade are more difficult to indentify due to their smaller cross section when compared to objects such as a handgun, hand grenade or wrist watch. This is not expected to constitute a serious problem as most threat objects are significantly larger than key or razor blade. This work demonstrates that many concealed metal objects with different sizes and shapes also various materials can be simultaneously detected, whether together or individually, by using the electromagnetic pulse induction. Through the simulated results can be find the small sensitive metal objects that pose dangerous for human and usually concealed or smuggled between the items and devices. The electromagnetic pulse induction by simulation models demonstrates the ability to effectively count and identify multiple objects carried in close proximity providing that the objects do not have very similar time constants.

5.7 Summary

Using the electromagnetic pulse induction for detection of metal objects has been validated successfully, and applied to several threat targets such as handgun, hand grenade, razor blade and a knife and non-threat targets for example mobile phone, wrist watch and key. These targets (objects) were different sizes and shapes but of the same material which was stainless steel. The study has shown the orientation, sensitivity of small objects, size, shape and the material component. The pulse of

current causing eddy current to flow and excited in the metal object and generate scatter signal after reflection from the object and which takes an exponential form that decays with time. This is the time constant which is determined for each target separately and together as group.

This study achieved its purpose for detection of metallic objects and finds the time constant for each target. It can be noted the time constant does not change for the handgun and knife for many orientations; neither it is affected by position. Investigations were performed to detect objects in a variety of conditions; using combinations involving a single and multiple objects up to a maximum of five targets. It was possible to detect individual targets within a group of objects. Smaller objects such as a razor blade were also detectable.

Chapter 6

CONCLUSION AND FUTURE WORK

6.1 Conclusion

This thesis has presented advanced feature based techniques for the detection and identification of metallic objects. The research is conducted using a finite element time domain electromagnetic solver, to simulate electromagnetic pulse induction with low frequency electromagnetic fields. The approach involves inducing eddy currents, by a transmitted electromagnetic pulse signal; into the concealed object and measuring the characteristic decay time of the received the signal. Comparison of the measured decay time with a library of time constants is the basis of object detection and identification..

The feasibility study of detecting and identifying multiple objects they are grouped in close proximity and the work been achieved through an integrated study of a group of targets for this purpose. Furthermore to improve the detection results and reduce the false alarm rates for metallic objects detection especially the threat targets.

The literature survey has identified some advantages and disadvantages of the detection of concealed and buried metal objects by several different techniques. The technologies reviewed include magnetic gradiometer, inductive magnetic field, acoustic and ultrasonic, EMR, MMW, THz, IR, X-Ray. All these technologies need to meet the main requirements of high penetration of clothing or soil for detection the metallic objects concealed under clothing or underground; suitable stand-off distance and accurate discrimination of threat and non-threat items for reliable and effective deployment. From this brief review it is evident that electromagnetic induction based techniques offer a good solution, because of the ability to identify multiple objects grouped together, unlike other reviewed technologies. EMI offers both good penetration ability and high resolution advantages for metallic objects can be detected with no ionising radiation hazard.

The comparison of different techniques is necessary, the advantages and disadvantages of different techniques need to be understood. Most of the concealed metal object methods described here are complementary. New concealed metal object systems need to be an amalgamation of the technique mentioned above permitting a reduction in the number of false alarms.

In this research to detect the concealed metallic objects by using the electromagnetic pulse induction and low frequency with simulation models which is used in the detection applied in the testing models to verify the effect of this method over many figures of spheres and cylinders with different sizes and material components. The models were validated by simulation of stainless steel cylinders and spheres of different radii. The fundamental time constants from the simulations were compared to the theory results are done it perfect and agree very well. This validation permits us more confidence to the model complex targets of different sizes.

The important at this research the progress is found the several concealed metallic objects (threat and non-threat) that pose a dangerous on the human in a way directly or indirectly with different sizes, shapes and mix jointly of two objects up to five objects simultaneously at the same material, and find the results of fundamental time constant and the time decay for these metallic objects. From result of detection on the testing data set comes out, it is easy to obtain the conclusion that the electromagnetic pulse induction has very good effect on the targets detection result.

The influence of the separation of two objects is also investigated, two spheres and two cylinders of many materials components; copper, aluminium, stainless steel and titanium where are applied simulated at varying separations. From these important results can be suggesting detection and identified the multiple metallic objects of their time constants even when they are close together. It is very important consequence as it suggests that multiple metallic objects can be detected, counted and identified even when the targets are close together. So that we apply that to a group of threat objects and non-threat objects were seven targets; hand grenade, hand gun, knife, razor blade, mobile phone, wrist watch and key at same materials components, all they simulated individually and with each other. The sensitivity for gun and knife of multi-

orientations (different directions) were acceptable and little variation in the fundamental time constant.

Then the simulations demonstrate the feasibility of being able to detect, count and identify a range of commonly carried objects and whether a range of threat or non-threat objects. It can be Discriminated of weapons from benign objects is feasible, at least for the objects simulated, as the fundamental time constants are sufficiently distinct.

The results of fundamental time constant for two objects together or more as group (multi objects), mixed targets and different sizes also different shapes whichever threat and benign targets were agreement and satisfied the result of single target and at the same time, can be detected, counted and identified multi targets up to five targets when applied close together as group and the fundamental time constant was clear and little change for results, but no affect on the result, in spite of the accuracy of the determination of the individual objects' fundamental time constants is made worse increasing number of objects especially the small targets such as key and razor blade.

The reason is due to the eddy currents flowing in the object give rise to a changing magnetic field which induces eddy currents in neighbouring (around) objects and therefore blurs the fundamental time constants that already affect on the small targets.

The small objects for example key and razor blade are more difficult to indentify due to their small cross section when compared to another objects, such as a handgun, hand grenade or wrist watch. This is not expected to pose a serious problem because the threat objects are bigger than the key and the razor blade.

From these proves, can be detecting at the same time many concealed, hidden and buried metal objects with different sizes, shapes and various materials components, whether these objects as group or individual by using a finite element time domain electromagnetic pulse induction solver. Through the simulated results can be find the small sensitive metal objects that constitute dangerous for human and usually concealed or smuggled between the items, devices and in the baggage or containers. The electromagnetic pulse induction by simulation models demonstrate the ability to

effectively count and identify multiple objects carried in close proximity providing that the objects do not have very similar time constants.

6.2 Future Work and Recommendation

In this work has shown the potential of the using the electromagnetic induction for metal objects detection and identification by using the fundamental time constant as parameter to discrimination and classification the multiple items of threat and non-threat objects.

- This investigation is ready to extend to the laboratory that this work will enhance the capability of current screening procedures; it is not complicated and low price and will be activated.

- Multiple metal objects can be include over five objects with different materials in the concealed target detection system to have more views of the items and improved detection.

- Make signature database to discriminate the threat and benign targets by collected the signal response of classes of many metallic objects.

- It is very important to make test for sensitivity of concealed metal items to target materials components.

- To development this work and obtained the robust pattern recognition system, need to use another signals of pulses and low frequency.

- When using simulation software must be taking into account time factor, it is very important used high quality of hardware (computer) in terms of fast processor and high memory to get the perfect results.

REFRENCES

1. V. Sutton, and D. Bromley, Understanding technologies of terror Technology in Society, vol. 27, Issue 3, pp. 263-285, 2005

2. N. Paulter, Users' Guide for Hand-Held and Walk-Through Metal Detectors, National Institute of Justice Guide 600-00, January 2001,pp 20-39.

3. N. Paulter, Guide to the Technologies of Concealed Weapons and Contraband Imaging and Detection National Institute of Justice Guide 602-00, February 2001, pp. 33 - 50.

4. http://www.ceia.net/security, access 21.09.2012.

5. L. G. Roybal, P. M. Rice, and J. M. Manhardt, A new approach for detecting and classifying concealed weapons, Proceedings of the SPIE, The International Society for Optical 54 Engineering, Conference on Surveillance and Assessment technologies for Law Enforcement, Vol. 2935, Boston, MA, November 1996, pp. 95-107

6. P. V. Czipott and M. D. Iwanowski, Magnetic sensor technology for detecting mines, UXO, and other concealed security threats, Proceedings of the SPIE, The International Society for Optical Engineering, Conference on Terrorism and Counter-terrorism Methods and Technologies, Boston, MA, November 1996, pp. 67-76.

7. http://www.cflhd.gov/resources/agm/engApplications/SubsurfaceChartacter/632DetectingUndergroundStorageTanks.cfm, 22, November, 2012.

8. S. Kumar, A. R. Perry, C. R. Moeller, D. C. Skvoretz, M. J. Ebbert, R. K. Ostrom, S. L. Bennett, and P. V. Czipott, "Real-Time Tracking Magnetic Gradiometer for Underwater Mine Detection", Proceedings of Oceans 2004. MTTS/IEEE Techino-Ocean '04, Vol. 2, pp. 874-878, 2004.

9. B. Anastassia, the detection of concealed firearm carrying trough CCTV: the role of affect recognition, thesis of Loughborough University, 2011.

10. C. Nelson, Metal Detection and Classification Technologies Johns Hopkins APL technical Digest, Vol. 24. Number 1, 2004. pp.62-66.

11. A. Agurto, Y. Li, G. Tian, N. Bowring, S. Lockwood, a Review of Concealed Weapon Detection and Research in Perspective, IEEE International Conference, on Networking, Sensing and Control, London, UK, 15-17 April 2007.

12. C. Nelson, Wide-Area Metal Detection System for Crowd Screening in Proc. SPIE AeroSence 2003 Conf. Sensors and Command, Control, Communication, and Intelligence (C3T) Technologies for Homeland Defense and Law Enforcement II, Orlando, FL(22-25 Apr 2003).

13. P. Pati, P. Mather, Open Area Concealed Weapon Detection System, Detection and Sensing of Mines, Explosive Objects, and Obscured Targets XVI, Proc. of SPIE Vol. 8017 801702-1, 2011.

14. C. Nelson, D. Mendat, and T. Huynh, Three-dimensional Steerable Magnetic Field Antenna for Metal Target Classification, in Proc. SPIE AeroSense 2003 Conf., Detection and Remediation Technologies for Mines and Minelike Targets, Orlando, FL, 22-25 Apr 2003, pp. 707-717.

15. A. Al-Qubaa, G. Tian, J. Wilson, Electromagnetic Imaging System for Weapon Detection and Classification, the fifth international conference on sensor technologies and applications, 2011.

16. J. DuChateau, M. Hinders, Using Ultrasound in Concealed Weapons Detection", NDE Lab, Department of Applied Science, College of William and Mary, April 2005.

17. D. Donskoy, Acoustic/Seismic Methods (Paper II), Stevens Institute of Technology, http://www.rand.org/publications/MR/MR1608/MR1 608.

18. C. Gooneratne, S. Mukhopahyay and G. Sen Gupta, a Review of Sensing Technologies for Landmine Detection, Unmanned Vehicle Based Approach, 2nd International Conference on Autonomous Robots and Agents, December 13-15, 2004.

19. C. Kuo, Full Wave 2D Modeling of Scattering and Inverse Scattering for Layered Rough Surfaces with Buried Objects, thesis of University of Michigan, 2008.

20. J. Duchateau, M. Hinders, Using Ultrasound in Concealed Weapons Target Detection, NDE Lab, Department of Applied Science, College of William and Mary, April 2005.

21. (http://wwwjaycor.com), access 22.09.2012.

22. A. Achanta, M. McKenna., Non-linear Acoustic Concealed Weapons Detections 34th Applied Imagery and Pattern Recognition Workshop, 2005, pp. 21-27.

23. A. Achanta, L. Innovations, Inc, Non linear Acoustic Concealed Weapons Detector, Storming Media, 2006.

24. D. K. Kotter, L. G. Roybal, R. E. Polk, Detection and classification of concealed weapons using a magnetometer-based portal, Proceedings of SPIE - Vol. 4708 Sensors, and Command, Control, Communications, and Intelligence (C31) Technologies for Homeland Defense and Law Enforcement, Edward M. Carapezza, Editor, August 2002, pp. 145-155.

25. M. Al-Azzo, Resolution Enhancement of Holographic Imaging of Concealed Object using Burg Method, International Journal of Recent Trends in Engineering, Vol. 2, No. 1, November 2009.

26. AKELA; US Department of Justice Final Report-Demonstration of a Concealed Weapons Detection System Using Electromagnetic Resonances January 2001.

27. E. Knott, J. SHAEFFER, and M. TULEY, Radar cross section, 2nd edition Tech Publishing, pp. 82-83, 2004.

28. A. R. Hunt, R.D. Hogg, W. Foreman, Concealed weapons detection using electromagnetic resonances, Proc. SPIE Vol. 3575, Enforcement and Security Technologies, A. Trent De Persia; John J. Pennella; Eds. SPIE, pp. 62-67, 1998.

29. Jarkko, TSA announces new millimeter wave security screening system, October 17, 2011 in Aviation.
30. A. Agurto, New proposal for the detection of concealed weapons electromagnetic weapon detection for open areas," Ph.D. Thesis, Huddersfield, UK, 2009.

31. D. Rauscher and M. Hartnett, concealed weapon detection programme, decision science applications, Inc, 1998.

32. R. McMillan, Currie, Concealed weapon detection using microwave and millimetre wave sensors, microwave and millimetre wave technology proceedings, ICMMT. International conference, Beijing, China, 1998.

33. T. Bosq, M. Alonso, G. Boreman and D Dillery, Millimeter wave imaging system for the detection of non-metallic objects Proc. SPIE, 6217, (2006).

34. J.R. Lockwood, J. Mcfee, Alternatives for Landmine Detection, online book, 0-8330-3301-8, 2003.

35. R. Appleby, R. Anderton, Millimeter-Wave and Submillimeter-Wave Imaging for Security and Surveillance Proceedings of the IEEE Volume 95, Issue 8, P 1683 – 1690, 2007.

36. H. Essen, H. Fuchs, M. Schlechtweg, A. Tessmann, Concealed Weapon Detection with Active and Passive Millimetre wave Sensors, Two Approaches, (FGAN-FHR) and (IAF), Germany.

37. D. Sheen, D. McMakin, and T. Hall, Three-Dimensional Millimeter-Wave Imaging for Concealed Weapon Detection, IEEE transaction on microwave theory and techniques. Vol. 49, No. 9, September 2001.

38. S. Stanko, D. Notel, A. Wahlen, Active and passive mm-wave imaging for concealed weapon detection and surveillance Infrared, Millimeter and Terahertz Waves, IRMMW-THz 2008.

39. M. Kemp, a Review of Millimetre-Wave and Terahertz Technology for Detection of Concealed Threats, IEEE, 2008.

40. L. Moeller, PI, Standoff Detection of Concealed Weapons using a Terahertz illuminator with an Uncooled Imager, NIJ Award: 2007.

41. M. Châteauneuf, J. Dubois, Detection of explosives using THz time domain spectroscopy, Proc. of SPIE Vol. 6796, 67962D, 2007.

42. T. Kleine-Ostmann, P. Knobloch, M. Koch, S. Hofmann, M. Hofmann, G. Hein, K. Pierz, Compact and cost-effective continuous wave THz imaging system Lasers and Electro-Optics, 2002.

43. E. Gerecht, A Passive Heterodyne Hot Electron Bolometer Imager Operating at 850 GHz IEEE Transactions on microwave theory and techniques, vol.56, NO. 5, May 2008.

44. T. Rudeger, Alessandro; F. Beltram, E. Harvey, field, Edmund, Terahertz semiconductor-heterostructure laser Nature, vol. 417, no. 6885. Page(s) 156 - 169. May 2002.

45. M. R. Leahy-Hoppa and M. J. Fitch, Terahertz spectroscopy techniques for explosives detection, Anal Bioanal Chem, 395:247–257, (2009).

46. E. L. Jacobsa, S. Moyera, C. C. Franckb Concealed weapon identification using terahertz imaging sensors, Proc. of SPIE Vol. 6212, 62120J, (2006).

47. M. J. Fitch, D. Schauki, C. A. Kelly and R. Osiander, Terahertz imaging and spectroscopy for landmine detection Proc. SPIE 5354 45, 2004.

48. R. Osiander, J. Miragliotta, Z. Jiang, J. Xu and X. C. Zhang, Mine field detection and identification using THz spectroscopic imaging Proc. SPIE 5070 1, 2003.

49. K. Cooper, R. Dengler, Fast high-resolution terahertz radar imaging at 25 meters, SPIE Vol. 7671, 76710Y, 2010.

50. R. W. Mc-MILLAN, terahertz imaging millimetre wave radar, conference surveillance and assessment, technologies for law, Alabama, USA, 2004.

51. H. Roskos, Terahertz success relies on research investment, Optics & Laser Europe, p15, 2008.

52. R. W. McMillan, O. Milton, Detection of Concealed Weapons Using Far Infrared Bolometer Arrays, 2000.

53. A. Rogalski and K. Chrzanowski, Infrared devices and techniques, OPTO-electronics review 10(2), 111-136, 2002.

54. T. Nguyen, D. Hao, P. Lopez, Thermal Infrared Identification of Buried Landmines, SPIE Vol. 5794, USA, Mar. 2005.

55. P. KRUSE and D. Skatrud, Uncooled Infrared Systems in Semiconductors and Semimetals, R.K WillardsoPress, New York, 1997.

56. B. Abidi, Y. Zheng, A. Gribok, and M. Abidi,. Improving Weapon Detection in Single Energy X-Ray images through pseudo-colouring, IEEE Transactions on systems, Vol. 36, No. 6, Nov. 2006.

57. M. Roomi, R. Rajashankari, Detection of concealed weapons in x-ray images using fuzzy K-NN, International Journal of Computer Science, Engineering and Information Technology (IJCSEIT), Vol.2, No.2, April 2012.

58. N. Shanks and A. Bradley, Handbook of Checked Baggage Screening: Advanced Airport Security Operation, Wiley Blackwell, 2004.

59. R. Feynman, The Feynman Lectures On Physics, volume 2: Addison-Wesley Publishing Company, 1964.

60. S. Qaten, Assessment of defects in ferromagnetic metals with eddy currents, thesis of University of Brunel, 1989.

61. L. Pasion, Detecting Unexploded Ordnance with Time Domain Electromagnetic Induction, Thesis, University od British Colombia, 1999.

62. J.Reitz, J. Frederick, R. W. Christy, Foundations of Electromagnetic Theory, 1979.

63. J. D. Jackson, Classical Electrodynamics: John Wiley and Sons, 1975.

64. S. Ward, and G. Hohmann, Electromagnetic Theory for Geophysical Applications, in Nabighian, M.N., Ed., Electromagnetic Methods In Applied Geophysics: Society of Exploration Geophysicists, 1991, Volume 1, Theory, 131-311.

65. J. Weaver, Mathematical Methods for Geo-electromagnetic Induction: John Wiley and Sons, Inc, 1994.

66. B. Chalmers, A. Williamson, A. Machines: Electromagnetics and design Jone Wiley and sons INC, 1991, p (2-20).

67. P. R. Karmel, G. D. Caler, Introduction to electromagnetic and microwave Engineering, John Wiley and Sons, 1998.

68. G. Caloz, M. Dauge, *Skin* effect in electromagnetism, workshop ‘‘ Non standard Numerical methods for PDE’s, Pavia, June 29 – July 2, 2010.

69. Vector Fields Software, Cobham Technical Services, Version 13.014, 2009.

70. Y. Li, T. Theodoulidis, Magnetic Field-Based Eddy-Current Modeling for Multilayered Specimens, IEEE transactions on magnetics, vol. 43, No. 11, 2007.

71. A. A. Kaufman, P. A. Eaton, The Theory of Inductive Prospecting, Amsterdam, Netherland, 2001.

72. G. Y. Tian, A. Sophian, D. Taylor and J. Rudlin, Multiple Sensors on Pulsed Eddy-Current Detection for 3-D Subsurface Crack Assessment, IEEE Sensors Journal, 5 (1). pp. 90-96, 2005.

73. C. Nelson, C. Cooperman, W. Schneider, D. S. Wenstrand, and D. G. Smith, Wide bandwidth time-domain electromagnetic sensor for metal target classification, IEEE Trans. on Geosci. Remote Sens., Vol. 39, No. 6, 1129{1138, Jun. 2001.

74. C. Nelson, Wide-area metal detection system for crowd screening, Proc. SPIE AeroSense 2003 Conf., Sensors and Command, Control, Communication, and Intelligence (C3T) Technologies for Homeland Defense and Law Enforcemnt II, Orlando, FL, Apr. 22-25, 2003.

75. M. Gashinova, UWB signature analysis for detection of the body-worn weapons, IEEE, 0-7803-9582-4/06, 2006.

76. S. Singh, M. Singh, Explosives detection systems (EDS) for aviation security, Elsevier, signal processing 83, 31-55, 2003.

77. T. Bell, AETO Inc., Subsurface discrimination using electromagnetic induction sensors, Transactions on geo-science and remote sensing, Vol. 39, No. 6, June 2001.

78. A. R. Hunt, Demonstration of a Concealed Weapons Detection System Using Electromagnetic Resonances, Final Report, National Institute of Justice US Dept. of Justice Washington, 2001.

79. C. E. Baum, Detection and Identification of visually obscured targets, p 243 – p 281, 1998.

80. N. Har field and J. R. Bowler, Theory of thin-skin eddy-current interaction with surface cracks, J. Appl. Phys., Vol. 82, 4590, 1997.

81. B.-H. Cao, M. Fan, and X. Yang, Analytical time-domain model of transient eddy current field in pulsed eddy current testing, Acta Phys. Sin., Vol. 59, No. 11, 7570-7574, 2010.

82. A. Sophian, Characterisation of surface and sub-surface discontinuities in metals using pulsed eddy current sensors, thesis of University of Huddersfield, 2003.

83. A. A. Kaufman and G. V. Kellier, Inductive Mining Prospecting Part 1: Theory, 620, Elsevier, Amsterdam, 1985.

84. J. R. Wait and K. P. Spies, Quasi-static transient response of a conducting permeable sphere, Geophysics, Vol. 34, No. 5, 789-792, 1969.

85. C. V. Nelson, C. B. Cooperman, W. Schneider, D. S. Wenstrand, and D. G. Smith, Wide bandwidth time-domain electromagnetic sensor for metal target classification, IEEE Trans. on Geosci. Remote Sens., Vol. 39, No. 6, 1129-1138, Jun. 2001.

86. C. V. Nelson, Wide area metal detection (WAMD) system and method for security screening crowds, the Johns Hopkins University, US 6970086 B2, 2005.

87. A. Fainberg, Explosives detection for aviation security, Science, 14-15, 1992.

88. C. Wilker, detection of contraband using nuclear quad-pole resonance, US 7,106,058 B2, 2006.

89. P. Gao, Classification of Landmine-Like Metal Targets Using Wideband Electromagnetic Induction, Transactions on geo-science and remote sensing, Vol. 38, No. 3, May 2000..

90. A. G. Agurto, New proposal for the detection of concealed weapons, School of computing and engineering researcher's conference, Huddersfield, UK, 2007.

91. A. R. Hunt, Stepped- frequency CW radar for concealed weapon detection and through- the wall, SPIE Vol. 4708, 2002.

92. D. G. Sower, Eddy current resonances of canonical metallic targets Theory and measurements EG & G MSI, Interaction Note, Feb. 1997.

93. C. E. Baum, Detection and Identification of Visually Obscured Targets, p 434-544, Taylor and Francis, 1999.

94. J. R. Wait and K. P. Spies, Quasi-static transient response of a conducting permeable sphere, Geophysics, Vol. 34, No. 5, 789-792, 1969.

95. A. A. Kaufman and P. A. Eaton, The theory of Inductive Prospecting, Amsterdam, Netherland, 2001.

96. G. D. Sower and S. P. Cave, Detection and identification of mines from natural magnetic and electromagnetic resonances, Proc. SPIE, Vol. 2496, 1015-1024, Orlando, FL, 1995.

97. N. Geng and C. E. Baum, On the low-frequency natural response of conducting and permeable targets, IEEE Trans. on Geosci. Remote Sens., Vol. 37, No. 1, Jan. 1999. Progress In Electromagnetics Research M, Vol. 26, 2012 67.

98. C. E. Baum, Low-frequency near - field magnetic scattering from highly, but not perfectly, conducting bodies, Interaction Note 499, Phillips Laboratory, Nov. 1993.

99. C. E. Baum, On the singularity expansion method for the solution of electromagnetic interaction problems, Interaction Notes, Note 88, Air Force Weapons Laboratory, 1971.

100. C. E. Baum, The singularity expansion method and its application to target identification, Proc. of the IEEE, Vol. 79, No. 10, 1481 1492, 1991.

101. Y. Wang and N. Shuley, Complex resonant frequencies for the identification of simple objects in free space and lossy environments, Progress In Electromagnetics Research, Vol. 27, 1-18, 2000.

102. S. Harmer, S. E. Cole, N. J. Bowring, N. D. Rezgui, and D. Andrews, ‘‘On body concealed weapon detection using a phased antenna array," Progress In Electromagnetics Research, Vol. 124, 187-210, 2012.

103. S. Harmer, D. A. Andrews, N. D. Rezgui, and N. J. Bowring, ‘‘Detection of handguns by their complex natural resonant frequencies," IET Microw. Antennas Propag., Vol. 4, No. 9, 1182-1190, Sep. 2010.

104. S. Harmer, D. Andrews, N. Bowring, N. Rezgui, and M. Southgate, Ultra wide band detection of on body concealed weapons using the out of plane polarized late time response, Proc. SPIE, Vol. 7485, 748505, 2009.

105. L. Zhang, Y. Hao, and C. G. Parini, Natural resonant frequency extraction for concealed weapon detection at millimetre wave frequencies, 2nd European Conference on Antennas and Propagation (Eu CAP), 2007/11961, Edinburgh, UK, Nov. 11-16, 2007.

106. C. Alabaster, The microwave properties of tissue and other lossy dielectrics, Ph.D. Thesis, Cranfield, UK, Mar. 2004.

107. N. Geng and C. E. Baum, on the low-frequency natural response of conducting and permeable targets, IEEE Trans. on Geosci. Remote Sens., Vol. 37, No. 1, Jan. 1999.

108. M. Secman and G. Turhan-Sayan, Radar target classification method with reduced aspect dependency and improved noise performance using multiple signal classification algorithm, IET Radar, Sonar and Navigation, Vol. 3, No. 6, 583-595, 2009.

109. Y. Hua and T. K. Sarkar, Generalized pencil-of-function method for extracting poles of an EM system from its transient response, IEEE Trans. Antennas Propag., Vol. 37, No. 2, 229-234, 1989

APPENDICES

Appendix 1: The Figures Dimension:

1.1 The Handgun:

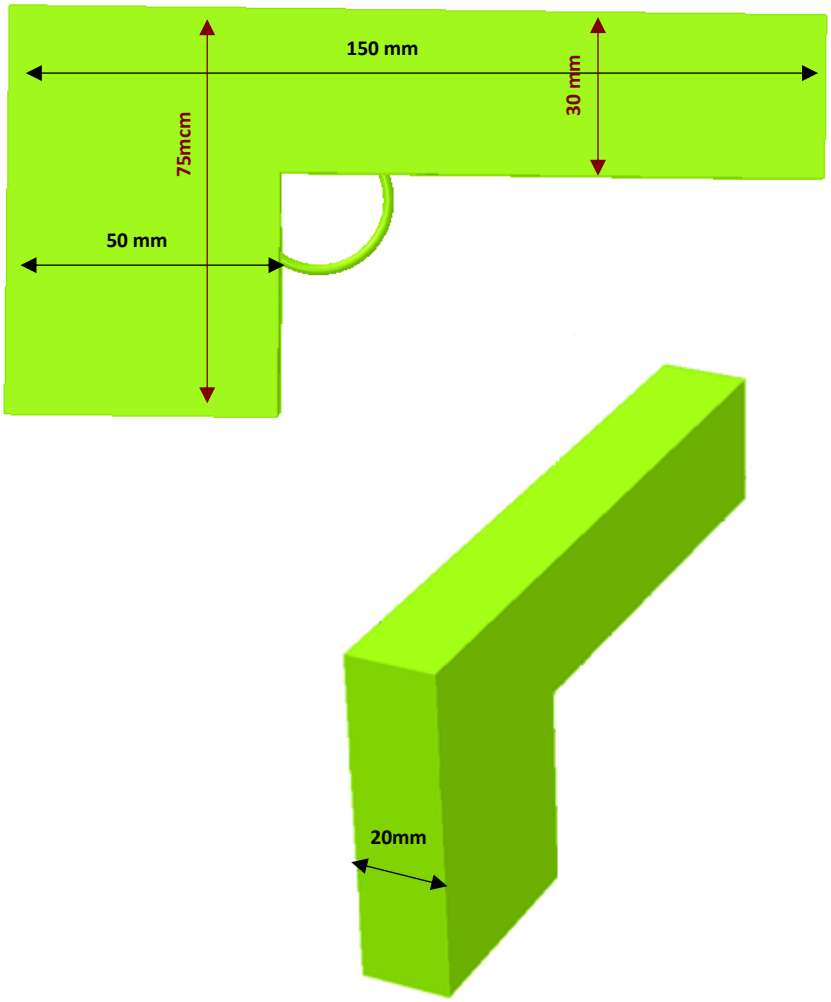

1.2 The Hand Grenade:

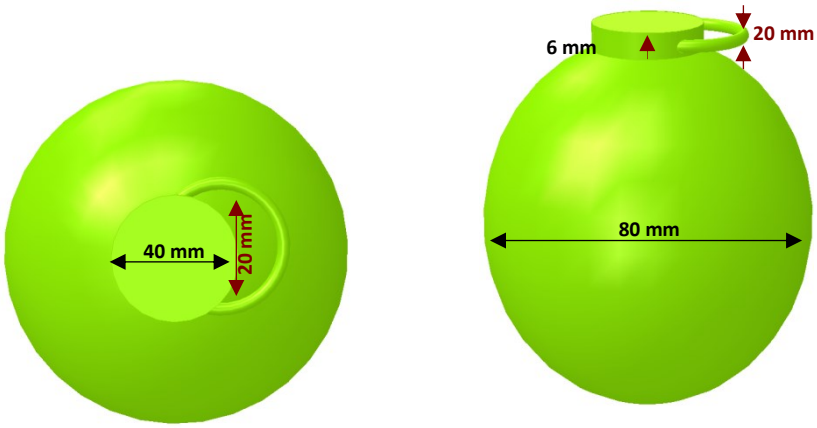

1.3 The Razor Blade:

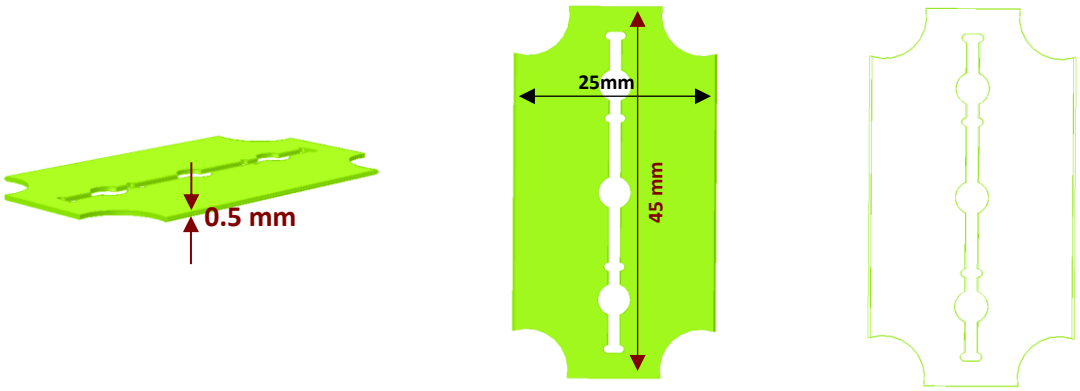

1.4 The Key:

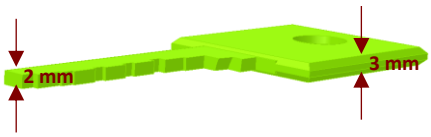

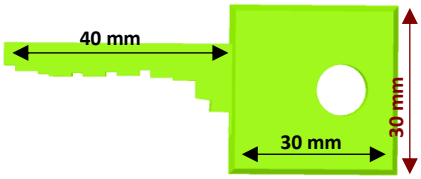

1.5 The Wrist Watch:

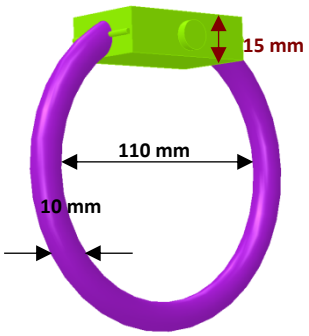

1.6 The Mobile Phone:

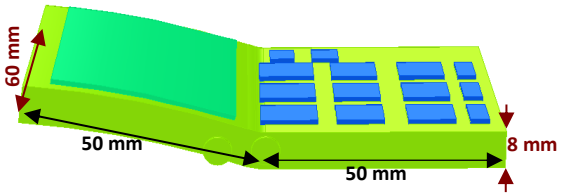

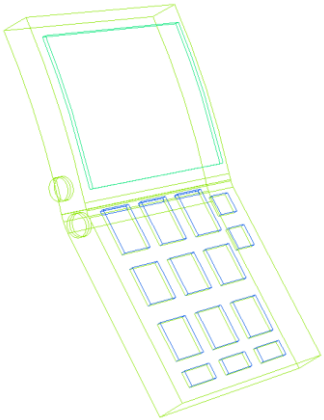

2.7 The Knife:

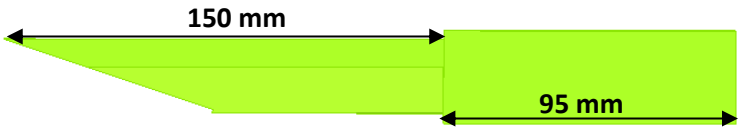

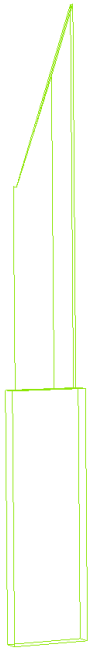

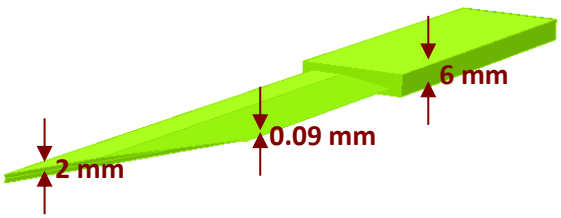

Appendix 2: Author's Publications:

2.1 Journal Papers:

Progress In Electromagnetics Research M, Vol. 26, 55- 68, 2012.

Resolution of Multiple Concealed Threat Objects using Electromagnetic Pulse Induction

Abdulbast Elgwel[1], Stuart William Harmer[2], Nicholas Bowring[3] & Shaofei Yin[4]

Sensing & Imaging Group, Manchester Metropolitan University, England

Abstract: The detection and identification of conducting objects using electromagnetic pulses to excite circulating eddy currents within the object is demonstrated by numerical simulation using a finite element time domain electromagnetic solver. The ability to discriminate between objects is based on the decay rate of the induced currents in the object, typically ~ 100 μS. The decay rates are different for a wide variety of everyday objects, allowing threat objects such as handguns, grenades and knives to be discriminated from benign objects such as mobile phones handsets, watches, keys, etc. Crucially, the time constant characterising an object depends only upon the electrical properties of the object (conductivity) and the shape and size of the object; the orientation of the object is irrelevant. This aspect independence of temporal current decay rate forms the basis of a potential object detection and identification system. By application of an algorithm based on the generalized pencil of function method, the authors demonstrate the ability to effectively count and indentify multiple objects carried in close proximity providing that the objects do not have very similar time constants.

1. I*n*troduction

Pulse Induction techniques for the detection and identification of metallic objects have been reported and studied as a possible method for concealed weapon detection [1]-[7], both on the human body and in carried baggage. Electromagnetic Pulse Induction (EMI) relies on a generating a rapidly changing, spatially uniform magnetic field which penetrates and encompasses the concealed metallic object. The temporally changing magnetic field induces transient eddy currents [8]-[13] in the conducting object which then decay by dissipative (resistive) losses. These eddy currents decay exponentially with time and have a characteristic time constant which depends only upon the size and shape of the object and the materials from which it is made; the orientation of the object does not influence the time constant [14]-[20]. This aspect independence which forms the basis of a simple object identification system:

[1] baset245@yahoo.com
[2] Corresponding author: s.harmer@mmu.ac.uk
[3] n.bowring@mmu.ac.uk
[4] s.yin@mmu.ac.uk

a library of time constants, measured *a-priori*, can be compared with the measured time constant of an unknown sample to assess the presence or absence of a particular object or objects of interest. EMI for concealed object detection has one important advantage over resonant electromagnetic aspect independent phenomena: that is the human body has a very much smaller perturbing effect in EMI than at the microwave frequencies (~ 0.4 – 2 GHz) required for excitation of natural resonances of typical concealed threat objects such as handguns and knives [21]-[27]. At microwave frequencies the human body is opaque and scatters and reflects microwave energy very effectively [28], undermining the ability to extract clean and uncluttered signatures from concealed objects [24], [26]. EMI operates at much lower frequencies ~ 10 KHz, where the human body is nearly transparent, does not support appreciable eddy currents and is therefore 'invisible' [19]. In the case where excitation occurs at frequencies where the electromagnetic wavelength is comparable with the concealed object size (Mie scattering regime), resonant effects give a second aspect independent parameter: resonant frequency and decay time. However, because EMI operates at large electromagnetic wavelengths when compared to object size, the concealed object is electrically small, and there is no resonant condition and consequently there is only one aspect independent parameter. EMI is at a disadvantage here as mapping an object in complex frequency space (two independent parameters) provides a less degenerate and more robust identifier than is possible with a single, aspect independent parameter [29].

2. Theoretical Basis

There is published work in the field of EMI for a variety of uses, concealed weapons detection [1]-[7]; non destructive testing [30]-[32] ground penetrating radar for unexploded ordnance detection [18] and mining [17]. These applications rely on the same phenomena and share a common theoretical underpinning. The time domain dependence of the induced voltage on the secondary, receiver coil can be expressed as [1],

$$V(t) = \delta(t)\sum_{n=1} A_n \exp\left(-\frac{t}{\tau_n}\right) \qquad (1)$$

where A_n and τ_n are the amplitudes and time constants respectively, of the n^{th} eddy current mode circulating in the object. In general, an analytic solution giving the values of A_n and τ_n is not possible for all, but a few very simple cases where symmetry allows for an analytical expression. A conducting sphere is one such case [13], [16]. For a sphere of radius *R*; conductivity σ and relative permeability μ, the time constants τ_n are given by,

$$\tau_n = \frac{\mu\mu_0\sigma R^2}{\chi_n^2} \tag{2}$$

where χ_n are the solutions of the equation,

$$\tan(\chi_n) = \frac{(\mu-1)\chi_n}{\mu-1+\chi_n^2} \tag{3}$$

The time dependence given by Equation 1 simplifies further for times which are long, when compared to the time constants of the higher ($n \geq 2$) order modes. For example the higher order modes of a sphere possess shorter time constants than the fundamental, see Equation 2, and it is assumed that this is true for other, more complex, objects. In this late time regime, after the excitation pulse or the switching off of the current in the primary coil that provides the spatially uniform magnetic field, the voltage induced in the secondary coil is simply

$$V(t) \sim A\exp\left(-\frac{t}{\tau_1}\right) \tag{4}$$

Thus we may identify an object by its aspect independent, fundamental time constant which is dependent only upon the shape, size and material that form the object.

When *M* multiple objects are present within the magnetic field the detected signal, again for times which are long compared to high order modes, will simply be the superposition of the signals for the objects individually,

$$V(t) \sim \sum_{n=1}^{M} A_n \exp\left(-\frac{t}{\tau_n}\right) \tag{5}$$

3. Object Counting and Identification

A pre-requisite of a security screening system based on EMI is the capability to detect and classify multiple objects that may be within close proximity to one another. As an example, a person could quite conceivably be carrying a handgun in a briefcase, a knife in their pocket and may well also have a mobile phone and other benign objects on their person. A robust and effective EMI based system is required to detect, count and identify these objects whatever their separations. Without doubt, the most serious problem posed by application of aspect independent EMI techniques is that of a single parameter being used to identify a concealed object, the fundamental time constant. There is an inherent degeneracy in this approach which may well prevent certain objects that share similar time constants being counted as individual items and therefore discriminated from one another. As can be seen from Equation 2, an object's time constant may be matched by an appropriately sized sphere.

To ascertain whether this problem is significant enough to seriously limit the effectiveness of an EMI system requires the measurement or simulation of a very wide variety of objects, both threat and non-threat, which may be encountered. In this study the authors present a representitive study of six commonly carried objects: A wristwatch, key and mobile phone handset as representative of benign objects and a knife, handgun and hand grenade as representative of threat objects.

Non-linear recursive fitting algorithms are not particularly suitable for the extraction of multiple time constants from a decaying temporal signal of the form of Equation 5. The fitting is sensitive to the starting points and is slow and computer intensive. The greatest problem is counting the number of objects present, as this is generally unknown *a-priori* and applying a model with an increasing number of fit parameters, terms and starting points quickly results in an unwieldy and unreliable method. The authors have investigated the application of the Generalised Pencil of Function (GPOF) method [33]-[34], which is a far more suitable and rapid algorithm for the intended application as it is a generalised Eigen value problem and therefore does not need multiple iterations to arrive at a solution. This approach is suggested by *Geng et al*. [19] for the extraction of time constants from non resonant objects.The GPOF algorithm decomposes the signal into a discrete set of complex frequency components; in the case of an exponentially decaying signal of the form of Equation 5, only the real parts of the complex frequency are non-zero and the imaginary (oscillatory) frequencies are ignored. The number of objects M is unknown but can be estimated, in the absence of degeneracy of time constants, by iteratively increasing the model order (the number of complex frequencies expected) of the GPOF algorithm until any new complex frequencies found have amplitude which is lower than a preset threshold value. See Figure 1. Comparison of the time constants thus obtained can then be made with a library of time constants for common or expected objects and a list of likely carried objects may then be formed. Output may be an autonomous alarm or informing the user, by screen, that a person is carrying only benign objects or that a person is likely carrying a threat object or objects.

The simulated transient data were windowed by selecting the temporal data 100 μS after the current driving the magnetic field is turned off. This is done to weight the fundamental resonance of the object. If this is not done spurious detections can arise, as higher order time constants can have sufficient amplitude to confuse the system, meaning a single object could be counted as two or more objects and the higher order time constants possibly mistakenly identified as being the fundamental time constants of other objects which are not actually present. 100 μS was chosen as this is the longest time constant of the limited objects simulated, with the exception of the hand grenade which has an unusually long time constant.

However this choice of waiting 100 μS is a somewhat arbitrary choice as the exact start of the late time is dependent on the object; for spheres the start of the late time region is given as the period of the fundamental time constant [13] and for handgun sized objects as ~ 100 μS [6]. A threshold discriminator of 5% of the maximum amplitude is applied to the amplitudes extracted using GPOF, below this value the associated time constant is not recorded.

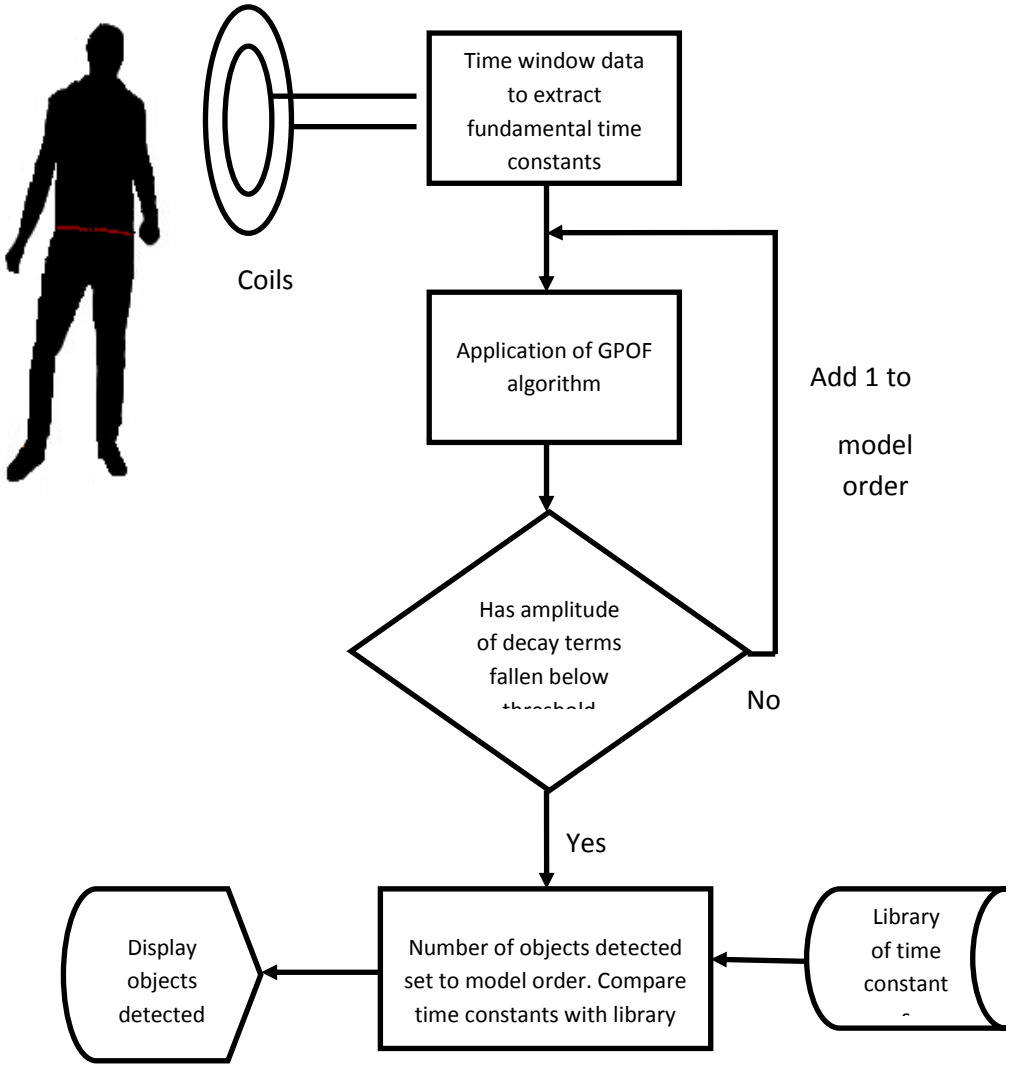

Figure 1: Flowchart depicting the processing steps and application of the GPOF algorithm to extract multiple time constants from the receiver coil time data.

4. Simulation

Numerical simulation is carried out using the commercially available finite element, time domain, electromagnetic solver software from *Vector Fields*. A large, circular coil is suitable for the purpose of generating a spatially uniform field over distances that are commensurate to typical concealed weapon

sizes (~20 cm). The model was validated by simulation of stainless steel spheres (conductivity 1.1×10^{6} sm^{-1}) and different radii. The fundamental time constants from simulations were compared to Equation 2, and the simulated results agree well with theory see table I.

Table I: Comparison of theoretical and simulated recovered time constants for stainless steel spheres of different radii

Material	Radius cm	Time Constant µS (simulation)	Time Constant µS (theory)
Stainless Steel	3.0	121	126
	4.0	221	224
	5.0	350	350
	6.0	507	504

The influence of the separation of two spheres (radii 4 and 6 cm) where simulated at varying separations, see Table II and both time fundamental time constants where accurately recovered irrespective of the separation between the two spheres. This important as it suggests that multiple objects can be detected and identified by means of their time constants even when they are located close together, for example when carried in a bag, providing they are not in direct electrical contact.

Table II: Influence of object separation on two stainless steel spheres (radii 4 and 6 cm respectively). The separation indicated between objects is for their closest surfaces and there is no electrical contact for the zero separation case.

Material	Objects separation - cm	Time Constant one - µS	Time Constant two - µS
Stainless Steel	100	221	526
	50	215	529
	25	220	527
	0.2	223	526
	0.0	222	527

5. Results

The aspect independence of the time constant of objects is the central and key effect on which the potential of EMI for concealed threat screening rests. A handgun was simulated in four different orientations (see figure 3) and the fundamental time constant recovered in the

absence of noise, there is little variation between the aspects, see Table III. Similar aspect independence is reproduced for the other simulated objects listed in Table IV.

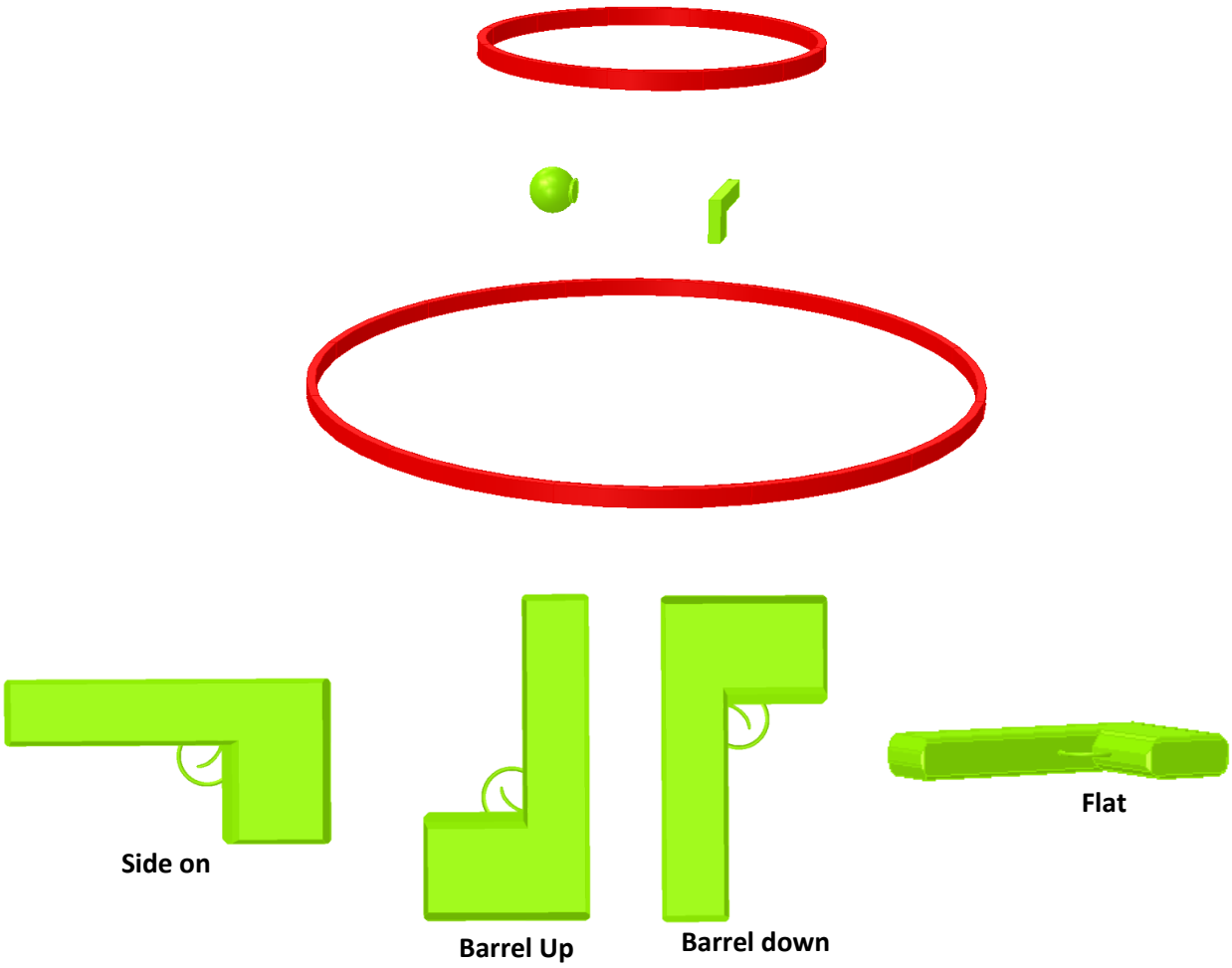

Figure 3: Examples of simulations of a handgun and hand grenade in the space between the drive (larger coil) and receiver (smaller coil) and some orientations of handgun used to validate the aspect independent nature of an object's time constant - see Table III.

Table III: Influence of object orientation

Material	Object & orientation		Time Constant µS
Stainless steel	Handgun	Side on	72.4
		Barrel up	72.1
		Barrel down	72.0
		Flat	73.6

Six objects were simulated in a single aspect, three benign objects and three threat objects. These were simulated individually and their characteristic time constants obtained in the absence of noise by the process described in Figure 1.

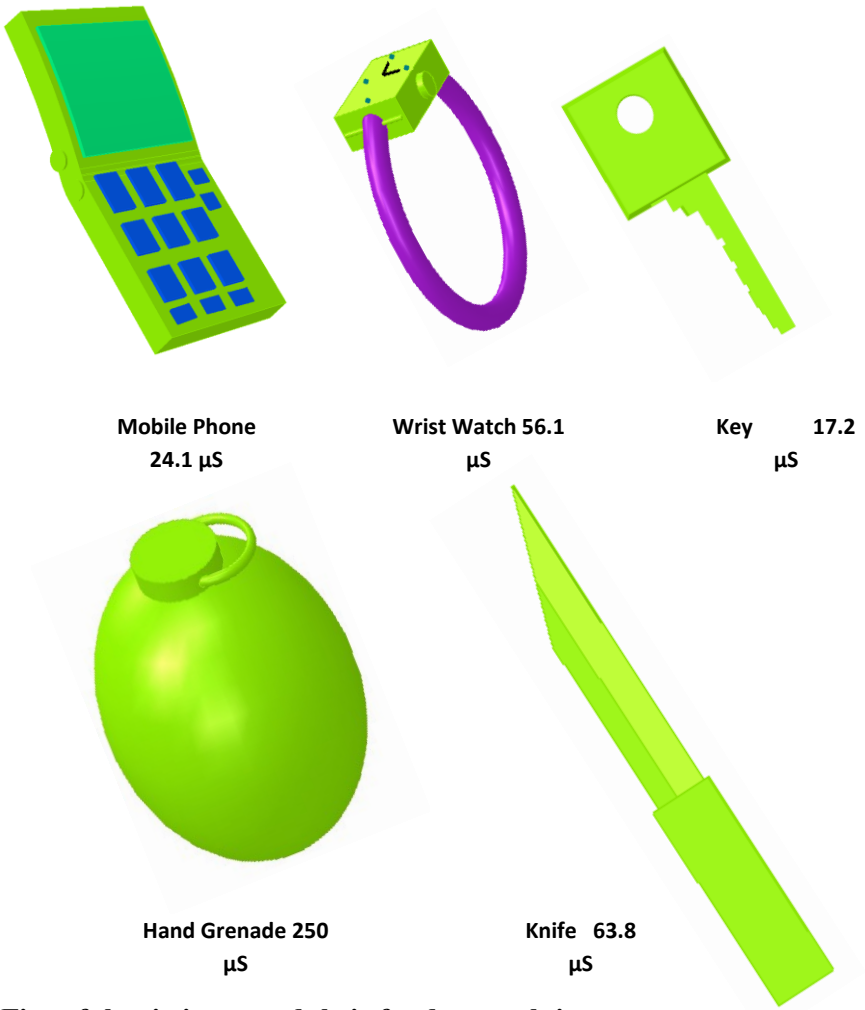

Figure 4: Five of the six items and their fundamental time constants as measured

when the object is simulated individually without noise; the handgun is shown in Figure 3 and has a fundamental time constant of 72.4 μS. See table IV for grouped objects results. All objects are stainless steel.

Table IV: Groups of two to five objects and the fundamental time constants obtained from these groupings; comparison is made to the time constants obtained for the Individual objects.

Objects	SNR	Hand grenade 250 μS	Handgun 72.4 μS	Knife 63.8 μS	Wrist watch 51.6 μS	Mobile phone 24.1 μS	Key 17.2 μS
Hand grenade & handgun	**Infinity**	**250**	**74.7**	**-**	**-**	**-**	**-**
	100	245.01	34.05	-	-	-	-
	50	240.16	14.52	-	-	-	-
	10	224.26	-	-	-	-	-
Wrist watch & key	**Infinity**	**-**	**-**	**-**	**53.9**	**-**	**12.4**[5]
	100	-	-	-	44.22	-	-
	50	-	-	-	46.60	-	-
	10	-	-	-	51.30	-	-
Hand grenade, handgun & wrist watch	**Infinity**	**253**	**86.0**[1]	**-**	**52.0**	**-**	**-**
	100	237.69	64.4	-	-	-	-
	50	215.17	59.06	-	-	-	-
	10	201.77	-	-	-	-	-
Hand grenade, handgun, wrist watch & knife	**Infinity**	**252**	**77.4**	**79.5**[1]	**43.0**[1]	**-**	**-**
	100	235.85	27.63	-	-	-	-
	50	210.27	39	-	-	-	-
	10	204.001	-	-	-	-	-
Hand grenade, handgun, wrist watch, knife & mobile phone	**Infinity**	**250**	**75.1**	**65.5**	**53.6**	**20.9**[1]	**-**
	100	231.96	74.84	-	-	-	-
	50	226.47	43.6	-	-		-
	10	230.88	32.46	-	-	-	-
Hand grenade, handgun, knife, mobile phone & key	**Infinity**	**232**	**69.1**	**65.6**	**-**	**25.1**	**9.25**[1]
	100	222.20	54.19	33.46	-	-	-
	50	221.46	30.55	-	-	-	-
	10	212.24	26.58	-	-	-	-

The time constants for these objects are presented in Table IV along with the retrieved time constants for groups composed of different numbers of the six simulated objects. The time constants are retrieved under noise free conditions (SNR of _) and with different levels of Gaussian noise applied (SNR of 100, 50 and 10). The hand grenade has by far the longest time constant, which is related to its near spherical and smooth shape giving rise to relatively

[5] Results with a greater than 10% discrepancy to the individually measured time constants

long lived eddy current distributions. Application of the simple algorithm described to the simulations of multiple objects, in the absence of noise, comprising combinations of the six objects listed in Table IV, successfully retrieves the fundamental time constants of the individual objects reasonably accurately. There is some discrepancy of time constants, notably in groups that contain more objects. The key seems to pose the greatest problem, the fundamental time constant is not accurately estimated when it is included in a group of other objects (See Table IV). The inaccuracy is probably due to the small size of the key relative to the other objects; the small size giving a much shorter fundamental time constant and a weaker contribution to the signal compared to the other, larger, objects. This results in the signals from the larger objects dominating and a greater inaccuracy in the retrieved time constant. However this interpretation seems to be incompatible with the data obtained for two spheres in proximity; see Table II, where the larger sphere's time constant is less accurately determined than the smaller.

When noise is added to the signal at a relatively low level (SNR of 100), the identification of multiple objects is significantly impaired, with only the largest and dominant objects being counted and the smaller objects either missing or their time constants considerably corrupted to the extent that identification would not be possible. For example, in the case where the handgun, hand grenade and wristwatch are presented together, only the handgun and hand grenade are counted for an SNR of 100; the wristwatch is absent. As the SNR increases the situation worsens, for an SNR of 10, using the same example scenario, only one object is counted (the hand grenade) and the time constant is highly corrupted (~20% different from accepted value). With five items present the addition of noise prevents the smaller objects from being counted and corrupts the time constants so that identification is not feasible, in fact only the hand grenade, which has a large cross section and long time constant, seems to remain detectable and identifiable.

7. Summary

The simulations demonstrate the feasibility of being able to detect, count and identify a range of commonly carried objects and also a range of weapons. However, this capability is lost if the signal is noisy and under these conditions smaller objects are not detected and aspect independent time constants are significantly corrupted, rendering identification unlikely. SNR

must be better than 100 if the proposed technique is to have reasonable chance of success. If SNR can be kept suitably low then discrimination of weapons from benign objects is feasible, at least for the objects simulated, as the fundamental time constants are sufficiently distinct.

The presence of multiple objects within the sensor range does not prevent counting and identification, although the accuracy of the determination of the individual objects' fundamental time constants is made worse increasing number of objects. The reason for this worsening of performance is undoubtedly due to the interaction (scattering) of the magnetic fields from the objects, i.e. the eddy currents flowing in one object give rise to a changing magnetic field which induces eddy currents in neighbouring objects and therefore blurs the time constants. In the absence of noise, the distortion of time constants when multiple objects are present is not so strong as to prevent the counting and identification of five objects from one another, with the possible exception of the key, see Table IV. Smaller objects such as a key or coins are more difficult to indentify due to their smaller cross section when compared to objects such as a handgun, hand grenade or knife. This is not expected to constitute a serious problem as most threat objects are significantly larger than a key or a coin. This investigation is now being extended to the laboratory, where a demonstrator system is now being built and it is anticipated that this work will enhance the capability of current screening procedures.

References

1. Nelson, C. V., Cooperman, C. B., Schneider, W., Wenstrand, D. S., and Smith, D. G., "Wide Bandwidth Time-Domain Electromagnetic Sensor for Metal Target classification," *IEEE Trans. Geosci. RemoteSens*. 39(6), 1129–1138 (Jun 2001).
2. Nelson, C. V., "Wide-Area Metal Detection System for Crowd Screening," in *Proc. SPIE AeroSense 2003 Conf., Sensors and Command, Control,Communication, and Intelligence (C3T) Technologies for Homeland Defense and Law Enforcemnt II,* Orlando, FL (22–25 Apr 2003).
3. C. V. Nelson, "Metal Detection and Classification Technologies", *Johns Hopkins APL technical Digest*, Vol. 24, Number 1, 2004, pp. 62-66.
4. Nicholas G. Paulter, "Guide to the Technologies of Concealed Weapon and Contraband Imaging and Detection," NIJ Guide 602–00 Electricity Division, National Institute of Standards and Technology Gaithersburg, MD 20899. Prepared for: National Institute of Justice Office of Science and Technology Washington, DC 20531 February 2001.
5. Alan Agurto, Yong Li, Gui Yun Tian, Nick Bowring and Stephen Lockwood, "*A Review of Concealed Weapon Detection and Research in Perspective,"*

Proceedings of the 2007 IEEE International Conference on Networking, Sensing and Control, London, UK, 15-17 April 2007

6. Agurto Goya, Alan, "New Proposal for the Detection of Concealed Weapons: Electromagnetic Weapon Detection for Open Areas," Thesis PhD. 2009, Huddersfield UK.
7. Hunt, A.R., Hogg, R.D., and Foreman, W., "Concealed weapons detection using electromagnetic resonances," *Proc. of the SPIE, The International Society for Optical Engineering Conference of Enformcement and Security Technologies*, Vol. 3575, pp. 62-67, Boston, MA. November 1998.
8. Baum, C. E., "On the singularity expansion method for the solution of electromagnetic interaction problems," Interaction Notes, Note 88, Air Force Weapons Laboratory, 1971.
9. Baum, C. E., E. J. Rothwell, K. M. Chen, et al., "The singularity expansion method and its application to target identification," *Proc. IEEE*, Vol. 79, No. 10, 1481-1492, 1991.
10. Wang, Y. and N. Shuley, "Complex resonant frequencies for the identifcation of simple objects in free space and lossy environments," *Progress In Electromagnetics Research*, Vol. 27, 1-18, 2000.
11. S. W. Harmer, S. E. Cole, N. J. Bowring, N. D. Rezgui, and D. Andrews, "On body concealed weapon detection using a phased antenna array," *Progress In Electromagnetics Research,* Vol. 124, 187-210, 2012
12. Harmer, S. W., D. A. Andrews, N. D. Rezgui, and N. J. Bowring, "Detection of handguns by their complex natural resonant frequencies," *IET Microw. Antennas Propag.*, Vol. 4, No. 9, 1182-1190, Sep. 2010.
13. Harmer, S., D. Andrews, N. Bowring, N. Rezgui, and M. Southgate, "Ultra wide band detection of on body concealed weapons using the out of plane polarized late time response," *Proc. SPIE*, Vol. 7485, 748505, 2009.
14. Zhang, L., Hao, Y., and Parini, C.G. "Natural resonant frequency extraction for concealed weapon detection at millimetre wave frequencies," *2nd European Conference on Antennas and Propagation (EuCAP 2007)* (2007/11961), Edinburgh, UK, 11-16 Nov. 2007.
15. Clive M. Alabaster, "The microwave properties of tissue and other lossy dielectrics," PhD. thesis, Cranfield UK, March 2004.

16. A. A. Kaufman, P. A. Eaton, "*The Theory of Inductive Prospecting,"* Amsterdam, Netherland, 2001.
17. Norbert Geng and Carl E. Baum, "On the Low-Frequency Natural Response of Conducting and Permeable Targets," *IEEE Transactions on geoscience and remote sensing*, Vol. 37, No. 1, Jan. 1999
18. C. E. Baum, "Low-frequency near-field magnetic scattering from highly, but not perfectly, conducting bodies," Phillips Lab., Interaction Note 499, Nov. 1993.
19. G. D. Sower and S. P. Cave, "Detection and identification of mines from natural magnetic and electromagnetic resonances," in *Proc. SPIE*, Orlando, FL, vol. 2496, pp. 1015–1024, 1995.
20. G. D. Sower, "Eddy current resonances of canonical metallic targets—Theory and measurements," EG&G MSI, Interaction Note, Feb. 1997.
21. Gui Yun Tian, Ali Sophian, David Taylor, and John Rudlin, "Multiple Sensors on Pulsed Eddy-Current Detection for 3-D Subsurface Crack Assessment," *IEEE Sensors Journal*, 5 (1). pp. 90-96, 2005.
22. Wait, J.R., and Kenneth P. Spies, "Quasi-static Transient Response of a Conducting Permeable Sphere," *Geophysics*," Vol. 34, issue 5, p. 789-792, 1969.
23. Hua, Y. and T. K. Sarkar, "Generalized pencil-of-function method for extracting poles of an EM system from its transient response," *IEEE Trans. Antennas Propag.*, Vol. 37, No. 2, 229-234, 1989.

.

2.2 Conference Papers:

Research day at Manchester Metropolitan University, 20th April 2012
Detection of Metallic Objects using Electromagnetic Pulses

Abdulbast Elgwel, Nicholas Bowring and Stuart Harmer, Sensing and imaging group, School of Science and Engineering, Manchester Metropolitan University, Oxford Road, Manchester M1 5GD

Detection of Metallic Objects using Electromagnetic Pulses

Abdulbast Elgwel, Nicholas Bowring and Stuart Harmer

School of Engineering ,Manchester Metropolitan University, Oxford Road, Manchester M1 5GD

Abstract:

Concealed threat objects such as handguns, grenades and knives are still a challenge to detect, especially in crowded areas. In this research we apply the commercially available finite difference time domain electromagnetic solver software *Vector Fields* to simulate the interaction of electromagnetic pulses with various metallic objects. A transmitter coil generates low frequency pulses which induce eddy currents to flow on the concealed objects. The decay time of the electromagnetic pulses measured by a receiver coil positioned some distance away. The voltage induced in the receiver coil has the form of an exponential decay in time. The time constant of the decay depends only upon the electrical properties of the object (conductivity) and the shape of the object. By mathematical analysis of the data multiple objects can be detected and indentified.

Simulation programme:

Vector Fields V13

The scheme of the model consists of two coils as seen figure 1. The first solenoid coil is the **Transmitter coil** and has 200 cm radius and 1 turn with a thickness of 1.5 cm. The second coil is the **Receiver Coil** with radius 100 cm and 1 turn, also with a 1.5 cm thickness. The driving signal is a saw tooth pulse and the target placed in the space between the coils.

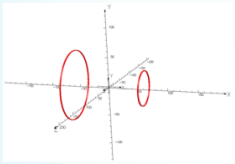

Figures 1: Transmitter coil & Receiver coil

Results & Discussion:

1. Sphere

Spheres with different radii can be used to validate the finite element model by comparison with theory:

$$\tau_{Theoritical} = \frac{\sigma \mu a^2}{\pi^2} \qquad (1)$$

where σ the conductivity, μ permeability and a the radius.

So the time constant from the simulation determine from fitting curve produce by mathematical method is:

$$Y = A * \exp(-b * x), \qquad (2)$$

$$\tau_{Simulation} = \frac{1}{b} \qquad (3)$$

Comparison of theoretical and simulation time constants show good agreement, see table 1, and the time constants depend on the size and shape, see fig 2.

Material	Radius	b	$\tau_{Simulation}$	$\tau_{Theortical}$
Stainless steel	3.0 cm	8249	0.0001212	0.0001260
	4.0 cm	4520	0.0002212	0.0002241
	5.0 cm	2855	0.0003502	0.0003501
	6.0 cm	1973	0.0005068	0.0005042

Table 1: Spheres with different radii

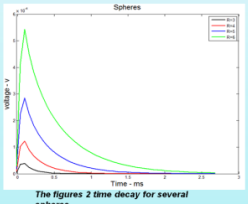

The figures 2 time decay for several spheres

2.Hand Bomb, Gun & : Knife

These shapes, simulated in stainless steel, are studied by modelling with each target separately, as show figure 3. The induced eddy currents decay exponentially with time. This decay is aspect independent and can be determined from equation (3). Table 2 displays the time constants for a variety of threat objects and the temporal decay curves are displayed in figure 4. Table 3 indicates the orientations for targets are irrelevant, i.e. the orientation does not affect the time decay rate

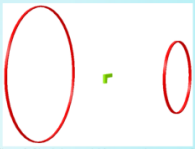

Figure 3: Simulation model for separating target - Gun

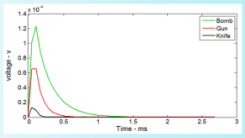

Figures 4: time decay for Gun, Hand Bomb & Knife

Material	Target	b	$\tau = \frac{1}{b}$
Stainless steel	Bomb	4005	0.0002496
	Gun	1.377e+4	0.0000724
	Knife	1.567e+4	0.0000638

Table 2: Time constant for separating targets

Material	Target		b	$\tau = \frac{1}{b}$
Stainless steel	Bomb	Side	4005	0.0002496
		Up	4021	0.0002486
	Gun	Normal	1.337e+4	0.0000724
		Up	1.386e+4	0.0000721
		Down	1.387e+4	0.0000720
	Knife	Normal	1.567e+4	0.0000638
		Up	1.684e+4	0.0000593
		Down	1.6e+4	0.0000625
		Side	1.563e+4	0.0000639

Table 3: The individually targets with various in direction

3. Two targets together:

In this step, two targets are placed together with variable separation and in **horizontal & vertical positions** as shown in figures 5(a) and 5(b). The temporal voltage induced becomes and the equation becomes:

$$Y = A * \exp(b * x) + c * \exp(d * x) \qquad (4)$$

$$\tau_1 = \frac{1}{b} \qquad (5)$$

$$\tau_2 = \frac{1}{d} \qquad (6)$$

Table 4 indicates the time constants for two targets in a horizontal position and table 5 for two targets in a vertical position. The decay curves are shown in figures 6 & 7:

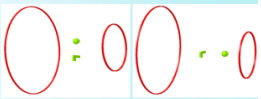

Figure 5(a) *Figure 5(b)*

Material	Target	b	d	$\tau_1 = \frac{1}{b}$	$\tau_2 = \frac{1}{d}$
Stainless steel	Bomb & Knife	1.521e+4	4011	0.0000657	0.0002493
	Bomb & Gun	1.351e+4	3992	0.0000740	0.0002505
	Gun & Knife	1.579e+4	1.412e+4	0.0000633	0.0000708

Table 4: two targets together at horizontal position

Material	Target	b	d	$\tau_1 = \frac{1}{b}$	$\tau_2 = \frac{1}{d}$
Stainless steel	Bomb & Knife	1.549e+4	3999	0.0000645	0.0002500
	Bomb & Gun	1.362e+4	3983	0.0000734	0.0002510
	Gun & Knife	1.701e+4	1.314e+4	0.0000587	0.0000761

Table 5: two targets together at vertical position

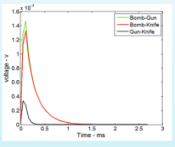

Figures 6 time decay for Gun-Hand Bomb, Hand Bomb-Knife & Gun-Knife – at horizontal position

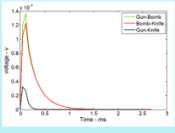

Figures 7 time decay for Gun-Hand Bomb, Hand Bomb-Knife & Gun-Knife – at vertical position

Conclusion:

Through our study of the models developed above we find a very good agreement between theoretical and simulated time constants for spheres. This validation permits us to apply, with confidence, the model to more complex and interesting objects in many of orientations. It was noted that the time constant depends only on the size, shape and material from which it is made and does not change by alteration of orientation. Two targets close to each other can be detected and indentified by their characteristic time constants. It is hoped that three and more objects could be detected and discriminated, opening the way for a powerful concealed threat detection solution.

2.3 Conference Papers:

Research day at Manchester Metropolitan University; 25th April, 2013

Electromagnetic Pulses Induction for Detection of Metal Items

Abdulbast Elgwel, Nicholas Bowring and Stuart Harmer, Sensing and imaging group, School of Science and Engineering , Manchester Metropolitan University, Oxford Road, Manchester M1 5GD

Electromagnetic Pulse Induction for Detection of Metal Items

Abdulbast Elgwel, Nicholas Bowring and Stuart Harmer

Sensing & Imaging Group, School of Engineering ,Manchester Metropolitan University,

Oxford Road, Manchester M1 5GD

Abstract:

It is undeniable that the detection of hidden contraband and concealed threats such as knives and handguns in baggage or on the body is a significant challenge, especially when screening of crowded areas is required. In this research we apply the commercially available finite difference time domain electromagnetic solver software, *Vector Fields*, to simulate the interaction of a low frequency electromagnetic pulse with different metal objects. Electromagnetic Pulse Induction (EMI) relies on a generating a rapidly changing, spatially uniform magnetic field which penetrates and encompasses the concealed metallic object. The temporally changing magnetic field induces eddy currents in the conducting object which then decay by dissipative (resistive) losses. These currents decay exponentially with time and exhibit a characteristic time constant which depends only upon the size, shape and material composition of the object. Mathematical analysis is by implementing the generalised pencil of function (GPOF) method. The GPOF algorithm decomposes the signal into a discrete set of complex frequency components; providing the capability to obtain the time constants from data. The results show that, theoretically, multiple objects can be detected and indentified.

Material	Length	Radius	$\tau_{Simulation}$ ms	$\tau_{theoretical}$ ms
Titanium	4 cm	2 cm	0.0936	0.0932
	8 cm	4 cm	0.3736	0.3730
	10 cm	4 cm	0.4660	0.4663
	10 cm	6 cm	0.6990	0.6995

Table 1: Fundamental time constants for a variety of different sized Titanium Cylinders.

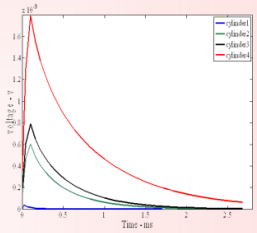

Figure 3: Eddy current decay curves for Titanium Cylinders

Simulation programme:

Vector Fields V13

A model was used that consists of two coils as seen figure 1. The **Transmitter coil** has 200 cm radius and 1 turn with a wire diameter of 1.5 cm. The **Receiver Coil** with radius 100 cm and 1 turn, also with a 1.5 cm wire diameter. The object under test is placed between these coils in which a nearly spatially uniform magnetic field exists over the scale of the object.

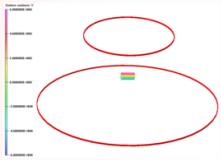

Figures 1: Object between Transmitter coil and Receiver coil

Results:

1. Cylinder

Cylinders of different sizes and of different materials were modelled; the results can be used to validate the finite element model by comparison with theory:

$$\tau_{theory} = \frac{\sigma \mu a^2 h}{18} \qquad (1)$$

where σ is the conductivity, μ the permeability, *a* the radius and h the length.

So the time constant from the simulation determine from fitting curve produce by mathematical method is:

$$v(t) = A\exp(-\frac{1}{\tau_0}) \qquad (2)$$

The model confirms agrees well with theory, see Tables 1 & 2. The eddy current decay curves are plotted in the figures 2 & 3.

Material	Length	Radius	$\tau_{Simulation}$ ms	$\tau_{theoretical}$ ms
Stainless steel	4 cm	2 cm	0.0622	0.0614
	8 cm	4 cm	0.2483	0.2457
	10 cm	4 cm	0.3088	0.3071
	10 cm	6 cm	0.4607	0.4607

Table 1: Fundamental time constants for a variety of different sized Stainless steel Cylinders.

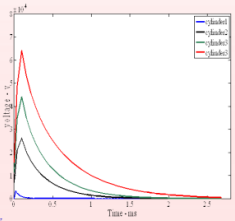

Figure 2: Eddy current decay curves for Stainless steel Cylinders

2. Mobile Phone, Watch & Key:

Three objects used as examples of non-threat objects are a mobile phone, watch and key, all composed of stainless steel. The time constant for these objects are presented in table 3 Results for groups of objects comprising combinations of these three objects are listed in table 4. The decay time is dependent on the size, shape and electrical and magnetic properties of metallic objects, so a smaller sized object gives a shorter fundamental time constant and a weaker contribution to the signal compared to larger objects.

Material	Target	$\tau_{Simulation}$ ms
Stainless steel	Mobile Phone	0.0241
	Watch	0.0516
	Key	0.0172

Table 3: Fundamental time constant for mobile phone, watch & key

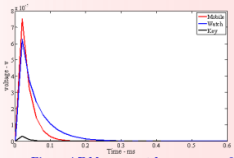

Figure 4 Eddy current decay curves of mobile phone, watch & key

Objects	Mobile Phone 0.0241 ms	Watch 0.0516 ms	Key 0.0172 ms
Mobile Phone & Watch	0.0261	0.0541	-
Mobile Phone & key	0.0256	-	0.0153
Watch & key	-	0.0539	0.0124
Mobile Phone , Watch & Key	0.0262	0.0537	0.0118

Table 4: Grouped objects and their fundamental time constants

Conclusion:

The model was validated by simulation of stainless steel cylinders of different radii. The fundamental time constants from the simulations were compared to the theory results and agree very well. This validation permits us more confidence to the model complex targets of different sizes. The time constant depends on the size, shape and material of the object. When two and three objects are placed together there is some discrepancy of time constants, notably in groups that contain more objects. The key seems to pose the greatest problem, the fundamental time constant is not accurately estimated when it is included in a group of other objects and the inaccuracy is probably due to the small size of the key relative to the other objects. This is an important result as it suggests that multiple objects can be detected and identified by means of their time constants even when they are close together, for example when carried in a bag, providing they are not in direct electrical contact.